TOWARDS THE TOTAL SYNTHESIS AND STEREOCHEMISTRY DETERMINATION OF STRESGENIN B

by

Michael P. Cook

B.S., The University of Pittsburgh, Pittsburgh, PA, 2004

Submitted to the Graduate Faculty of the

Kenneth P. Dietrich School of

Arts and Sciences in partial fulfillment

of the requirements for the degree of

Master of Science

University of Pittsburgh

2016

UNIVERSITY OF PITTSBURGH

DIETRICH SCHOOL OF ARTS AND SCIENCES

This dissertation was presented

by

Michael P. Cook

It was successfully defended on

April 5, 2011

and approved by

Dissertation Advisor: Dr. Kazunori Koide, Associate Professor

Committee Member: Dr. Peter Wipf, Distinguished University Professor

Committee Member: Dr. Craig Wilcox, Professor

Dissertation Advisor: Kazunori Koide, Associate Professor

Dedicated to my mother and also to my wife…

ABSTRACT

TOWARDS THE TOTAL SYNTHESIS AND STEREOCHEMISTRY DETERMINATION OF STRESGENIN B

Michael P. Cook, M.S.

University of Pittsburgh, 2016

The natural product stresgenin B has been shown to inhibit the up-regulation of HSPs in vivo. Since HSPs are known to protect cancerous cells from a variety of internal and applied stress (such as drug treatments and radiation), this makes stresgenin B a potentially new chemotherapeutic agent.

Herein is described the development and application of a new synthetic method that efficiently installs a primary amide-bearing acetonide group. Based on extensive Reaxys and SciFinder searching, we have found this to be only the second example of such a moiety, and the first in the class of 5,5-bicyclic systems. This methodology has the potential to be expanded to include esters, carboxylic acids, and other more exotically functionalized acetonides. In addition, we have held in reserve analogous compounds (synthesized during the course of this work), very similar in structure and composition to the natural product, for future SAR studies.

TABLE OF CONTENTS

Towards The Total Synthesis and Stereochemistry Determination of Stresgenin B i
Abstract v
Table of Contents vi
List of Tables viii
List of Figures ix
List of Schemes xi
Abbreviations xiii
Acknowledgements xv
1.0 Heat Shock Proteins as Therapeutic Targets 1
2.0 Inhibitors of HSPs and Current State of the Art in Drug Development 5
2.1 Radicicol 7
3.0 Discovery and biological significance of stresgenin B 11
4.0 Background and Previous Routes 15
4.1 Carl R. Johnson's Approach 16
4.2 Fulvenes 17
4.3 Second Generation Scheme 19
4.4 Generation 3 Scheme 22
4.5. Conclusions from Previous Routes 26
5.0 Background for Current Synthetic Plan 27
5.1 Retrosynthetic analysis 28
5.2 Acetonide formation. 29
5.3 Lead Attempts 30
5.4 Installation of the methyl ester 31
5.5 Early Attempts at Acetonide Formation 36
6.0. Revision to the 4th Generation Route 42
6.1 Revised retrosynthetic analysis 42
6.2 Deprotection 45
7.0 Summary and Future Experiments 48
8.0 Experimental Section 49
8.1 General Techniques 49
8.1.1 Preparation of Ester 40 50

8.1.2 Product Mixture 40a 51
8.1.3 Product mixture 40b 51
8.1.4 Compound 40 52
8.1.5 Compound 51 Z 53
8.1.6 Compound 51 E 53
8.1.7 Preparation of 51-E from 51-Z 54
8.1.8 Preparation of diol 73 55
8.1.9 Compound 73 55
8.1.10 Preparation of benzyl ether 83 55
8.1.11 Compound 83 56
8.1.12 Preparation of diol (80) 57
8.1.13 Compound 80 57
8.1.14 Preparation of 79 58
8.1.15 Preparation of sulfoxide 84 58
8.1.16 Preparation of aldehyde 85 59
8.1.17 Preparation of carboxylic acid 86 60
8.1.18 Compound xx diastereomer 86 60
8.1.19 Preparation of amide 87a-d 61
8.1.20 Compound 47a 62
8.1.21 Compound 47b 62
8.1.22 Compound 87c 62
8.1.23 Compound 87d 63
8.1.24 Preparation of bi-cyclic amide 95 63
8.1.25 Compound 95 64
9.0 NMR Spectrums 65
10.0 Bibliography 110

LIST OF TABLES

Table 1: Spectral Assignments (in CDCl3) 14
Table 2: Solvent Effects on the Wittig Reaction 32
Table 3: Model Reactions to Scan Reagents for Acetonide Formation..... 37
Table 4: Examination of Deprotection Routes using Model Compound 83..... 45

LIST OF FIGURES

Figure 1: HSP90 N-Terminal Binding Domain[5] 3
Figure 2: Geldanamycin and Analogues 6
Figure 3: 17-AAG 6
Figure 4: 17-DMAG 6
Figure 5: Radicicol and its biotinylated derivative 7
Figure 6: Radicicol analogue bound to the ATP binding site of HSP90* 7
Figure 7: Oxime analogues 8
Figure 8: Novobiocin and Coumarin 8
Figure 9: Purine Derivatives 9
Figure 10: Quercetin 9
Figure 11: Current Heat Shock Protein Inhibitors 10
Figure 12: Stresgenin B 12
Figure 13: NOESY Correlation 14
Figure 14: 5,5-enone (4S, 5S)-(isopropylidenedioxy)-2-cyclopentenone 15
Figure 15: Prostaglandin E_2 16
Figure 16: Aromatic and Antiaromatic Properties of 7 18
Figure 17: Resonance structure Analysis of 18 19
Figure 18: Steric Interactions in the Wittig Reaction (Vedejs Model) 31
Figure 19: An Examination of Dipole and Steric Interactions in the Wittig Reaction 33
Figure 20: Sterics Influence Z:E selectivity 35
Figure 21: Carbon Number Assignments 50
Figure 22: ^{1}H NMR spectrum of compound 23 (300 MHz, $CDCl_3$, 293K) 66
Figure 23: ^{1}H NMR spectrum of compound 22 (300 MHz, $CDCl_3$, 293K) 67
Figure 24: ^{1}H NMR spectrum of compound 35 (300 MHz, $CDCl_3$, 293K) 68
Figure 25: ^{1}H NMR spectrum of compound 37 (300 MHz, $CDCl_3$, 293K) 69
Figure 26: ^{1}H NMR spectrum of compound 34 (300 MHz, $CDCl_3$, 293K) 70
Figure 27: ^{1}H NMR spectrum of compound 40 R_f=0 .60 (300 MHz, $CDCl_3$, 293K) 71
Figure 28: ^{13}C NMR spectrum of compound 40 R_f=0 .60 (300 MHz, $CDCl_3$, 293K) 72
Figure 29: ^{1}H NMR spectrum of compound 40 R_f=0 .47 (300 MHz, $CDCl_3$, 293K) 73
Figure 30: ^{1}H NMR spectrum of compound 40 R_f=0 .47 (continued) 74
Figure 31: ^{13}H NMR spectrum of compound 40 R_f=0 .47 (300 MHz, $CDCl_3$, 293K) 75
Figure 32: ^{1}H NMR spectrum of compound 45 R_f=0 .38 (300 MHz, $CDCl_3$, 293K) 76
Figure 33: ^{1}H NMR spectrum of compound 45 R_f=0 .28 (300 MHz, $CDCl_3$, 293K) 77
Figure 34: ^{1}H NMR spectrum of compound 52 (300 MHz, $CDCl_3$, 293K) 78
Figure 35: ^{1}H NMR spectrum of compound 50 (300 MHz, $CDCl_3$, 293K) 79
Figure 36: ^{1}H NMR spectrum of compound 48 (300 MHz, $CDCl_3$, 293K) 80
Figure 37: ^{1}H NMR spectrum of compound 2 (300 MHz, $CDCl_3$, 293K) 81
Figure 38: ^{1}H NMR spectrum of compound 51-Z (300 MHz, $CDCl_3$, 293K) 82
Figure 39: ^{13}C NMR spectrum of compound 51-Z (300 MHz, $CDCl_3$, 293K) 83
Figure 40: ^{1}H NMR spectrum of compound 51-E (300 MHz, $CDCl_3$, 293K) 84
Figure 41: ^{13}C NMR spectrum of compound 51-E (300 MHz, $CDCl_3$, 293K) 85
Figure 42: ^{1}H NMR spectrum of compound 73 (300 MHz, $CDCl_3$, 293K) 86
Figure 43: ^{1}H NMR spectrum of compound 83 (400 MHz, $CDCl_3$, 293K) 87
Figure 44: ^{13}C NMR spectrum of compound 83 (400 MHz, $CDCl_3$, 293K) 88

Figure 45: ^{1}H NMR spectrum of compound 80 mix. diastereomers (400 MHz, $CDCl_3$, 293K) .. 89
Figure 46: ^{1}H NMR spectrum of compound 80 mix. diastereomers (400 MHz, $CDCl_3$, 293K) .. 90
Figure 47: ^{13}C NMR spectrum of compound 80 single diastereomer (400 MHz, $CDCl_3$, 293K) 91
Figure 48: ^{1}H NMR spectrum of compound 79 (400 MHz, $CDCl_3$, 293K)..... 92
Figure 49: ^{1}H NMR spectrum of compound 79 (continued)..... 93
Figure 50: ^{13}C NMR spectrum of compound 79 (400 MHz, $CDCl_3$, 293K)..... 94
Figure 51: ^{1}H NMR spectrum of compound 84 (400 MHz, $CDCl_3$, 293K)..... 95
Figure 52: ^{1}H NMR spectrum of compound 84 (continued)..... 96
Figure 53: ^{1}H NMR spectrum of compound 84 (continued)..... 97
Figure 54: ^{1}H NMR spectrum of compound 85 (400 MHz, $CDCl_3$, 293K)..... 98
Figure 55: ^{1}H NMR spectrum of compound 85 (400 MHz, $CDCl_3$, 293K)..... 99
Figure 56: ^{1}H NMR spectrum of compound 85 (continued)..... 100
Figure 57: ^{1}H NMR spectrum of compound 87a (400 MHz, $CDCl_3$, 293K)..... 101
Figure 58: ^{13}C NMR spectrum of compound 87a (400 MHz, $CDCl_3$, 293K)..... 102
Figure 59: ^{1}H NMR spectrum of compound 87b (400 MHz, $CDCl_3$, 293K)..... 103
Figure 60: ^{13}C NMR spectrum of compound 87b (400 MHz, $CDCl_3$, 293K)..... 104
Figure 61: ^{1}H NMR spectrum of compound 87c (400 MHz, $CDCl_3$, 293K)..... 105
Figure 62: ^{13}C NMR spectrum of compound 87c (400 MHz, $CDCl_3$, 293K)..... 106
Figure 63: ^{1}H NMR spectrum of compound (600 MHz, $CDCl_3$, 293K)..... 107
Figure 64: ^{13}C NMR spectrum of compound 95 (600 MHz, $CDCl_3$, 293K)..... 108
Figure 65: NOESY correlation spectrum of compound 87a (600 MHz, $CDCl_3$, 293K) 109

LIST OF SCHEMES

Scheme 1: Johnson's Approach to Enone 2 16
Scheme 2: Armstrong's Approach to 2 via Fulvene Chemistry 17
Scheme 3: Test Reaction Using Fulvene Chemistry 18
Scheme 4: Retrosynthetic analysis of Second Generation Scheme 20
Scheme 5: Synthesis of Enone 2 20
Scheme 6: A HWE Transformation Leads to 2 in low/inconsistent yields 21
Scheme 7: Possible Pathway of Decomposition 22
Scheme 8: Retrosynthetic analysis of Generation 3 Scheme 22
Scheme 9: Synthesis of diol 34 23
Scheme 10: Preparation of ketal 39 24
Scheme 11: Unexpected Ester Formation 24
Scheme 12: Plausible Mechanism of Ester Formation 25
Scheme 13: Oxidation Attempts 25
Scheme 14: Moon/Jin Inspired Retrosynthetic Analysis 26
Scheme 15: Complete Retrosynthetic Analysis of Current Route 28
Scheme 16: Kochetkov's Synthesis of a Primary Amide-Bearing Acetonide 29
Scheme 17: Key Synthesis of Enone 2 30
Scheme 18: Effects of Lithium of Acidity 34
Scheme 19: HWE Conditions lead to Enhances E selectivity 34
Scheme 20: Photoisomerization of 52-Z 36
Scheme 21: Decomposition of 51 37
Scheme 22: Loss of Ammonia from Product 38
Scheme 23: Attempts at One-Pot Deprotection/Protection to 1a 39
Scheme 24: Conjugate Addition to Multiple Michael Acceptors 39
Scheme 25: Model System/Scanning of Lewis Acids 40
Scheme 26: Diagnostic Testing of Reagent Reactivity 40
Scheme 27: Resonance and Induction Influence Reactivity of Carbonyl 41
Scheme 28: Final Scan of Reagent Reactivity with Protic Acid 41
Scheme 29: Revised Retrosynthetic Analysis 42
Scheme 30: Synthesis of 82 43
Scheme 31: Formation of Key Intermediate 79 43
Scheme 32: Synthesis of the Amide-Bearing Acetonide 44
Scheme 33: Plausible Mechanism for low Observed Reactivity 46
Scheme 34: Deprotection of Benzyl using DDQ 47
Scheme 35: Synthesis of Most Advanced Intermediate 47
Scheme 36: Ester 40 Preparation 50
Scheme 37: Compound 51 Preparation 52
Scheme 38: Compound 51 E Preparation 54
Scheme 39: Preparation of Diol 73 54
Scheme 40: Preparation of Benzyl Ether 83 55
Scheme 41: Preparation of Diol 80 56
Scheme 42: Preparation of 79 57
Scheme 43: Preparation of Sulfoxide 84 58
Scheme 44: Preparation of Aldehyde 85 59

Scheme 45: Preparation of Carboxylic Acid 86 60
Scheme 46: Preparation of Diastereomer 86 61
Scheme 47: Preparation of Amide 95 63

ABBREVIATIONS

[α]	specific rotation
appt	apparent
br	broad
^{13}C	carbon 13 nuclear magnetic resonance
CSA	camphorsulfonic acid
d	doublet
dd	doublet of doublets
ddd	doublet of doublet of doublets
δ	NMR chemical shift in parts per million downfield from a standard
DCM	dichloromethane
DDQ	2,3-dicloro-5,6-dicyano-1,4-benzoquinone
DMSO	dimethyl sulfoxide
dr	diastereomeric ratio
dtd	doublet of triplet of doublets
dt	doublet of triplets
ε	dielectric constant
equiv	equivalent
ESI	electrospray ionization
Et	ethyl
g	gram
h	hour(s)

^{1}H NMR	proton nuclear magnetic resonance
HSP	heat shock protein
HRMS	high resolution mass spectrometry
Hz	Hertz
IR	infrared
J	coupling constant
L	liter
m	milli; multiplet
M	molar
Me	methyl
MHz	megahertz
mol	mole
MW (or FW)	molecular (formula) weight
NMR	nuclear magnetic resonance
NOESY	nuclear Overhauser enhancement spectroscopy
Ph	phenyl
Pr	propyl
q	quartet
R_f	retention factor
s	singles; second
SiO_2	silica gel
t	triplet
THF	tetrahydrofuran

ACKNOWLEDGEMENTS

Since I joined the Koide group in 2007, I have made a long and often difficult journey of learning how to become a scientist. This process would have been impossible if not for the open-door policy of my advisor, Dr. Kazunori Koide. It is through his patience and guidance that I have learned how to become a scientist. It is important for me to recognize the past and present members of the Koide group, especially Brian Albert, Amanda Gardner, Sami Osman, Dr. Shin Ando, and Dr. Fengling Song, whose guidance and wisdom have led me to this point today.

I have deep appreciation for the opportunity given to me by Dr. Craig Wilcox to perform undergraduate research in his laboratory in 2003-2004, and to my third committee member, Dr. Peter Wipf, who encouraged me to keep working at my goals during the most difficult time in my life.

I would not be at this point today had it not been for the love and support of my mother who has infinite patience in dealing with me. The same goes out to my wife, Karen, who continues to support all the long hours I put into work to make our lives, and our families' lives, better one day.

Additionally, my thanks are given to Dr. Damodaran Krihanan and Sage Bower for support in NMR studies, and Dr. John Williams and Bhaskar Godugu for mass spectrometry

.

1.0 HEAT SHOCK PROTEINS AS THERAPEUTIC TARGETS

Cancer is a disease characterized by genetic mutations, which in turn gives rise to phenotypic expressions, such as rapid cell division and growth rate (tumorigenesis).1 These tumors can be classified in two types: malignant and non-malignant. The former, being untreated, leads to death. Although the current technology makes possible the identification of specific proteins and signaling pathways in this disease, the inherent genetic plasticity of such cells makes it difficult to battle cancer by a single biological route. Additionally, cancer cells are extraordinarily proficient at subverting toxic environments and externally applied shock. For example, cancer cells exposed to a deadly dose of radiation have the capability of activating multiple overlapping signaling pathways to protect themselves from further damage. Many cancer cells also have the ability to up-regulate a multifaceted transcriptional response, allowing them to successfully cope with an oxygen-deprived atmosphere (such as in treatments targeting angiogenesis).

In the case of therapeutic treatments for cancer, such as radiation therapy and concomitant drug therapy, it can be assumed that these cells are always under some form of moderate to severe shock. One approach in chemotherapeutics is to target the machinery responsible for the maintenance and vitality of such cells. In part, cells respond to such stress via the up-regulation of chaperone proteins called heat shock proteins (HSPs).

Serendipitously discovered[2] in the 1960s within the chromosomes of Drosophila, HSPs are a family of molecular chaperones responsible for a wide range of cellular functions.[3] Induced in response to a variety of stressors, including hyper/hypothermia, as well as to chemical stressors,

such as drugs and radiation, these proteins are responsible for the maintenance and vitality both normal and malignant cell.

More recently, the role of HSPs as a novel therapeutic target for cancer has become a major point of interest in the scientific community. In addition to the maintenance of the cell, HSPs possess the ability to bind peptide dendritus from cells that are cancerous, foreign, or otherwise altered (in other words, peptides a normal cell would not otherwise possess), and which serve as antigens for the immune response. Additionally, they play an active role in the prevention of events leading to non-functional proteins, such as protein misfolding and aggregation.

A major interest has arisen in one heat shock protein in particular, HSP90, as it appears to play a leading role in the survival of cancer cells.[1] As such, work worldwide is being devoted to discovering new agents that target this and other HSPs (see following section).

HSPs are divided into families based on molecular weight, and are divided into ten classes. For example, the HSP90 protein (a 90 kD protein) belongs to a family containing HSP90, in both α and ß forms in humans, 86 and 84 in mice, and 83 in drosophila.[4] HSP90 is a constitutive homodimer with its main intersubunit contacts within the 190 C-terminal residues. The highly conserved 25kD amino terminal domain is the binding site for ATP and geldanamycin (Figure 1).

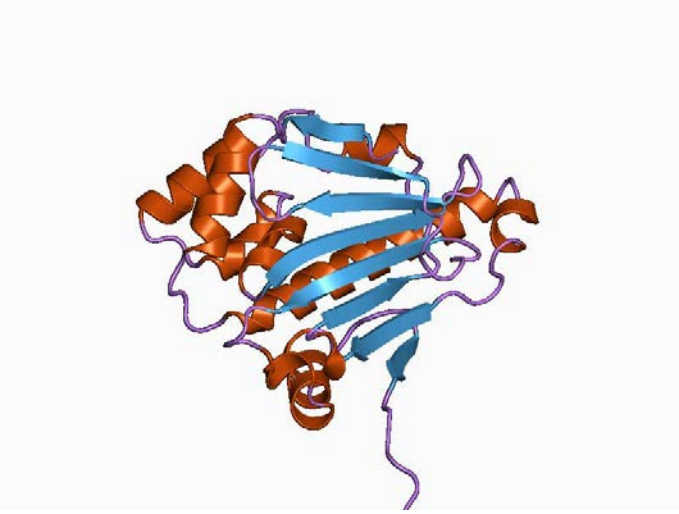

Figure 1: HSP90 N-Terminal Binding Domain[5]

Both the C and N terminals have been implicated in the binding of substrate polypeptides, which can then be presented to antigen presenting cells, thus eliciting an immune response. Additionally, nucleotides, and the adjacent charged sequence of HSP90 affect substrate binding at the N-terminal site.[6-10] Since the chaperone cycle that drives substrate loading and unloading is ATP-dependent,[11, 12] there is great potential in targeting the ATP binding site of this protein as a means to inhibit its function.

A variety of signal transduction proteins constitute the majority of HSP90 substrates *in vivo*.[13-15] These proteins are critically dependent on HSP90 for proper folding from their nascent to native state.[16] Disruption of HSP90 function by mutation or treatment of inhibitors leads to multiple physiological defects in cells (a result consistent with the importance of this protein to signal transduction networks). HSP90 affects the mitogenic signal cascade, cyclin-dependent progression through both G-1 and G-2, and centrosome function during mitosis.[17, 18, 19]

In addition to maintenance of the cell under normal conditions, HSP90 is also used under both stress and non-stressful situations to aid in protein folding, re-folding of denatured proteins, and stabilization of proteins undergoing stress often with the aid of co-chaperon HSP60.[17] However, the exact mechanism of recognition of these misshapen proteins remains elusive. The mode of activation for up-regulation of the HSP expression is, however, known. Heat shock factor 1, *hsf*-1, is the transcription factor allowing for the up-regulation of the *HSP* gene expression. Under normal conditions, this protein is in its monomeric form and is sequestered by HSP90. As the level of stress increases in the cell, and more proteins lose their structural integrity, *hsf-1* monomers are released into the surrounding environment. Upon release, *hsf-1* forms a trimer, which is in turn translocated to the nucleus, where it binds to the heat shock element (a conserved regulatory DNA sequence comprised of at least three contiguous inverted repeats of 5'-nGAAn-3' upstream of the heat shock gene). This, in turn, activates the gene for transcription to RNA. [20]

Susan Lindquist et al.[21] have demonstrated the direct role hsf-1 plays in carcinogenesis. Two types of mice ($hsf\text{-}1^{+/+}$ and $hsf\text{-}1^{-/-}$) were subjected to topical carcinogens for a period of days. While tumorigenesis had occurred in both types of mice, it was recorded that those bearing $hsf\text{-}1^{+/+}$ produced up to eight tumors/mouse, leading to a low percent survival rate after 45 weeks (~30%). However, mice bearing knocked-down $hsf\text{-}1^{-/-}$, showed on average only one tumor/mouse, with a much higher survival rate (90% after 45 weeks). This study demonstrated the vital importance HSPs play in tumorigenesis. Furthermore, this suggests HSP downregulators can be used in parallel with common chemotherapeutic treatments (such as radiation), thus increasing efficacy.

2.0 INHIBITORS OF HSPS AND CURRENT STATE OF THE ART IN DRUG DEVELOPMENT

Initially viewed as disadvantageous, HSP inhibitors interact with proteins in a stoichiometric manner.[16] However, the ATPase domains of HSPs have been identified as targets for HSP inhibitors. Although it would seem that proteins from both malignant and normal cells are targeted, only malignant cells are selectively inhibited. The pathway by which this type of selectivity occurs, however, remains elusive. There is always the concern, however, that in by exploring such chemotherapeutic routes, drug-resistant cells may evolve.

The natural products geldanamycin and radicicol were the first HSP inhibitors reported.[22] However, the natural geldanamycin went unnoticed for many years, due to a lack of understanding about its biological pathway. In 1992, Neckers et al. discovered that this compound was binding to HSP90.[23] Geldanamycin competes with ATP at the nucleotide binding site in the NH_2-terminal domain of HSP90.[24] The mode of action, through ATPase inhibition, leads to the destruction of several proteins by the ubiquitin-proteasome pathway,[25] resulting in apoptosis.[26-28] In preclinical trials, the drug proved too hepatotoxic for human use and was poorly soluble in aqueous media. Following these results, a less toxic analogue was developed. Analogues of the natural product (Figure 2) have been developed and will be discussed in further detail.

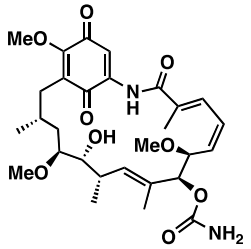

Figure 2: Geldanamycin and Analogues

The analogue 17-allylamino-17-demethoxygeldanamycin (17-AAG, Figure 3), with an IC50 of 31 nM for the inhibition of ERBB2 in SK-BR-3 cells is by far the most studied analogue. ErbB2 is a member of the ErbB receptor tyrosine kinase family. Through independent study, this analogue was shown to possess more potent biological activity than 17-AAG, and a 10-fold increase in solubility in pH 7.0 buffer.[29]

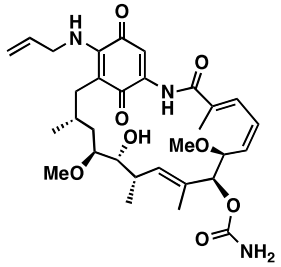

Figure 3: 17-AAG

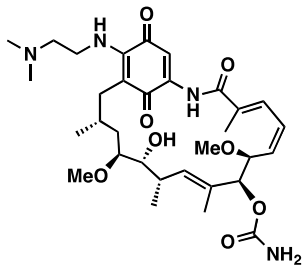

Figure 4: 17-DMAG

2.1 RADICICOL

Radicicol (Figure 5) was first isolated in 1953 from *Monosporium bonorden*, and a subsequent total synthesis reported in 1968 by McCapra and collegues.[30, 31]

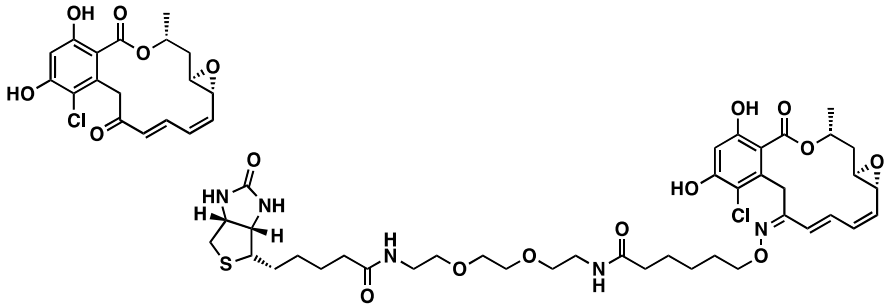

Figure 5: Radicicol and its biotinylated derivative

Affinity chromatography led to isolation of HSP90 (Figure 6).[32] X-Ray studies subsequently identified the binding site as the N-terminal ATPase domain with a K_D of 19 nM.

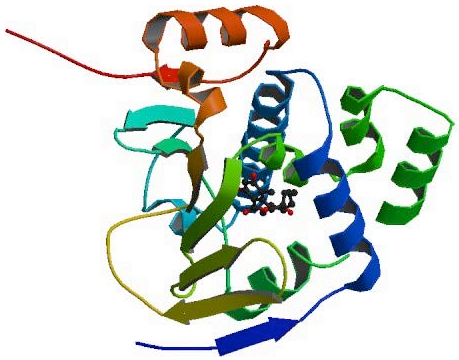

Figure 6: Radicicol analogue bound to the ATP binding site of HSP90*

However, Kwon and collaborators discovered that biological activity of radicicol vanishes in the presence of thiols, obviously a major problem to its introduction into biological systems.[33]

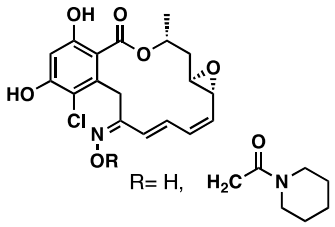

Figure 7: Oxime analogues

Novobiocin (Figure 8) binds to a site different than geldanamycin or radicicol. It has been shown to inhibit growth of gram-positive bacteria, hydrolysis of ATP, and binding of DNA topoisomerase II.[34]

Through a series of studies, it was discovered that novobiocin binds at a previously unrecognized ATP-binding site at the C-terminal region of HSP90, leading to destabilization and dissociation of client proteins.[35, 36]

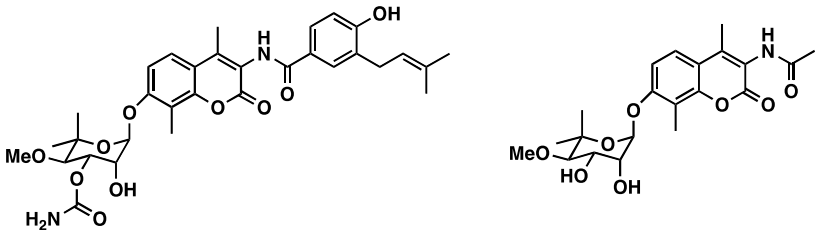

Figure 8: Novobiocin and Coumarin

In the beginning of the twentieth century, an interest in fully synthetic inhibitors gained notice with the discovery of purine derivatives. Examples of such agents are shown in Figure 9.

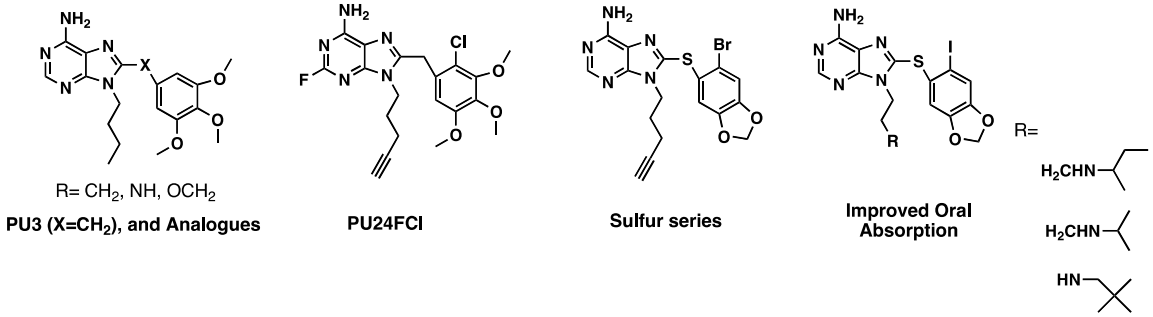

Figure 9: Purine Derivatives

PU3 was the first synthetic HSP90 inhibitor based on computer modeling studies with a K_D of 15-20 μM.[37] A library of PU3 analogues was subsequently produced with higher aqueous solubility with the most potent analogue possessing an IC_{50} of 300 nM.[38 39]

In addition to HSP inhibitors, there exist inhibitors of the transcription factor *hsf*-1. Among the most well-known of these is the naturally occurring flavonoid quercetin (3,3',4',5,7-pentahydroxyflavone) shown in Figure 10.

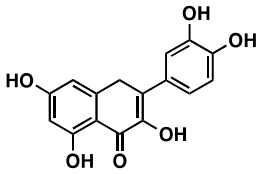

Figure 10: Quercetin

Quercetin works by affecting hsf-1 hyperphosphorylation, DNA binding, and transcriptional activity.

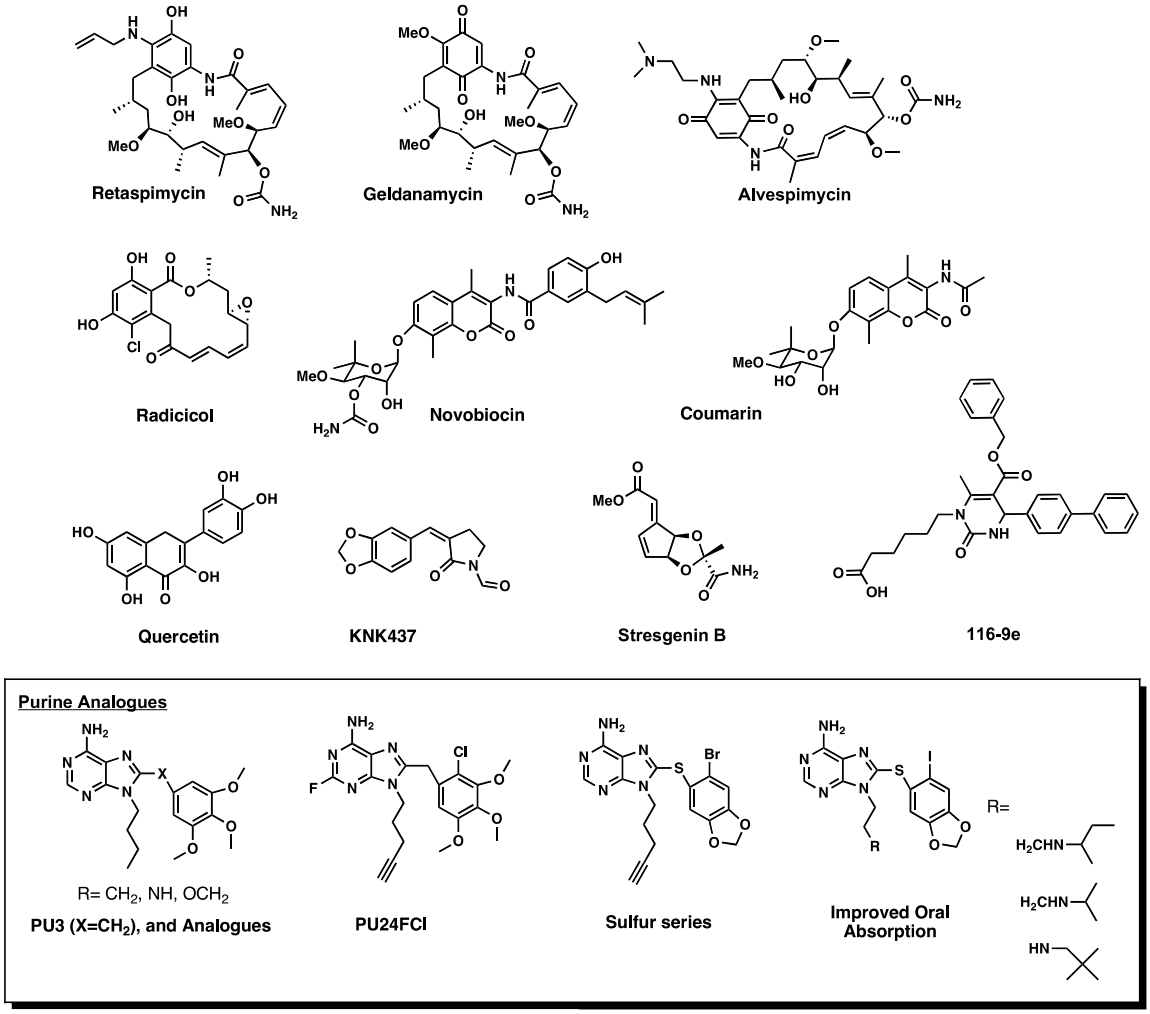

Figure 11: Current Heat Shock Protein Inhibitors

3.0 DISCOVERY AND BIOLOGICAL SIGNIFICANCE OF STRESGENIN B

Stresgenin B (Figure 12, Scheme 1a) was isolated (7.3 mg) in 1999 by the Akagawa group from a culture broth of *Streptomyces* sp. AS-9. It was shown to inhibit expression of heat shock protein genes *HSP*-72, 73, 90, and 110 with no effect on post-transcriptional processes.[40]

Identification of stresgenin B was achieved by three sequential screening assays. In the first screening assay, inhibitors of HS-Luc expression were added from the beginning of heat shock activation. Therefore, inhibitors of promoter activation, mRNA synthesis, and/or protein synthesis were detected. For example, actinomycin D (RNA synthesis inhibitor) and cycloheximide (protein synthesis inhibitor) inhibited HS-Luc expression.

In the second assay, inhibitors identified from assay one were added after the cells had been exposed to heat-shock. As such, inhibitors of downstream promoter activation would be found. cycloheximide showed the same activity in both screens, but actinomycin D showed less inhibition of assay two compared with assay one. By this manner, protein synthesis inhibitors were excluded from the second assay.

The third assay was used to determine those inhibitors with promoter specificity. As such, the inhibitors were compared to two assays, one for HS-Luc expression, the second for Dex-Luc expression. The Dex-Luc promoter is much more sensitive to promoter inhibition generally, therefore, an evaluation could be made between selectivity for the heat shock promoter (HS-Luc) and Dex-Luc.

The results showed that both promoters were equally sensitive to cycloheximide. Actinomycin D was less effective towards HS-Luc expression than Dex-Luc, and could thereby

be ruled out as a selective heat shock promoter inhibitor. As a positive control, quercetin, a known heat shock inhibitor, was tested and showed selectivity in inhibition of the HS-Luc over Dex-Luc promoter. Stresgenin B showed even more selectivity to the HS-Luc expression with better inhibition than quercetin. Therefore, stresgenin B was identified as a selective inhibitor of promoter activation. This assay did not exclude inhibition of events upstream of promoter activation, however, there were no effects on down-stream events.

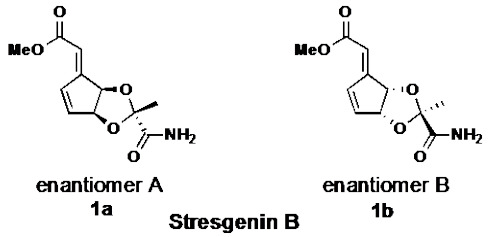

Figure 12: Stresgenin B

The AS-9 strain in this study was collected from a soil sample near Tokyo, Japan. A stock culture of this bacterium was inoculated into a flask containing 20 ml of a medium consisting of soybean meal, cornstarch, MS3600, and $MgSO_4 \cdot 7H_2O$ in tap water. The flask was incubated at 27 °C for 72 h on a reciprocal shaker (120 rpm), after which 0.75 ml portions were transferred to ten more identical flasks containing the same media. After incubation at 24 °C for 24 h on a reciprocal shaker, 1.5 g activated charcoal was added to each flask and incubating continued for 72 h. The entire collective contents were filtered through a pad of Celite 545, and the resulting carbon cake was extracted twice with 400 ml portions of acetone (50% aqueous). The extract was concentrated by rotary evaporation to 150 ml at 40 to 45 °C, and then extracted twice with 150 ml ethyl acetate.

The resulting organic layer was evaporated to dryness and the residue was taken up in 2.5 ml butyl acetate. 0.5 ml portions were subjected to silica column chromatography with butyl acetate as eluent. Active fractions collected from five columns were evaporated to dryness, and then taken up in 2.5 ml acetonitrile. Again, 0.5 ml fractions were subjected to silica gel column chromatography using acetonitrile as eluent. Active fractions showing absorbance at 275nm were collected and evaporated to dryness then taken up in 2.5 ml butanol saturated water. 0.5 ml portions were charged onto a Wakogel LP-60C18 column, and developed with saturated butanol water. UV active fractions were collected and evaporated to dryness, leaving 31.6 mg of crude powder. The crude powder was purified further using preparative HPLC using an Insertsil ODS-3 column and 15% acetonitrile in 0.03M ammonium acetate buffer (pH 6.0) as a mobile phase. Pure fractions active at 275 nm were collected and lyophilized to give 7.3 mg of pure stresgenin B as a white powder.

The molecular formula was determined by high resolution FAB-MS analysis. The UV spectrum in methanol shows a maximum at 275 nm, indicating the presence of a dienate moiety. The ^{1}H, and ^{13}C NMR HMQC spectra suggests one C-methyl, one O-methyl, two oxymethine carbons, and one quaternary carbon. The plane structure of stresgenin B was determined by the HMBC spectrum correlations shown below. Additionally, the relative stereochemistry was determined using NOESY ().

Table 1: Spectral Assignments (in CDCl3)

Carbon Number	*^{13}C Chemical Shifts (ppm)*	*^{1}H Chemical Shifts (ppm)*
C-1	164.5	
C-2	136.2	7.43 br
C-3	130.0	
C-4	124.4	6.43 ddd (*J* =9.7, 1.8, 1.8 Hz)
C-5	129.1	6.56 d (*J* =9.7 Hz)
C-6	80.9	4.42 m
C-7	79.2	4.46 m
C-1'	172.1	
C-2'	109.8	
C-3'	22.9	1.66 s
O-Me	52.2	3.79 s

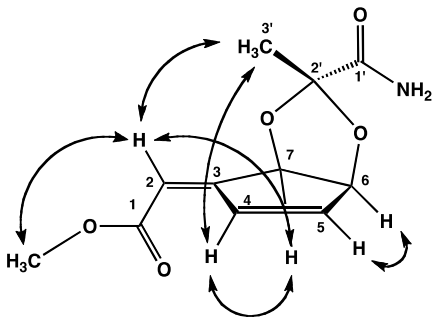

Figure 13: NOESY Correlation

Stresgenin B displayed an IC_{50} of 7.0 μM for HS-Luc expression (4.9 times lower than quercetin). The biological mechanism of inhibition by stresgenin B has yet to be identified and remains a goal of this research. This compound offers the hope of a powerful new tool in the regulation of the heat shock response. The densely functionalized and unique structure implies an interesting mode of action that has yet to be explored.

4.0 BACKGROUND AND PREVIOUS ROUTES

Cyclopentenones are a known building block used in natural product synthesis, especially in the case of prostaglandins and nucleoside/nucleotide chemistry.[41] The bicyclic 5,5-enone (4S, 5S)-(isopropylidenedioxy)-2-cyclopentenone (Figure 14) was employed as the key building block towards the synthesis of stresgenin B. In fact, so important is this intermediate, that it was incorporated into every retrosynthetic analysis within this study. As such, we examined known methodologies for the efficient syntheses of such building blocks. Early on, it was drawn to our attention that this enone could be constructed enantioselectively from common sugars, as the basic structure follows that of an unsaturated $C_nH_{2n}O_n$ framework. Our current, and most successful, route employs D-ribose (discussed shortly). This has been successful in making separation less problematic and in ensuring known chirality.

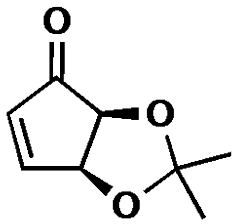

2

Figure 14: 5,5-enone (4S, 5S)-(isopropylidenedioxy)-2-cyclopentenone

4.1 CARL R. JOHNSON'S APPROACH

In 1986, Carl R. Johnson synthesized Enone 2 (Scheme 1) in 40% overall yield from cyclopentadiene in their route towards (-)-Prostaglandin E_2 (Figure 15).[42]

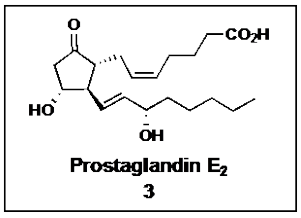

Figure 15: Prostaglandin E_2

They claimed to use this chemistry to suppress enolate formation from the acetonide side of the ketone through a combination of electrostatic charge repulsion and angle strain. As such, they were able to selectively alkylate the less hindered side of the compound.

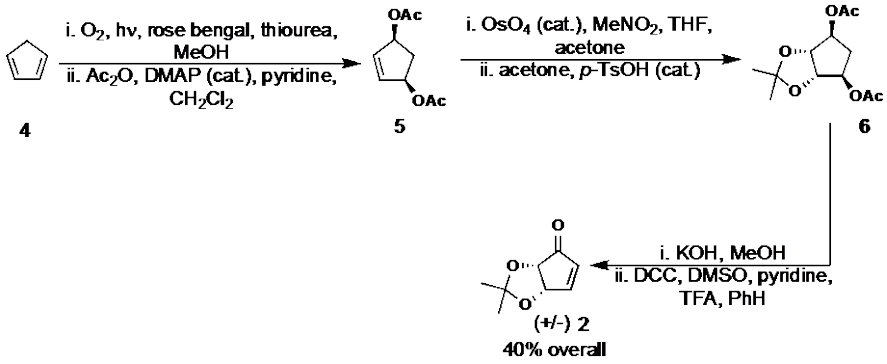

Scheme 1: Johnson's Approach to Enone 2

Although a very concise synthesis, the pathway ultimately leads to ent-**2**, which had to be resolved using N,S-dimethyl-S-phenylsulfoxamine.

4.2 FULVENES

Among the more precarious routes, the Alan Armstrong group took advantage of the use of fulvene chemistry to synthesize **9** on their way to **2** (Scheme 2).[43, 44]

Starting from fulvene **7**, Sharpless dihydroxylation provided diol **8** in 36%. Acetonide protection of the diol and another dihydroxylation from **9** yielded **10** and **11** as inseparable isomers in a 1:1 ratio. However, selective protection of **10** allowed **11** to be separated, followed by oxidation using sodium periodate, yielding enone **2** in 18 %.

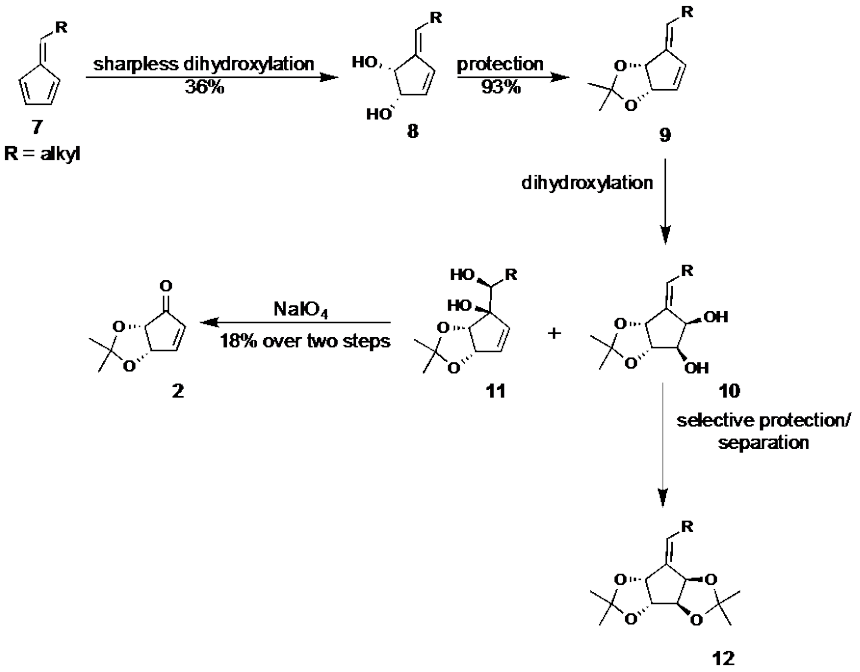

Scheme 2: Armstrong's Approach to 2 via Fulvene Chemistry

This synthesis, however, had issues that arose in the very first step. Especially interesting is the initial building block, a fulvene, which possesses antiaromatic, anti-Hückel character (Figure 16).

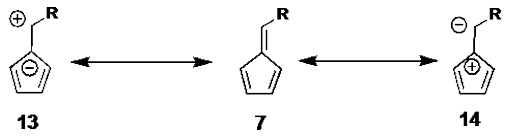

Figure 16: Aromatic and Antiaromatic Properties of 7

While the fulvene itself could be prepared from a simple condensation reaction using freshly distilled cyclopentadiene, and an aliphatic ketone or aldehyde in the presence of pyrrolidine, the real concern lay with the low yielding, non-regioselective dihydroxylation steps. In addition to forming two isomers with no desired selectivity in the second dihydroxylation, separation was not possible, thus leading to another chemical step to remove the undesired isomer.

Regardless of the difficulties in regioselectivity and separation, the methodology was indeed very enticing, as stresgenin B could potentially be formed in only three or four steps. As such, we used this protocol as precedence for the formation of an unstable intermediate with antiaromatic character. However, the reaction proved to be incompatible with **15**.

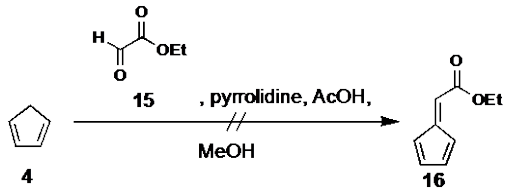

Scheme 3: Test Reaction Using Fulvene Chemistry

This result can be rationalized in that electron-withdrawing groups placed adjacent to the exocyclic olefin would greatly add to destabilization. Through resonance structure analysis of **17**, it is revealed that the electron withdrawing ester stabilizes the resulting negative charge on the α carbon. This in turn leads to high anti-aromatic character of the fulvene. As seen in the other resonance structure **19**, the induced aromaticity of the ring is stabilizing, but the positive charge is greatly destabilized positioned α to the electron withdrawing ester (Figure 17). With these results in hand, we concluded that this particular route would be ineffective in quickly synthesizing the core of stresgenin B.

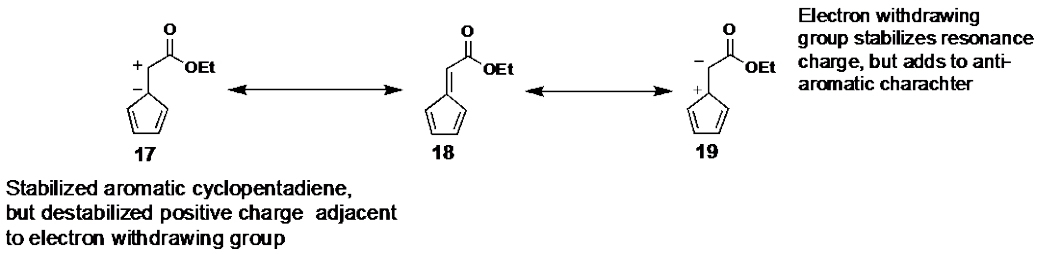

Figure 17: Resonance structure Analysis of 18

4.3 SECOND GENERATION SCHEME

We next turned our attention to a synthesis from the R. T. Borchardt group, in which enone **2** was synthesized in only three steps (enantiopure) with a 41% yield.[45] We envisaged our retrosynthetic analysis as shown in Scheme 4:

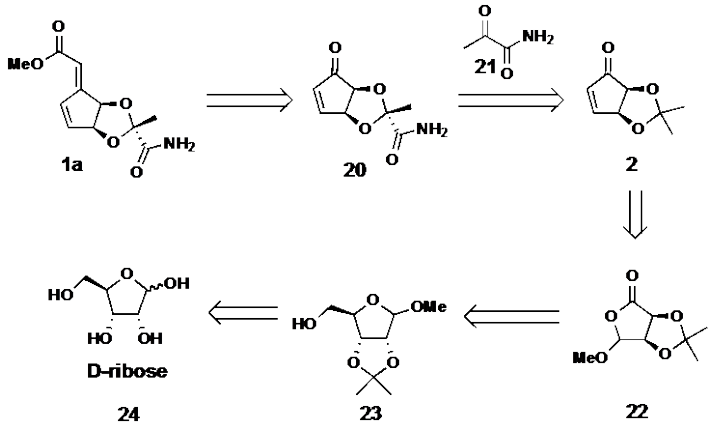

Scheme 4: Retrosynthetic analysis of Second Generation Scheme

Starting from D-ribose, acetonide protection of D-ribose under acidic conditions with 2,2-dimethoxypropane and methanol would yield **23**. The primary alcohol was oxidized to lactone **22** with concomitant loss of the methylene group using PCC. They discovered that the expected oxidation to the aldehyde could be suppressed by using 4.0 equivalents of PCC. From lactone **22**, the key intermediate would follow through a HWE reaction employing phosphonate ylide $(MeO)_2POCH_2Li$ (generated *in situ*). At this point we planned our chemistry for an interconversion of acetonide **2** to amide-bearing acetonide **20** via acidic deprotection/protection steps using reagent **21**. The natural product would finally be synthesized via a final stage Wittig or HWE reaction.

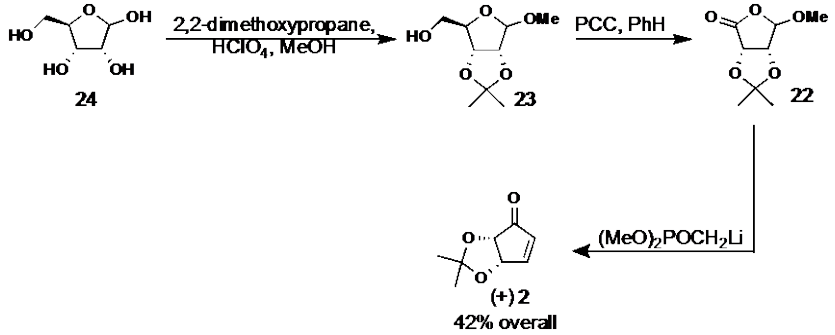

Scheme 5: Synthesis of Enone 2

Especially interesting in this scheme was the unexpected oxidation of **23** to **22**. The mechanism for this reaction remains unknown.

We began our synthesis with the protection and oxidation steps, proceeding smoothly and yielding the acetonide and lactone in 67 and 60% yields respectively. However, the third step of the synthesis was inconsistent, with maximum yields of only 20%. Additionally, reactions above a 100 mg scale resulted in complete decomposition of the substrate yielding an intractable (by HPLC) mixture. A possible rationale is discussed below:

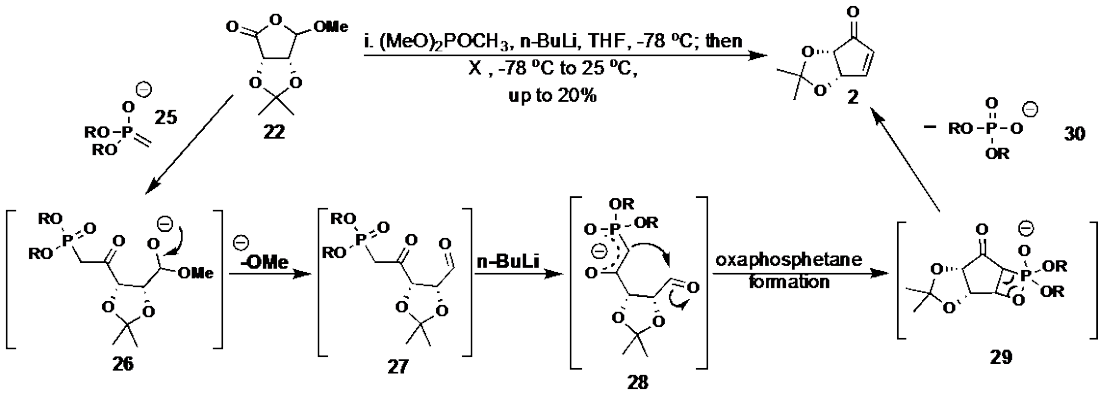

Scheme 6: A HWE Transformation Leads to 2 in low/inconsistent yields

Because the HWE reaction in this case must be allowed to warm to room temperature for conversion to take place, it is possible that other, less stable enolates, (on the acetonide carbon α to the ketone or aldehyde) may form. This would allow for undesired additions to take place, especially centered toward the aldehyde, leading to undesired additions to the substrate. Among these possible reactive intermediates are **31** and **32**

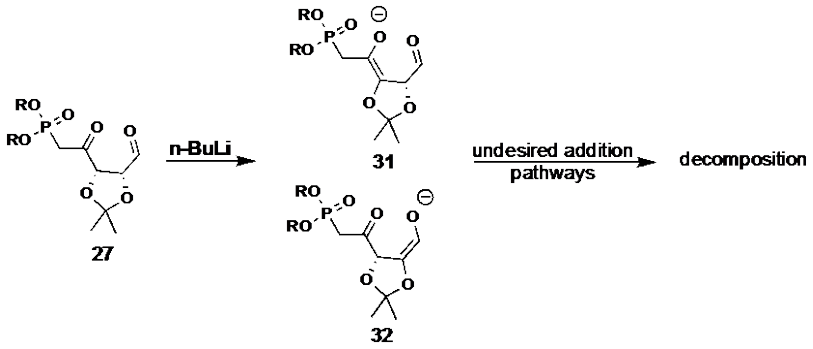

Scheme 7: Possible Pathway of Decomposition

4.4 GENERATION 3 SCHEME

Since formation of enone **2** had thus far proven to be problematic, giving unpredictably low yields, we modified the retrosynthetic analysis so that the enone moiety would be installed after acetonide formation. As such we envisaged the following retrosynthetic analysis would lead to a successful synthesis.

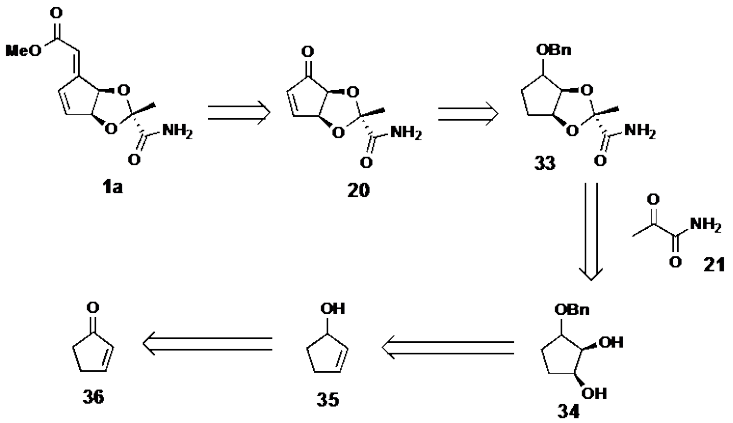

Scheme 8: Retrosynthetic analysis of Generation 3 Scheme

Starting from commercially available cyclopenteneone **36**, we first envisaged a Luche reduction, followed by benzyl protection and osmium mediated dihydroxylation to lead to the benzyl-protected diol **34**. We would next employ **21** in the 'protection step' to obtain the second key intermediate in our synthesis (the amide-bearing acetonide). Deprotection followed by IBX oxidation would yield enone **20**, by which a Wittig or HWE reaction would afford the natural product.

As a pitfall, we knew many diastereomers would be formed during the course of the reaction that would make characterization very difficult. This in fact turned out to be the case as most of the diastereomers were inseparable by HPLC. However, we planned that by the end of the synthesis, we would eventually eliminate these unnecessary stereogenic centers via oxidation.

2-cyclopenteneone was exposed to Luche conditions to yield alcohol **35** in quantitative yield.[46] Benzyl protection followed by Upjohn dihydroxylation provided the key diol **34** in 64 % yield over three steps as a mixture of isomers.[47]

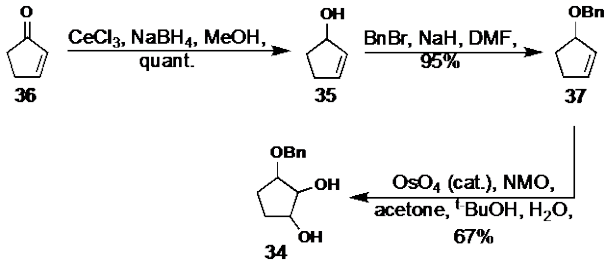

Scheme 9: Synthesis of diol 34

We were now ready for the key step in the reaction, the formation of the primary amide-bearing acetonide. We thus synthesized reagent **39** from commercially available lactamide with IBX in boiling EtOAc.[48] We additionally synthesized ketal **39** to use in further testing.

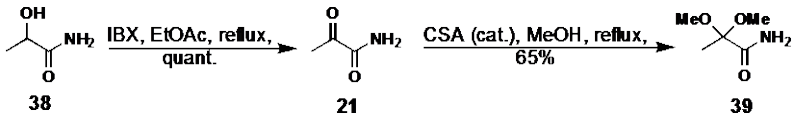

Scheme 10: Preparation of ketal 39

While **21** was unreactive under these harsh conditions, we were unable to affect a transformation using ketal **39** with catalytic CSA in xylenes at 160 °C. Purification of the product revealed not the desired amide, but ester **40** in 75% yield. When 3Å molecular sieves were added to adsorb methanol, the yield increased to 86%, however, no amide was isolated.

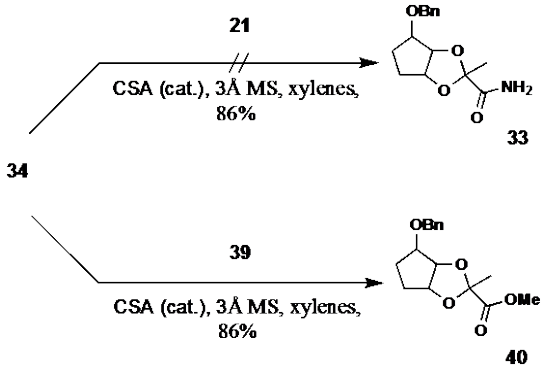

Scheme 11: Unexpected Ester Formation

We proceeded on with the synthesis, knowing another step would be necessary for the conversion to the amide. A significant amount of time was invested in separating these isomers (by column, followed by prep-TLC, finally HPLC). While we isolated two isomers from the mixture, complete separation was not possible.

We discovered the *in situ* conversion of the amide to the ester and attributed this finding to methanol's nucleophilicity, the strong organic catalyst, and high reaction temperature. It is

important to note that this feature of the synthesis carried on in many future attempts using different routes.

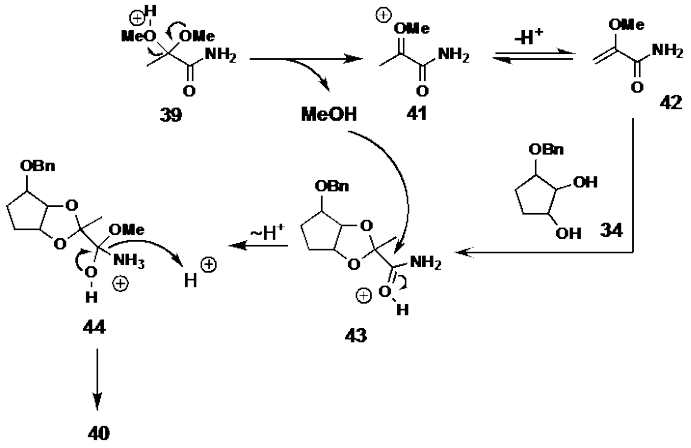

Scheme 12: Plausible Mechanism of Ester Formation

Continuing forward, benzyl deprotection was performed under hydrogenolysis conditions with $Pd(OH)_2$ under 1 atm H_2 in ethanol, yielding the corresponding alcohol **45** in quantitative yield. We envisaged the alcohol could be oxidized to yield the enone directly via IBX oxidation.[49] However, we were unable to affect the desired transformation, the reaction only leading to decomposition of substrate.

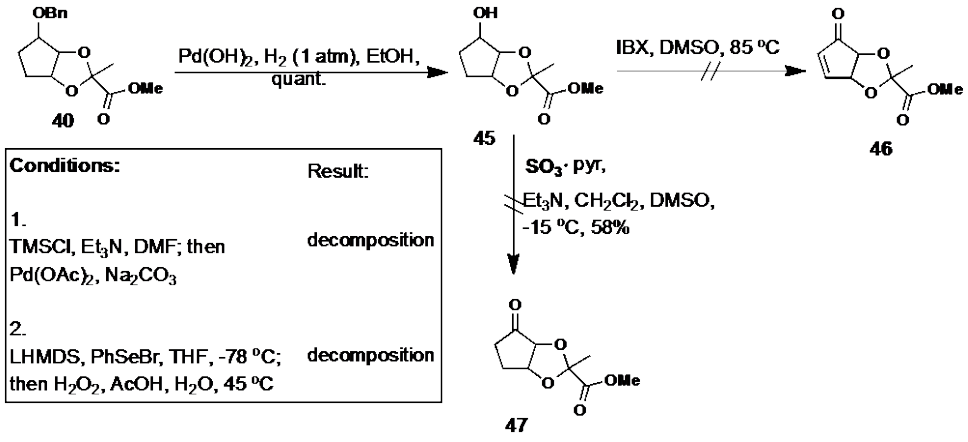

Scheme 13: Oxidation Attempts

Since the IBX oxidation proved unsuccessful, we planned for a two-step process in obtaining **46**. After scanning several oxidation conditions, we initially thought the Parikh-Doering oxidation was successful. [50] Analysis of the product IR showed two carbonyl absorptions at 1758 and 1642 cm^{-1}. However, 1H NMR revealed only trace amounts of product, which was inseparable (HPLC) from the starting material.

4.5. CONCLUSIONS FROM PREVIOUS ROUTES

Based on our previous findings, it became clear that a successful synthesis of this natural product would proceed through a route in which the requisite olefin and corresponding allylic alcohol were synthesized prior to acetonide formation. Additionally, characterization of products in these pathways had proven difficult and tedious, as even HPLC was, in most cases, ineffective in resolving all diastereomers within the given mixtures (up to eight at times). We felt that this was not acceptable for a natural product synthesis, as regio, stereo, and chemoselectivity along with expedition of synthesis (including ease of purification) are paramount factors creating success.

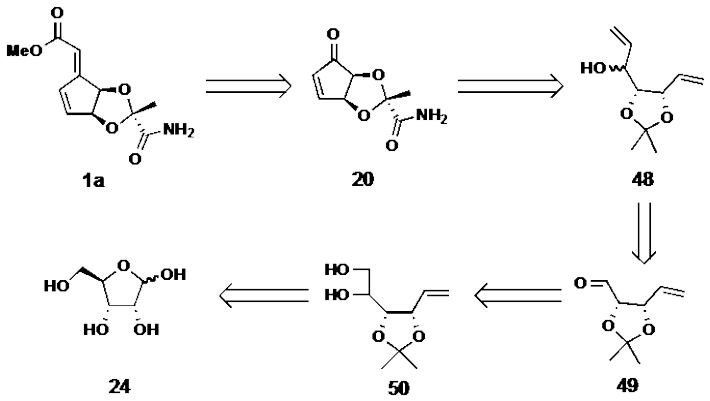

Scheme 14: Moon/Jin Inspired Retrosynthetic Analysis

5.0 BACKGROUND FOR CURRENT SYNTHETIC PLAN

Our attention was directed to common sugars, such as D-ribose, as an inexpensive starting point. Especially appealing is that, in using such a reagent, direct access to both enantiomers of stresgenin B could be accessed. This is especially useful in the determination of the absolute stereochemistry of the natural product.

Recent research from the Moon and Chu groups showed that enone **2** could be synthesized from D-ribose in moderate yield.[51, 52] As such, we anticipated a synthesis of stresgenin B from **2** via a Wittig or HWE reaction followed by acetonide deprotection/protection with amide **21**.

Creation of quaternary stereocenters is a challenging task in organic synthesis.[53] The single quaternary stereocenter in stresgenin B is an example of unique acetonide group bearing a primary amide. In searching SciFinder and Reaxys databases for related structures, we were unable to locate any other examples other than a single case N. K. Kochetkov reporting in the *Proceeding of the Academy of Sciences of the USSR*. We will discuss this particular case shortly.

Searching for related compounds led to the discovery of a few examples of acetonides with esters; however, all of them were related to the single example of the amide-acetonide previously mentioned (more details will follow).

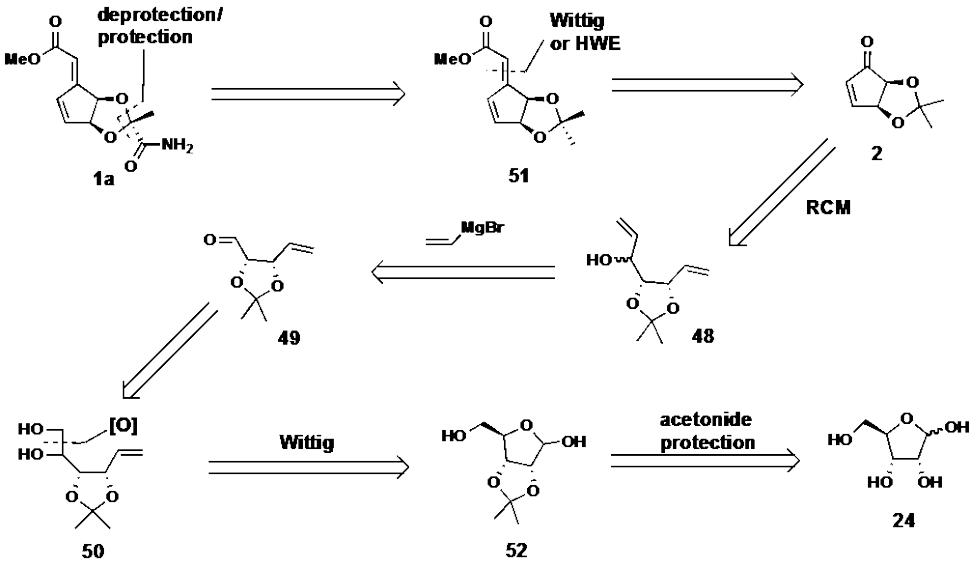

Scheme 15: Complete Retrosynthetic Analysis of Current Route

5.1 RETROSYNTHETIC ANALYSIS.

We envisaged that we could form stresgenin B in one step from compound **51** via an acetonide deprotection/protection step, ideally in one pot. We anticipated that a Wittig or HWE reaction would affect the transformation of ketone **2** to ester **51** with a low preference for the E isomer. A RCM reaction of compound **48** would be used to install enone **2**. Installation of the necessary terminal olefin using vinylmagnesium bromide and aldehyde **49** would yield **48**. As such, through a series of Wittig and oxidation steps, using D-ribose as an inexpensive chiral pool starting material, the desired aldehyde **49** could be formed. As such, we began the synthesis of enone **2** using the scheme developed in the Moon and Jin labs to take us to the heart of the synthesis, formation of the primary amide-bearing acetonide.

5.2 ACETONIDE FORMATION.

There are over 20 methods to install the isopropylidene ketal protecting group using a wide variety of reagents.[54] These most commonly utilize 2,2-dimethoxypropane or acetone as the reagent of choice, largely under acidic conditions.

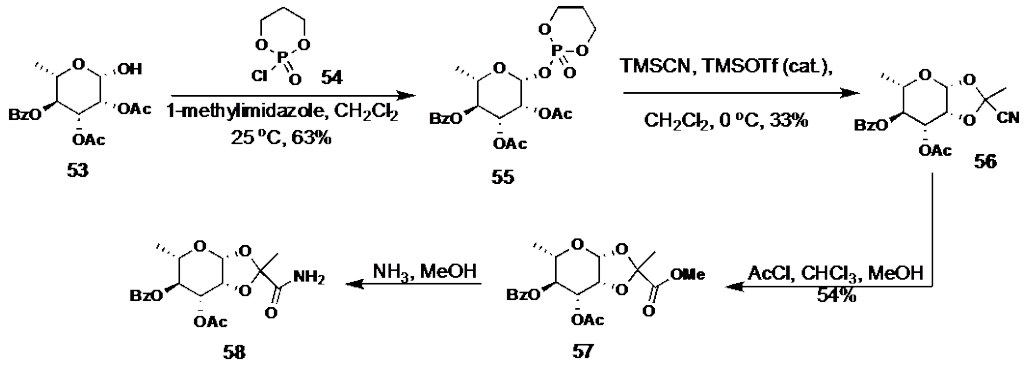

Scheme 16: Kochetkov's Synthesis of a Primary Amide-Bearing Acetonide

In Kochetkov's protocol for formation of primary bearing acetonide **58**, no details are provided into the synthesis of the cyano acetonide intermediate **56**. Regardless, starting from the **56**, he reported the conversion to the corresponding methyl ester **57** was achieved through in-situ generated HCl formation and addition of methanol in 54% yield. Ammonia in methanol converts the ester to the amide, which was used directly in another step in their route. It is possible that they utilized a route such as the one reported by Singh.[55] In this case, the transformation is initiated via hydroxy protection/activation of compound **53** to yield **55**, followed by intramolecular attack on the resulting oxocarbenium ion by the adjacent acetal. This intermediate, in turn, undergoes nucleophilic attack with cyanide to form the cyano acetonide.

5.3 LEAD ATTEMPTS

We began our synthesis with the initial goal of forming enone **2**.[51, 52] As such, starting from D-ribose in acetone, acetonide **52** was formed under acidic conditions at room temperature (Scheme 17).

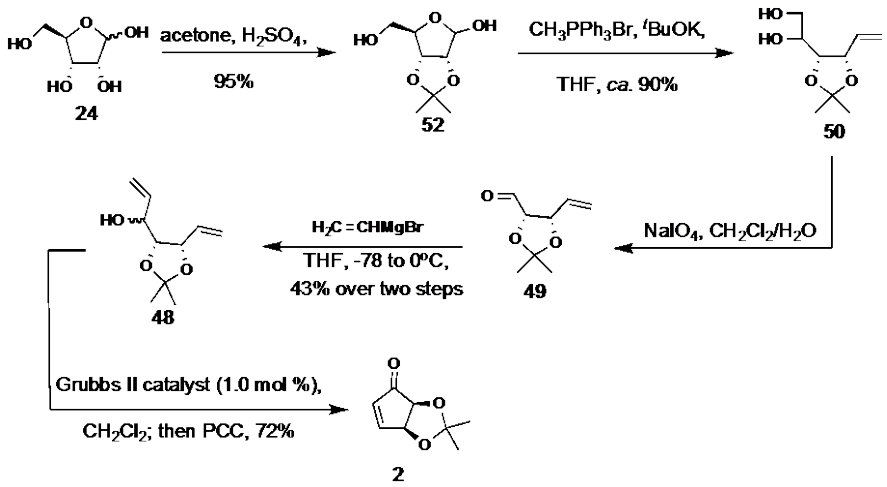

Scheme 17: Key Synthesis of Enone 2

A Wittig reaction was then used to form the terminal diol/olefin **50**. Oxidation with sodium periodate led us to aldehyde **49.** Aldehyde 49 was found to be very volatile and unstable. We therefore continued the synthesis with this material as a crude in CH_2Cl_2, exposing it directly to vinylmagnesium bromide to yield **48**.

The key enone **2** was formed in one pot via an RCM reaction using Grubbs II catalyst followed by PCC oxidation in 43% over two steps from **48**.

5.4 INSTALLATION OF THE METHYL ESTER

In examples of aldehyde substrates employing non-stabilized ylides, unfavorable 1,3 and 1,2 interactions are minimized in an early transition state leading to a puckered transition state that favors Z olefin formation. (Figure 18)[56] Correspondingly, there is a reduction of unfavorable 1,2 interaction amongst stabilized ylides (in a later, more oxaphosphatene-like transition state), leading predominately to the E geometry. Unfortunately, no rational models can be built when using ketones as substrates, due to more demanding steric effects on a substrate-to-substrate basis.

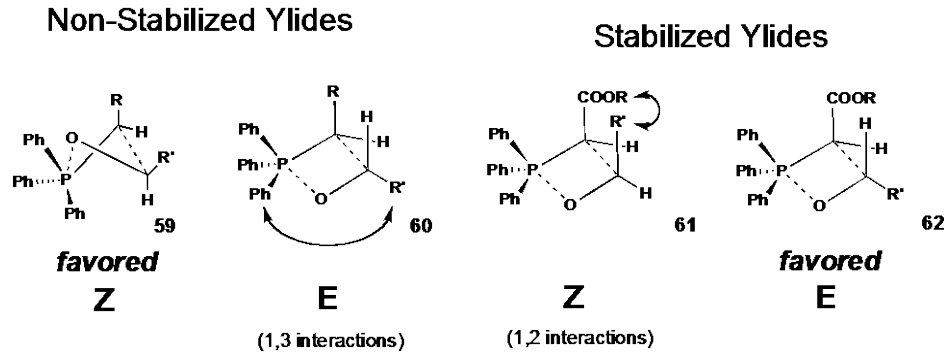

Figure 18: Steric Interactions in the Wittig Reaction (Vedejs Model)

As mentioned, the olefin geometry in these cases is substrate controlled. As such, compound **5**, when exposed to various Wittig conditions (Table 2), yielded **51** in good yield and poor selectivity (73%, 1:3 E/Z, NOE correlation).[5]

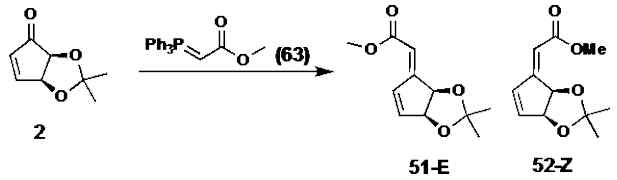

Table 2: Solvent Effects on the Wittig Reaction

Solvent	Temperature (˚C)	Time	(E:Z)
PhH	80	2 d	1:3
MeOH	80	1.5 h	intractable mixture
MeCN	50	16 h	1:4
THF	80	16 h	1:4
DMF	80	4 h	intractable mixture

It was hypothesized that dipole interactions could be the determining factor in driving the selectivity to the Z isomer (Figure 18).[56] We expected that by using solvents with higher dielectric constants than benzene, we could effectively disrupt these dipole interactions. However, the results in Table 2 suggests that dipole interactions were not the key in determining the selectivity, as the ratio of E:Z remained essentially unchanged and did not follow a rational trend. In an attempt to rationalize the results, the following transition states were postulated, suggesting that sterics may play the determining role in the outcome. According to research by Vedejs[57-60] selectivity in typical Wittig conditions employing aldehyde substrates can be rationalized via the transition states in Figure 18.

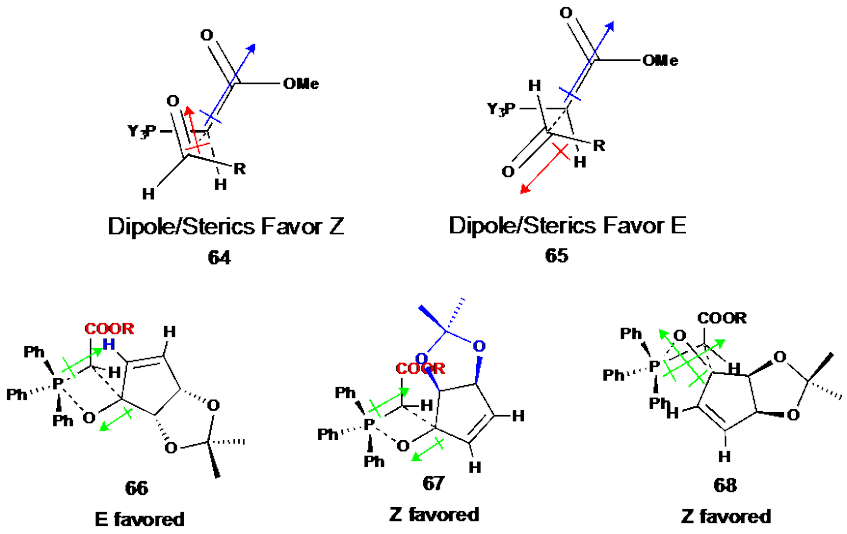

Figure 19: An Examination of Dipole and Steric Interactions in the Wittig Reaction

As such, transition states (Figure 19) were postulated to aid in the rationalization of the observed selectivity. In a puckered transition state (model **68**), large steric demands are avoided, thus favoring Z selectivity. Structure **66** and **67** possesses unfavorable 1,3 interactions, presumably leading to the shift in the selectivity from E to Z.

Despite the poor selectivity, both the E and Z isomer were readily separated via column chromatography. We stored these compounds for future SAR studies of the acetonide ring.

In order to improve selectivity, we began exploring Masamune's conditions which incorporate LiCl into a variation of the HWE reaction.[61] Lithium cation affects the pKa of the methelene protons adjacent to the phosphonate group by coordinating to the phospoester/ester moieties. The pKa value of these protons has been shown to be ~ 12.2 and thus should be easily deprotonated with mild bases such as DBU (pKa ~ 11.6) or $^{i}Pr_2NEt$ base (pKa ~ 10.5).

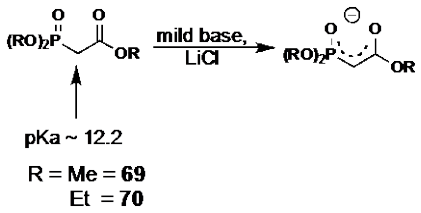

Scheme 18: Effects of Lithium of Acidity

The following reaction was carried out using phosphonate **69** and **70** and LiCl in stoichiometric amount (Scheme 18)

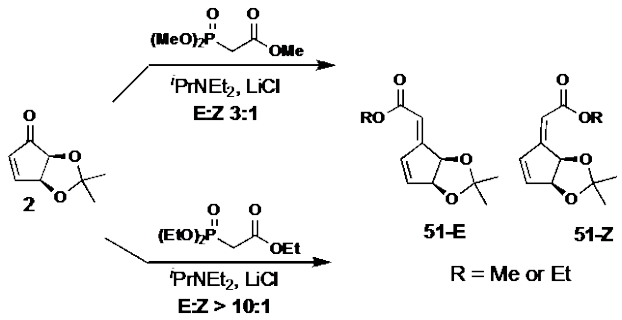

Scheme 19: HWE Conditions lead to Enhances E selectivity

We discovered that ester **51** was formed in a 3:1 E to Z ratio using reagent **69**. When reagent **70** was used the E:Z ratio increased to >10:1. These results may be in part rationalized by analyzing the transition states using Newman projections in Figure 20.

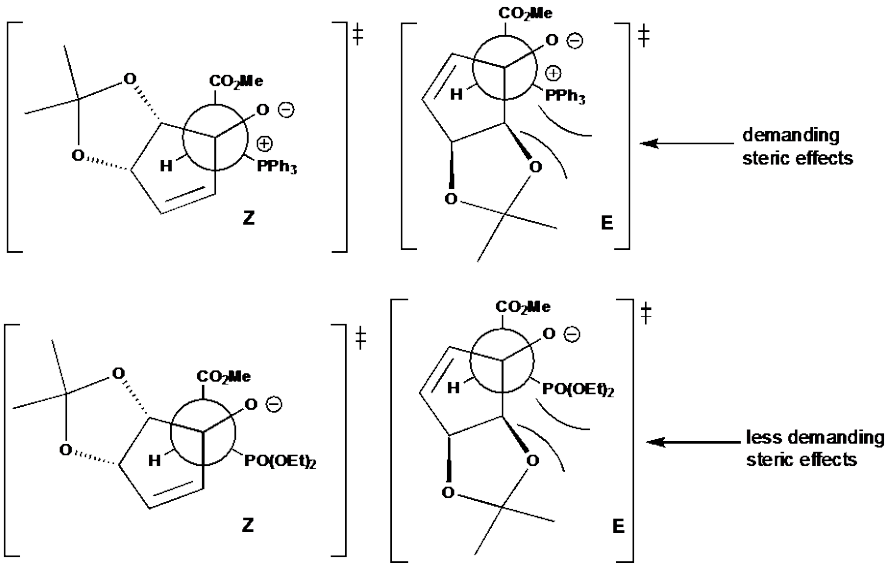

Figure 20: Sterics Influence Z:E selectivity

In the case of the observed E selectivity with the methyl phosphonate, the E transition state is less sterically encumbered by the smaller substituent on phosphorous. In addition, presuming the betaine formation is the next step (followed by oxaphosphatene formation), incorporation of Li leads to stereochemical drift between the *cis* and *trans* betaine intermediates (due to charge stabilization of the betaine by Li). This would allow for a greater percentage of the trans oxaphosphatene to be formed.

Regardless of the selectivity, we proposed that photoisomerization (254 nm) could be used to isomerize **51-Z** to **51-E** (with a small degree of E selectivity). When we conducted this test, however, it was found that there was no selectivity for either isomer (equilibration yielded a 1:1 ratio of E:Z). This implies only a minute difference in energy between the two structures.

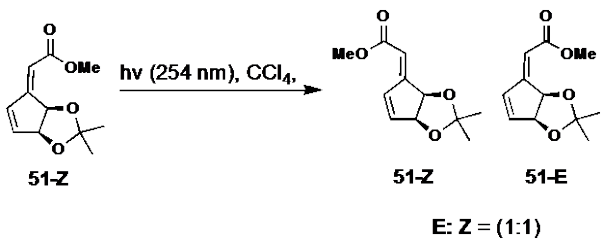

Scheme 20: Photoisomerization of 52-Z

This was surprising since it was implicit that relief of any steric strain from the acetonide and ester groups would shift the isomerization towards the E isomer. Computational studies have been carried out with aldehyde substrates using phosphonates activated by lithium, but none have been carried out with ketones. It is of great interest to incorporate further studies in the near future without Li and with lithium in a variety of mildly coordinating solvents (THF, diethyl ether, and acetonitrile) to fully understand the reaction dynamics. It is probable that, unlike the case of the previously studied Wittig reaction, dipole effects (further enhanced by coordinating Li) may play a role in the selectivity of the reaction. A computational study would lead to a better understanding of important reaction intermediates.

5.5 EARLY ATTEMPTS AT ACETONIDE FORMATION

With advanced intermediate **51-E** in hand, we began testing conditions for the acetonide deprotection/protection sequence. Cis-1,2-cyclopentanediol, **71**, was chosen for model studies. A variety of Lewis acids were tested and the results are listed in Table 3.

Table 3: Model Reactions to Scan Reagents for Acetonide Formation

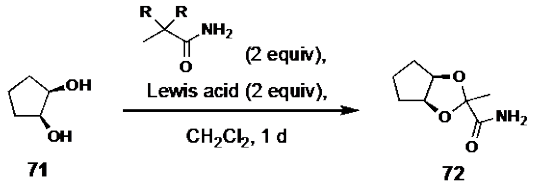

71 72

Temp °C	Lewis Acid	R	Results
25	$Hg(OAc)_2$	SEt	No reaction
80	$Sc(OTf)_3$	SEt	SM decomposed (rxn solvent = MeCN)
80	$Sc(OTf)_3$	OMe	No Reaction
25	$Cu(OTf)_2$	OMe	SM Decomposed
80	$Hg(OAc)_2$	OMe	No Reaction
25	$Zn(OTf)_2$	OMe	SM decomposed

Concurrently, we screened deprotection conditions of **51-E**, and found using Dowex WX-8 resin beads in wet methanol afforded the desired diol **73** in 82% yield. However, the substrate began to decompose within hours during solvent removal in the work-up stage (Scheme 21).

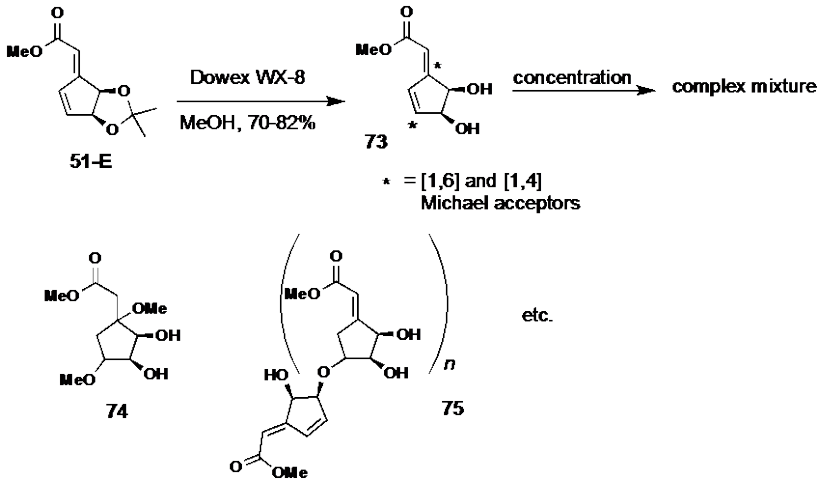

Scheme 21: Decomposition of 51

Crude ^{1}H NMR of the decomposed material showed multiple methoxy peaks leading us to believe that trace acid was catalyzing a combination of 1,4 and 1,6 conjugate additions, (as well as potential polymerization). In order to overcome this, the crude material was treated with base before solvent removal, followed immediately by protection. However, only starting material decomposition was observed.

As previously discussed, it was discovered that acetonide formation with methoxy-bearing ketal reagents did not lead to the amide-bearing acetonide, but to the corresponding ester. The amide itself in methanol did not form the ester. As such, transformation must have happened under the extremely high temperature employed (160 °C). Since this transformation was unavoidable under all conditions tested, we temporarily concluded that the formation of the amide bearing acetonide group would be the key step in the synthesis and may have to be installed in a last step reaction using ammonia.

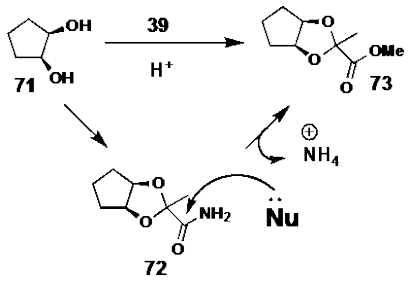

Scheme 22: Loss of Ammonia from Product

We believed that some of these issues might be overcome with the use of an appropriate Lewis acid based on the observation that conversion from the amide to ester was facilitated by protic acids (Scheme 22).

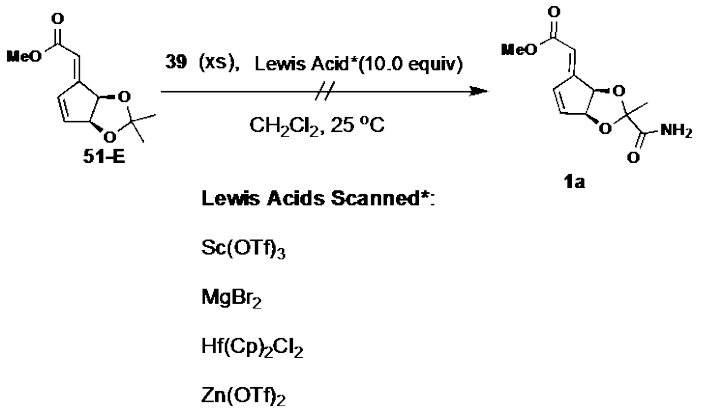

Scheme 23: Attempts at One-Pot Deprotection/Protection to 1a

However, the desired transformation did not proceed at room temperature or refluxing temperatures. In most cases, the starting material quickly decomposed in solution at room temperature, or began to decompose with the addition of heat. Activation of the ketal under acidic conditions, with concomitant generation of methanol, could lead to conjugate addition. In this scenario, multiple decomposition pathways can be envisioned leading to a variety of methyl-ether peaks, which was observed in the crude ^{1}H NMR. A few possible examples are listed below (Scheme 24).

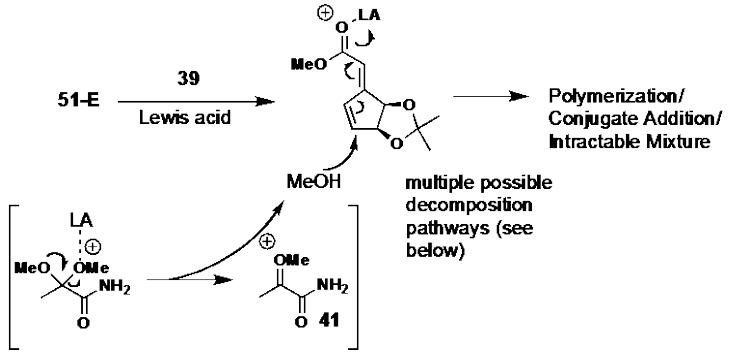

Scheme 24: Conjugate Addition to Multiple Michael Acceptors

We hypothesized that, due to the strain imposed by the acetonide ring, the more activated ketal would be needed to induce the transformation. As such, we tested a variety of reagents under various conditions (Scheme 5.10). However, no desired product was formed according to crude.

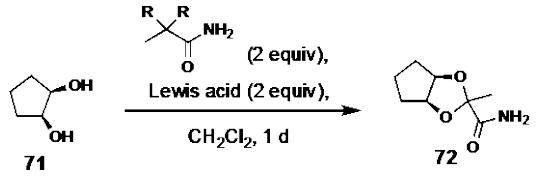

Temp °C	Lewis Acid	R	Results
25	$Hg(OAc)_2$	SEt	No reaction
80	$Sc(OTf)_3$	SEt	SM decomposed (rxn solvent = MeCN)
80	$Sc(OTf)_3$	OMe	No Reaction
25	$Cu(OTf)_2$	OMe	SM Decomposed
80	$Hg(OAc)_2$	OMe	No Reaction
25	$Zn(OTf)_2$	OMe	SM decomposed

Scheme 25: Model System/Scanning of Lewis Acids

We performed another control reaction to test if the substrate was prohibiting the transformation. However Scheme 5.11 demonstrated **71** is not problematic. This led us to consider that the reagents were not reactive.

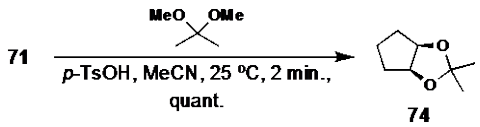

Scheme 26: Diagnostic Testing of Reagent Reactivity

Closer structural analysis reveals that those reagents bearing electron withdrawing groups adjacent to the site of nucleophilic addition are greatly destabilized via induction and resonance

(Scheme 26). Since the sigma cloud that forms a bond is never fully covalent, those atoms (groups) possessing higher electronegativity will pull electron density towards its nucleus. In effect, resonance structure a' is greatly destabilized being positioned adjacent to the amide. As such, we anticipated a reagent that minimized these effects would be significantly more reactive.

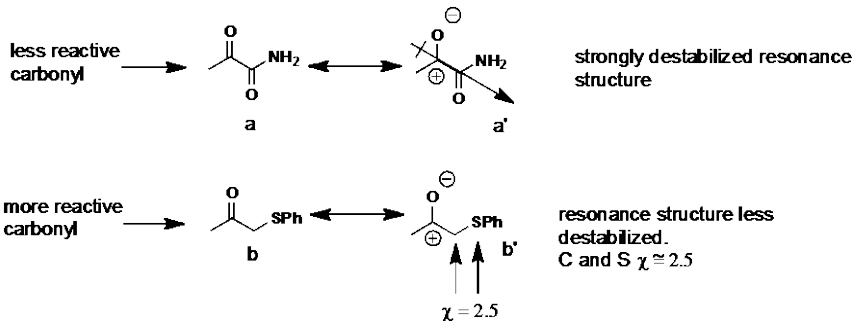

Scheme 27: Resonance and Induction Influence Reactivity of Carbonyl

As such, we searched the literature and located compound 82 (structure b, Scheme 27). Since sulfur and carbon have essentially equivalent electronegativities ($\chi \approx 2.5$), we postulated a more facile reaction under much milder conditions. In addition, sulfur is known to undergo facile oxidation. Our results are discussed shortly.

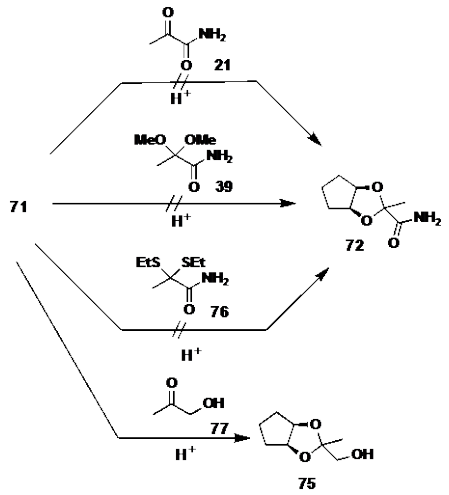

Scheme 28: Final Scan of Reagent Reactivity with Protic Acid

6.0. REVISION TO THE 4TH GENERATION ROUTE

6.1 REVISED RETROSYNTHETIC ANALYSIS

In response to the aforementioned problems, the amide bearing acetonide needed to be installed prior to enone formation. We thus developed the following modified retrosynthetic analysis.

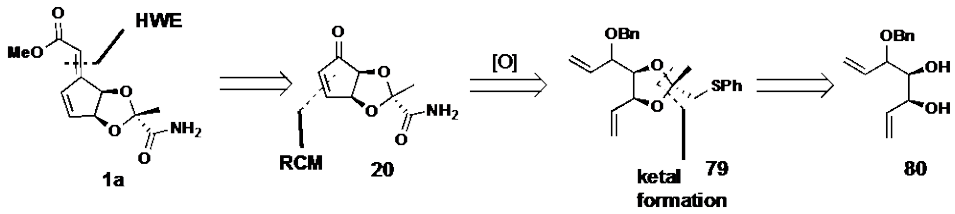

Scheme 29: Revised Retrosynthetic Analysis

Stresgenin B could be obtained directly via the aforementioned HWE transformation from **20**. First, through a series of functional group transformations (sequential oxidations), followed by a ring closing metathesis/oxidation, we could obtain **20** from **79**. We anticipated formation of **79** would be affected with use of a new reagent, **82**, under acidic conditions, from **80**.

As a first step, we prepared reagent **82** from 2-chloroacetone in the presence of K_2CO_3 and thiophenol in acetone.[62]

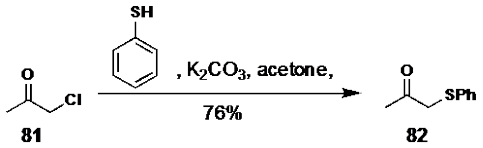

Scheme 30: Synthesis of 82

With this reagent, compound 79 was formed in 74% yield under acidic conditions from diol **80** as a 2:1 mixture of diastereomers. As validation to our hypothesis, this reaction proceeded at room temperature, and requiring less than 1 d, compared to a temperature of 160 °C needed to effect the similar transformation using previously discussed reagents.

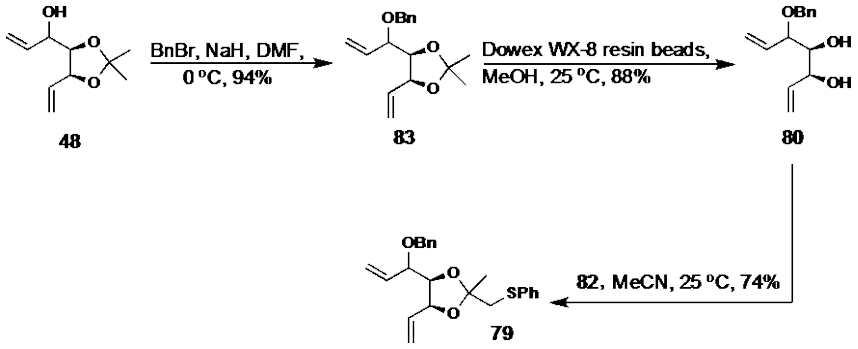

Scheme 31: Formation of Key Intermediate 79

From **79**, oxidation to sulfoxide **84** using *m*-CPBA, followed by a Pummerer rearrangement and hydrolysis, afforded aldehyde **85,** which was used as a crude mixture immediately in the next step (Scheme 32).[63]

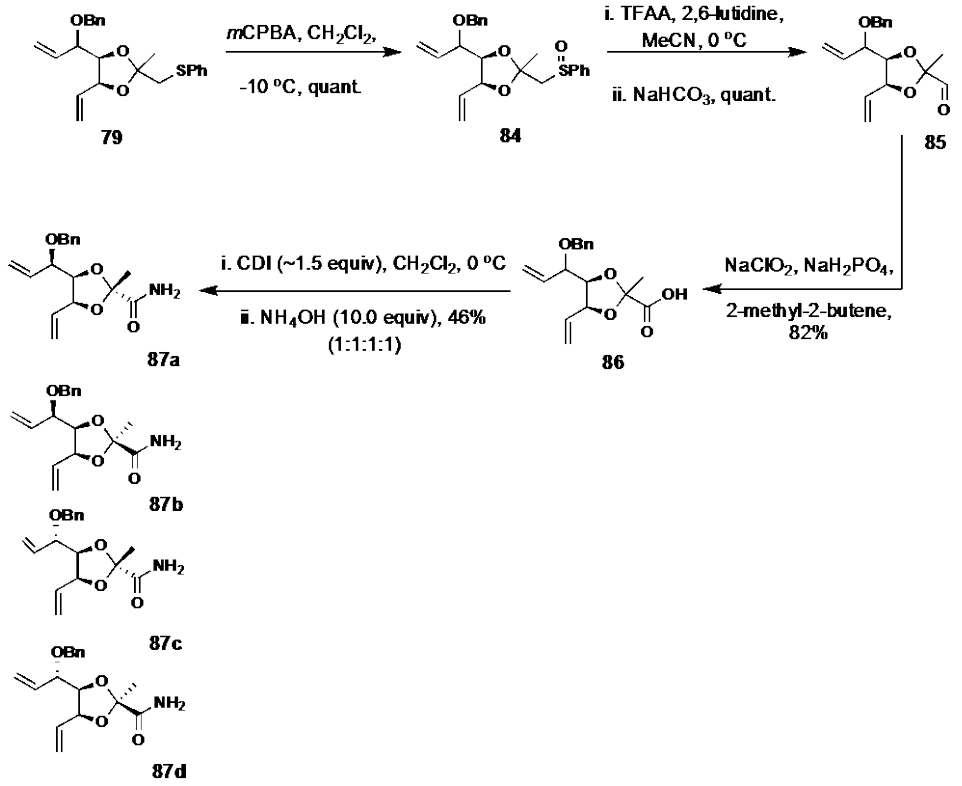

Scheme 32: Synthesis of the Amide-Bearing Acetonide

We continued forward with a mixture of diastereomers until they could be separated. Extensive purification of our intermediates was unnecessary, as the scheme was expedited with use of crude intermediates.

Compound **85** was then exposed to oxidation conditions with sodium chlorite yielding **86** as a crude oil, which was used directly in the next step without purification. With carboxylic acid **86** in hand, we were ready to complete the synthesis of the key acetonide. CDI coupling of **86** followed by addition ammonium hydroxide led to amides **87a-d** in 46% overall yield as a mixture of four column-separable isomers (Scheme 6.4). Isomer **87d** is currently being purified by HPLC because there is an inseparable (preparatory TLC/flash chromatography) impurity present.

6.2 DEPROTECTION

Several conditions were examined with compound **83** as a model for deprotection. Our initial results are listed in Table 4.

Table 4: Examination of Deprotection Routes using Model Compound 83

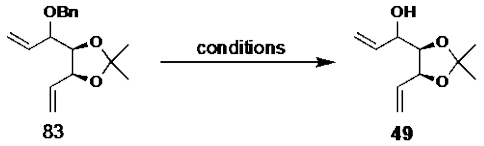

83 **49**

Conditions	Yield (%)
1. lithium di-tert-butyl biphenyl, THF, -78 °C	0
2. TMS-Cl, NaI, MeCN, reflux	0
3. i. TMSOTf, Ac_2O, CH_2Cl_2, -35 °C, then; ii. NaOH	0
4. DDQ, CH_2Cl_2/H_2O, 23 °C	27

Addition of lithium di-tert-butyl biphenyl at -78 °C led to decomposition of the starting material. We next used in-situ generated TMS-I; however, no reaction could be induced at a refluxing temperature.[64-66] Another attempt was made using TMSOTf to form an intermediate acetoxy moiety followed by hydrolysis.[67, 68] however, no desired product was formed.

However, DDQ[69] was effective in removing the benzyl group of our model compound in 27% yield. When we in turn applied these conditions to our amide-substrate **87a-d**, we observed no reaction. As a rationale, we proposed the following mechanism in which the primary amide aids in stabilizing the oxocarbenium intermediate of the reaction through reversible addition/elimination (Scheme 33).

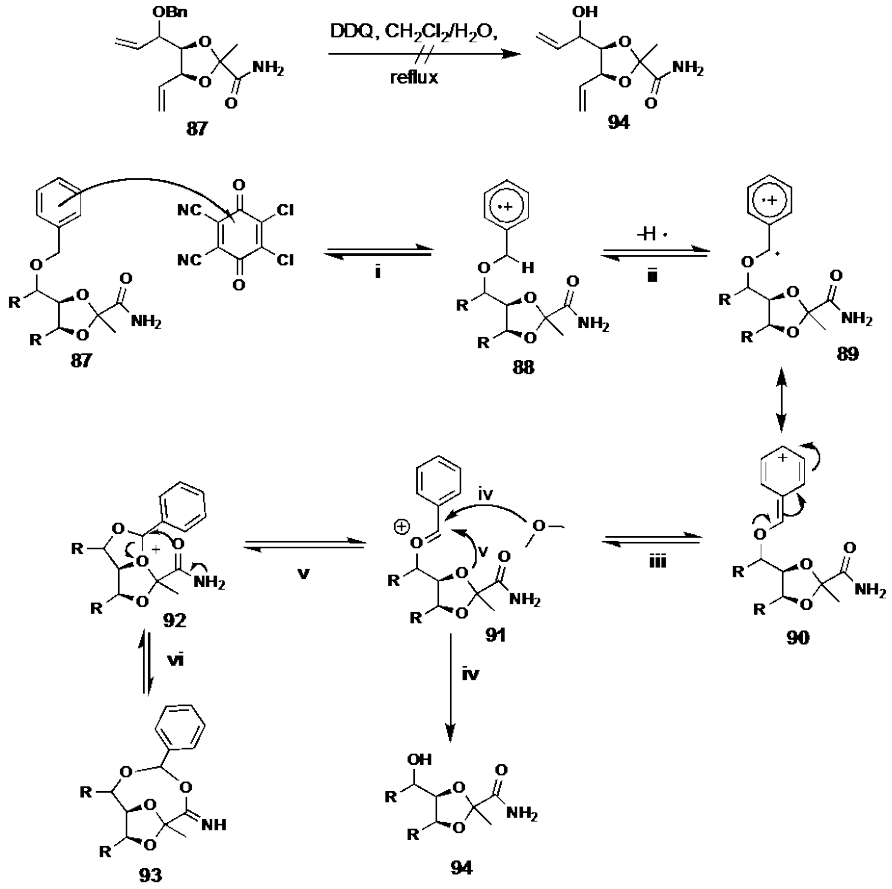

Scheme 33: Plausible Mechanism for low Observed Reactivity

The key to product formation, therefore, would be hydrolysis via water in step four. We anticipated that a higher temperature would allow us to overcome this effect. We changed solvents to nitromethane and water and heated to 110 °C. The desired product was thus isolated in 47% yield.

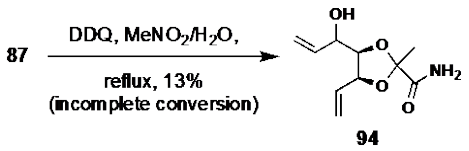

Scheme 34: Deprotection of Benzyl using DDQ

Since we were concerned with the possibility of the deprotected alcohol to undergo nucleophilic substitution/elimination with the amide group during deprotection, we are currently carrying out the RCM reaction before deprotection. The advantage of which would allow us to carry out the deprotection/oxidation in a single step perhaps with the use of catalytic DDQ and MnO_2.[70]

A Catalytic amount of Grela-Grubbs catalyst in toluene at 160 °C were found to afford the 5,5-bicyclic system **95** in 43% yield. NOESY assignments indicate the same stereochemistry at the quaternary center as the natural product. Furthermore, stereochemical assignments can now be made on previous intermediates

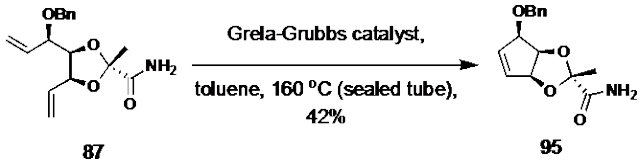

Scheme 35: Synthesis of Most Advanced Intermediate

7.0 SUMMARY AND FUTURE EXPERIMENTS

We have developed a methodology for the formation of an amide-bearing acetonide group. While this moiety had been reported only once in the literature, our method allows for access to a wider range of more exotically functionalized acetonides. To this extent, carboxylic acids, esters, and sulfoxides have already been demonstrated. In addition, we have demonstrated the synthesis can be streamlined by using crude intermediates, without need for purification, thus expediting the scheme.

The completion of this synthesis is anticipated to take a total of two more steps. A one-pot deprotection/oxidation followed by an E-selective HWE reaction.

8.0 EXPERIMENTAL SECTION

8.1 GENERAL TECHNIQUES

All reactions were carried out with dry, freshly distilled solvents under anhydrous conditions, unless otherwise noted. Tetrahydrofuran (THF) was distilled from sodium/benzophenone, and methylene chloride (CH_2Cl_2) was distilled from calcium hydride. Dimethyl formamide (DMF) was carefully purified by fractional distillation over calcium hydride using a vigruex column. Acetonitrile was dried by passing through a column of silica gel, and storing over 4Å molecular sieves.

Yields refer to chromatographically and spectroscopically (^{1}H NMR) homogeneous materials, unless otherwise stated. All reactions were monitored by thin layer chromatography (TLC) carried out on 0.25-mm EMD silica gel plates (60F-254) using UV-light (254 nm), 2.4% phosphomolybdic acid/1.4% phosphoric acid/5% sulfuric acid in water, anisaldehyde in ethanol, or 0.2% ninhydrin in ethanol and heat as developing agents. TSI silica gel (230–400 mesh) was used for flash chromatography. NMR spectra were recorded on AM300, AM400, AM500, or AM600 (Bruker) instruments and calibrated using a solvent peak as an internal reference.

The following abbreviations are used to indicate the multiplicities; s = singlet, d = doublet, t = triplet, q = quartet, m = multiplet, br = broad, app = apparent. High-resolution mass spectra were obtained using either a VG Autospec having EBE geometry and electron impact ionization (EI) or a Q-TOF API-US with electrospray ionization (ESI) in the positive ion modes.

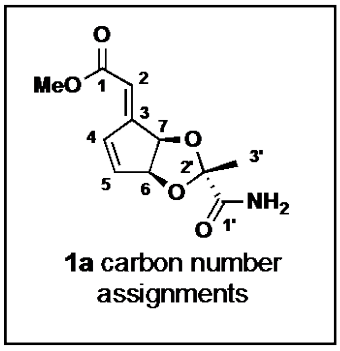

$^{1}H/^{13}C$ assignments for synthetic materials reflect the following assignments from the natural product

Figure 21: Carbon Number Assignments

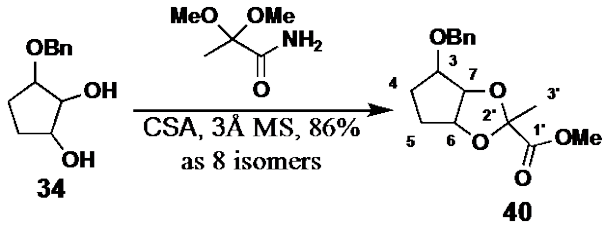

Scheme 36: Ester 40 Preparation

8.1.1 Preparation of Ester 40

To a 100-mL round bottom flask equipped with a Teflon coated stir bar was sequentially added diol **34** (2.3 g, 11.0 mmol) and xylenes (37 mL, 0.3 M) at 25 °C. To the mixture was added 3 Å MS (2.0 g) followed by ketal **39** (4.5 g, 3.0 equiv) at 25 °C. With stirring, CSA (1.03 g, 4.4 mmol) was added to the mixture in one portion at the same temperature. The reaction was equipped with a water-cooled condenser and subsequently heated to 160 °C for 1 d. The reaction was then cooled to 0 °C with a water/ice bath and quenched with the slow addition of Et_3N until the pH ~ 7.0. The entire mixture was placed on a column of silica gel (500 mL) and hexane (100

mL) was eluted through the column to remove xylenes. The column was further eluted (5% to 25% EtOAc in hexane) yielding the product as a clear oil composed of eight diastereomers (2.8g, 88%), four being resolved by ^{1}H NMR

8.1.2 Product Mixture 40a

R_f = 0.60-two diastereomers (50% EtOAc in hexanes); IR (thin film): 2945, 1759(C=O), 1454, 1370, 1141 cm^{-1}; *^{1}H NMR of isomer 1* (300 MHz, 293K, $CDCl_3$): δ 7.29-7.20 (m, 5H, H-Ar), 4.75 (dd, *J* = 5.7, 3.6 1H, 7-H), 4.50 (m, 5H, Bn-CH_2), 4.28 (q, *J* = 5.7, 1H, 6-H), 4.04 (dt, *J* = 9.3, 3.6 Hz, 1H, 3-H), 3.27 (s, 3H, -OMe), 2.16-1.96 (m, 2H, 5-H), 1.75-1.53 (m, 2H, 4-H), 1.51 (s, 3H, 3'-Me); 13C NMR (300 MHz, 293K, $CDCl_3$): *see attached spectra;* HRMS (ESI+) calcd for $C_{16}H_{21}O_5$ $[M+H]^+$ 293.1389, found 293.1397

^{1}H NMR of isomer 2 (300 MHz, 293K, $CDCl_3$): δ 7.29-7.20 (m, 5H, H-Ar), 4.96 (dt, *J* = 8.1, 3.6 Hz, 1H, 6-H), 4.50 (m, 2H, Bn-CH_2), 4.11 (app t, *J* = 4.2 Hz, 1H, 7-H), 3.93 (q, *J* = 5.4, 1H, 3-H), 3.26 (s, 3H, -OMe), 2.16-1.96 (m, 2H, 5-H), 1.75-1.53 (m, 2H, 4-H), 1.48 (s, 3H, 3'-Me); 13C NMR (300 MHz, 293K, $CDCl_3$): *see attached spectra*; HRMS: see above

8.1.3 Product mixture 40b

R_f = 0.47-two diastereomers (50% EtOAc in hexanes*); ^{1}H NMR of isomer 3* (300 MHz, 293K, $CDCl_3$): δ 7.35-7.15 (m, 5H, H-Ar), 4.75 (dd, *J* = 11.4, 5.7, 1H, 7-H), 4.58-4.41 (m, 2H, Bn-CH_2), 4.30 (dt, *J* = 7.5, 2.1, 1H, 6-H), 4.13 (dt, *J* = 7.5, 5.4 Hz, 1H, 3-H), 3.23 (s, 3H, -OMe), 2.19-1.89 (m, 2H, 5-H), 1.70-1.40 (m, 2H, 4-H), 1.52 (s, 3H, 3'-Me); 13C NMR (300 MHz, 293K, $CDCl_3$): *see attached spectra;* HRMS (ESI+) calcd for $C_{16}H_{21}O_5$ $[M+H]^+$ 293.1389, found 293.1399

^1H NMR of isomer 4 (300 MHz, 293K, $CDCl_3$): δ 7.35-7.15 (m, 5H, x-Ar), 4.58-4.41 (m, 2H, CH_2-Bn), 4.21 (dd, *J* = 5.1, 3.0 Hz 1H, 7-H), 4.03 (m, 1H, 6-H), 3.19 (s, 3H, -OMe), δ 2.19-1.89 (m, 2H, 5-H), δ 1.70-1.40 (m, 2H, 4-H), δ 1.51 (s, 3H, 3'-Me); 13C NMR (300 MHz, 293K, $CDCl_3$): *see attached spectra*; HRMS: see above

8.1.4 Compound 40

R_f = 0.38 (60% EtOAc in hexanes); *diastereomer b* (^{1}H NMR (300 MHz, 293K, 1% MeOD in $CDCl_3$): δ 4.60 (t, *J* = 5.1 Hz, 1H, 7-H), 4.38 (m, 2H, 6-H, 7-H), 3.34 (s, 3H, OMe), 2.25-2.102 (m, 2H, 5-H), 1.84-1.72 (m, 2H, 4-H); HRSM (ESI+) calcd for $C_9H_{14}O_5Na$ $[M+Na]^+$ 225.0739, found 225. 0726

R_f = 0.28 (60% EtOAc in hexanes); *diastereomer a* (^{1}H NMR (300 MHz, 293K, 1% MeOD in $CDCl_3$): δ 5.06 (dt, *J* = 9.0, 3.3 Hz, 1H, 6-H), 4.34 (dd, *J* = 11.4, 5.7 Hz, 1H, 3-H), 4.00 (t, *J* = 5.4 Hz, 1H, 7-H), 3.37 (s, 3H, -OMe), 2.34-1.90 (m, 4H, 4-H); HRSM (ESI+) calcd for $C_9H_{14}O_5Na$ $[M+Na]^+$ 225.0739, found 225. 0760

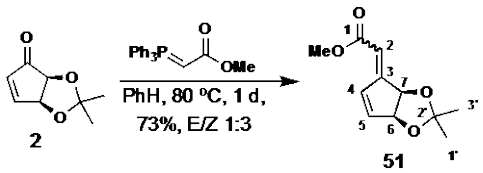

Scheme 37: Compound 51 Preparation

To a 100-mL, single-necked round bottom flask equipped with a Teflon coated stir bar was sequentially added enone **2** (1.7 g, 11.0 mmol) and benzene (55 mL, 0.2 M) at 25 °C. While stirring, the Wittig reagent was added in one portion (7.4 g, 22.1 mmol) at 25 °C. The mixture was connected to a water-cooled reflux condenser and heated to 80 °C for 1 d. After complete consumption of starting material by TLC analysis, the reaction was cooled to 25 °C and silica

gel (4 g) was added to the mixture. Solvents were removed *in vacuo* and the crude material was dry-packed on a silica gel column (125 mL). The material was purified by flash chromatography (100% hexanes to 30% EtOAc in hexanes). Diastereomers were easily separated yielding Z and E isomers as a clear, light yellow oil (1.7 g, 1:3 by mass E/Z). NOE experiment resolved the cis/trans isomers.

8.1.5 Compound 51 Z

R_f = 0.42 (30% EtOAc in hexanes); $[\alpha]_D$ = +115.1° (c 0.010, 23 °C, CH_2Cl_2); IR (CH_2Cl_2): 2289, 1716 (C=O), 1222, 1155, 1095 cm^{-1} ; (^1H NMR (300 MHz, 293K, $CDCl_3$): δ 7.38 (d, *J* = 5.7 Hz, 1H, 4-H), δ (apt dtd, *J* = 7.8, 3.6, 0.6 Hz, 1H, 5-H), 5.61 (app d, *J* = 0.9 Hz, 1H, 7-H), 5.16 (dd, *J* = 5.4, 2.1 Hz, 1H, 6-H), 5.10 (d, *J* = 5.4 Hz, 2H, x-H), 3.75 (s, 3H, -OMe), 1.42 (s, 3H, xH), 1.40 (s, 3H, xH), 8% NOE found between H-2 and H-4.; 13C NMR (300 MHz, 293K, $CDCl^3$): δ 166.3, 158.2, 143.6, 132.7, 113.7, 112.5, 81.6, 79.6, 51.1, 27.3, 26.1; HRSM (ESI+) calcd for $C_{11}H_{15}O_4$ $[M+H]^+$ 211.0975, found 211.0978;

8.1.6 Compound 51 E

R_f = 0.32 (30% EtOAc in hexanes); $[\alpha]_D$ = +150.0° (c 0.010, 22 °C, CH_2Cl_2); IR (CH_2Cl_2): 2289, 1719 (C=O), 1218, 1149, 1095 cm^{-1} ^1H NMR (300 MHz, 293K, CDCl3): δ 6.49 (app. dd *J* = 5.7, 1.8 Hz, 1H, 5-H), 6.34 (d, *J* = 5.4 Hz, 1H, 4-H), 5.96 (s, 1H, 2-H), 5.69 (d, *J* = 5.4 Hz, 1H, 6-H), 5.20 (dd, *J* = 5.4, 1.8 Hz, 1H, 7-H), 3.78 (s, 3H, -OMe), 1.46 (s, 3H, x-Me), 1.42 (s, 3H, x-Me); 13C NMR (400 MHz, 293K, $CDCl_3$): δ 166.6, 158.9, 143.6, 135.2, 115.1, 112.8, 83.6, 51.7, 29.3, 27.7, 26.4; HRSM (ESI+) calcd for $C_5H_{15}O_4$ $[M+H]^+$ 211.0970, found 211.0975

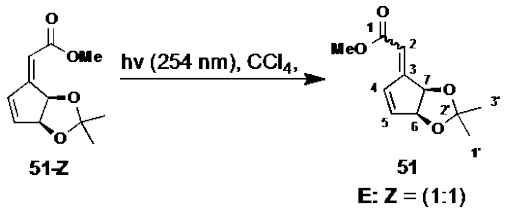

Scheme 38: Compound 51 E Preparation

8.1.7 Preparation of 51-E from 51-Z

To a 50-mL quartz reaction flask equipped with a Teflon-coated stir bar was sequentially added **51-Z** (1.4 g, 6.6 mmol) and CCl_4 (33 mL) at 25 °C. The quarts flask was placed in a TLC light box on top of a mechanical stirrer. A hand-held UV (254 nm) light was placed directly beside the reaction flask. While stirring, the UV light was applied and closing the TLC box eliminated excess stray light. After two minutes of stirring at 25 °C, TLC analysis showed equilibration between E and Z isomers. Solvents were removed *in vacuo* yielding a clear oil. Isomers were separated via flash chromatography (5% to 30% EtOAc in hexanes) on silica gel (100 mL). Removal of solvents by rotary evaporation yielded two separate isomers as a clear oil (1:1 E to Z by mass).

Spectra data matched that of 51-E and 52-Z previously synthesized.

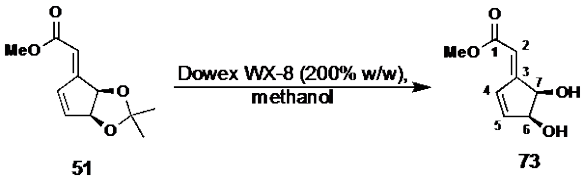

Scheme 39: Preparation of Diol 73

8.1.8 Preparation of diol 73

To a 25-mL round bottom flask equipped with a Teflon coated stir bar was sequentially added **51** (64 mg, 31 μM) followed by MeOH at 25 °C. The reaction was stirred vigorously as Dowex WX-8 resin beads (128 mg, 200% w/w) were added to the flask in one portion at the same temperature. The mixture was allowed to stir at 25 °C for 1 d at which point TLC analysis revealed complete consumption of starting material. The Dowex resin beads were filtered through a coarse frit. The crude material was then run through a small plug of solid $NaHCO_3$. before solvents were removed *in vacuo*. The crude material was used immediately in the next step as decomposition began during work-up.

8.1.9 Compound 73

R_f = 0.29 (50% EtOAc in hexanes; 1H NMR (300 MHz, 293K, CDCl3): δ 7.40 (d *J* = 6.0 Hz, 1H, 4-H), 6.49 (d, *J* = 6.0 Hz, 1H, 7-H), 5.89 (s, 1H, 2-H), 4.55(m, 2H, 4-H, 5-H), 3.73 (s, 3H, -OMe).

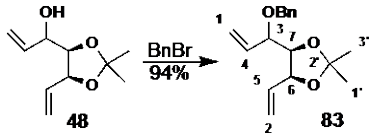

Scheme 40: Preparation of Benzyl Ether 83

8.1.10 Preparation of benzyl ether 83

To a 10-mL, single-necked round bottom flask equipped with a Teflon-coated stir bar was sequentially added **48** (4.12 g, 22.4 mmol) and DMF (75.0 mL, 0.3 M). The resulting solution was cooled to 0° C with an ice/water bath for 10 min. upon which was added NaH, (as a 60% dispersion in mineral oil; 896 mg, 37.3 mmol) in one portion. The mixture was stirred at this

temperature for 10 min then BnBr (3.2 ml, 29.1 mmol) was added via syringe over 10 min. The mixture was allowed to stir for 1 h at 0 ° and was subsequently poured over water (800 mL). The aqueous layer was extracted with ethyl acetate (3 x 160 mL). The combined organic layers were washed (2 x 100 mL brine). The combined organic layers were then dried over Na_2SO_4. Solvents were removed *in vacuo* and the crude material was purified by flash chromatography (100% hexanes to 5 % EtOAc in hexanes) on silica gel (500 mL) to afford 2 diastereomers **xx** as a light-yellow oil (4.9 g, 94%, dr = 1:1).

8.1.11 Compound 83

R_f = 0.56 (30% EtOAc in hexanes); IR (CH_2Cl_2): 2984, 1377, 1118, 1066 cm^{-1} ; ^1H NMR (400 MHz, 293K, $CDCl_3$): δ 7.39-7.24 (m, 5H, H-Ar), 5.98-5.76 (m, 2H, 4-H, 5-H), 5.35-5.18 (m, 4H, 1-H, 2H) 4.64 (d, *J* = 12.0 Hz, 1H, Bn-CH_2), 4.53 (app t, *J* = 6.4 Hz, 1H, 6-H), 4.46 (d, *J* = 12.0 Hz, 1H, Bn-CH_2), 4.19 (t, *J* = 6.0 Hz, 1H, 7-H), 3.82 (app t, *J* = 6.4, Hz, 1H, 3-H), 1.53 (s, 3H, -Me), 1.40 (s, 3H, -Me); 13C NMR (400 MHz, 293K, $CDCl_3$): δ 138.6, 135.8, 134.7, 128.5, 127.6, 127.4, 119.7, 118.9, 109.3, 80.9, 79.3, 79.2, 70.15, 27.7, 25.8; HRSM (ESI+) calcd for $C_{17}H_{22}O_3Na$ $[M+H]^+$ 297.1477, found 297.1467

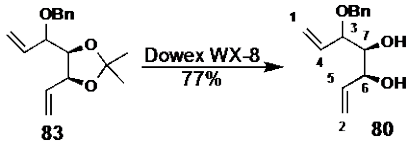

Scheme 41: Preparation of Diol 80

8.1.12 Preparation of diol (80)

To a 250-mL, single-necked round bottom flask equipped with a Teflon-coated stir bar was sequentially added **83** (1.24 g, 4.52 mmol) and methanol (90.0 mL, 0.1 M) at 25 °C. To the stirring solution was added Dowex W8-8 resin beads (2.48 g, 200 %w/w) in one portion at the same temperature. The resulting mixture was stirred for 36 h until no further conversion of starting material was observed on TLC. The reaction was filtered, and solvents removed *in vacuo*, yielding a crude yellow oil. The material was purified by flash chromatography (100% hexanes to 40% EtOAc in hexanes) using silica gel (70 mL). Rotary evaporation of solvents yielded a light-yellow oil (937 mg, 88% as two diastereomers). Diasteriomers were separated using preparatory-TLC (40% EtOAc in hexanes)

8.1.13 Compound 80

R_f = 0.18 (30% EtOAc in hexanes); IR (CH_2Cl_2): 3417 (O-H), 3076, 2873, 1064 cm^{-1}; ^1H NMR (400 MHz, 293K, $CDCl_3$): δ 7.38-7.31 (m, 5H, H-Ar), 5.97-5.85 (m, 2H, 4-H, 5-H), 5.43-5.21 (m, 4H, 1-H, 2-H), 4.62 (d, *J* = 11.2 Hz, 1H, Bn-CH_2), 4.32 (d, *J* = 11.2 Hz, 1H, Bn-CH_2), 4.19 (t, *J* = 5.6 Hz, 1H, 6-H), 3.95 (dd, *J* = 8.0, 4.8 Hz, 1H, 7-H), 3.60 (t, *J* = 4.8, 1H, 3-H); 13C NMR (400 MHz, 293K, $CDCl_3$): δ 137.7, 136.9, 134.8, 128.6, 128.2, 128.0, 120.0, 116.8, 80.9, 75.7, 73.9, 70.5; HRSM (ESI+) calcd for $C_{14}H_{18}O_3Na$ $[M+Na]^+$ 257.1154, found 257.1170

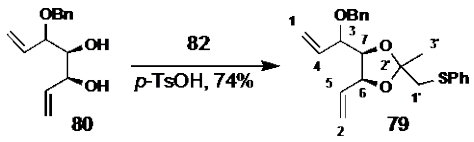

Scheme 42: Preparation of 79

8.1.14 Preparation of 79

To a 250 mL, single-necked round bottom flask equipped with a Teflon-coated stir bar was added diol xx (760 mg, 3.24 mmol), thioketone **82** (9.73 mmol), and acetonitrile (16 mL, 0.2 M). *p*-TsOH (123 mg, 20 mol%) was added to the reaction flask with vigorous stirring in one portion at 25 °C. The solution was allowed to stir for 24 h, during which time the reaction changed color from light yellow to green to brown. The reaction was cooled to 0 °C and quenched with saturated aqueous $NaHCO_3$ (10 ml). Acetonitrile was removed *in vacuo*, and the resulting biphasic layer was extracted with EtOAc (3 x 3 mL). Organic layers were combined, washed with brine (2 x 2 mL), and dried over Na_2SO_4. The semi-solid material was dry-packed and purified by flash chromatography using silica gel (170 mL) and 100% hexanes to 15 % EtOAc in hexanes as eluting solvents, yielding xx as a yellow oil (680 mg, 74 % yield, 4 diastereomers).

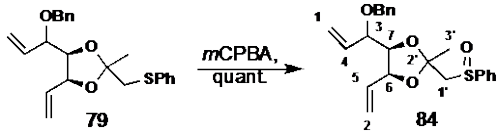

79 84

Scheme 43: Preparation of Sulfoxide 84

8.1.15 Preparation of sulfoxide 84

To a 50-mL, single-necked round bottom flask equipped with a Teflon-coated stir bar was sequentially added sulfide **79** (400 mg, 1.05 mmol) followed by CH_2Cl_2 (21 mL, 0.05 M). The solution was cooled to -10 °C using a NaCl/ice bath for 10 min, and *m*CPBA (~ 70% w/w; 362 mg, 2.10 mmol) was added in three portions over a period of 5 min. The solution was stirred at this temperature for 20 min and was subsequently quenched by addition of a saturated solution of $Na_2S_2O_3$ (20 mL) at 0 °C (ice/water bath). After the biphasic layer was stirred for 10 min at 25 °C, the organic layer was separated, and the aqueous layer was further extracted with CH_2Cl_2 (2

x 20 mL). The organic layers were dried over Na_2SO_4 and solvents removed *in vacuo* yielding **84** as a light yellow oil (The crude oil was used directly in the next step without further need of purification (422 mg). A sample of the crude material was purified by preparatory-TLC using 40% EtOAc in hexanes as developing solvent removing 6% w/w of impure materials. $^{1}H/^{13}C$ NMR attached

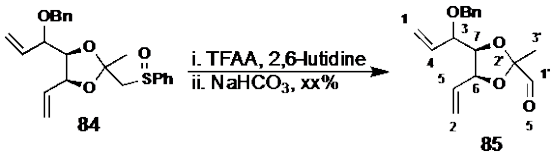

Scheme 44: Preparation of Aldehyde 85

8.1.16 Preparation of aldehyde 85

To a 100-mL, single-necked round bottom flask equipped with a Teflon-coated stir bar was sequentially added sulfoxide 84 (970 mg, 2.43 mmol), and acetonitrile (24 mL, 0.1 M) at 25 °C. The solution was cooled to 0 °C with an ice/water bath for 10 min and 2,6-lutidine (563 µL, 4.87 mmol) was added via syringe in one portion at the same temperature. TFAA (688 µL, 4.87 mmol) was added to the stirring solution at the same temperature via syringe over 15 min. After 10 min, TLC analysis showed complete consumption of starting material. Next, saturated $NaHCO_3$ (24 mL) was added. The reaction could be accelerated by the addition of solid $NaHCO_3$ (2.11 g, 2.04 mol) to ensure complete hydrolysis of the Pummerer intermediate. After complete consumption of the intermediate by TLC analysis, the excess solids were filtered using a fine filter-frit, and acetonitrile was removed *in vacuo*. The aqueous layer was extracted (EtOAc, 3 x 20 mL) and washed with brine (1 x 20 mL). The combined organic layers were dried over

Na_2SO_4. After removal of solvents by rotary evaporation, the resulting light yellow oil was subsequently used directly in the next step without further need of purification. $^1H/^{13}C$ attached

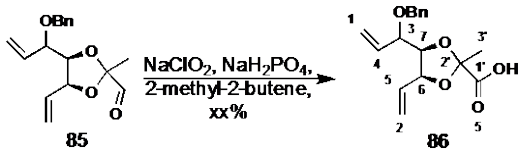

Scheme 45: Preparation of Carboxylic Acid 86

8.1.17 Preparation of carboxylic acid 86

To a 100-mL round bottom flask equipped with a Teflon-coated stir bar was sequentially added aldehyde **85** (700 mg, 2.34 mmol), 2-methyl-2-butene (2.57 mL, 20.43 mmol), and ^{t}BuOH (19 mL) at 25 °C. In a separate vial, a solution composed of $NaClO_2$ (264 mg, 2.92 mmol), and NaH_2PO_4 (2.68 g, 19.4 mmol) in H_2O (4.9 mL) was prepared. This solution was added via syringe over 10 min at 25 °C to the vigorously stirring solution of starting material and 2-methyl-2-butene. After 15 min, TLC analysis showed complete consumption of the starting material. Subsequently, Et_2O (20 mL) was added to the solution, and the solution was then brought to an acidic pH with the addition of 1M HCl (10 mL). The organic layer was separated, and the aqueous layer was further extracted with EtOAc (3 x 20 mL). The combined organic layers were washed successively with saturated aqueous $Na_2S_2O_3$ (2 x 20 mL), brine (1 x 20 mL), and then dried over Na_2SO_4. Solvent removal by rotary evaporation afforded a clear oil was used directly in the next step without need of further purification.

8.1.18 Compound xx diastereomer 86

R_f = 0.32 (1% AcOH and 4% MeOH in CH_2Cl_2); IR (thin film): 3417 (O-H), 3061, 1741 (C=O), 1476, 1578 1067 cm^{-1}; ^1H NMR (600 MHz, 293K, $CDCl_3$): δ 7.38-7.28 (m, 5H, x-Ar), 6.00-5.71

(m, 2H, x-H), 5.48-5.17 (m, 4H, x-H), 4.85 (t, *J* = 6.6 Hz, 1H, x-H), 4.79 (t, *J* = 6.6 Hz, 1H, x-H), 4.71 (app t, *J* = 6.6 Hz, 1H, x-H), 4.56 (d, *J* = 11.4 Hz, 1H, x-H), 4.39 (d, *J* = 11.4 Hz, 1H, x-H), 1.70 (s, 3H, x-H); HRSM (ESI+) *Sample submitted to HRMS facility.*

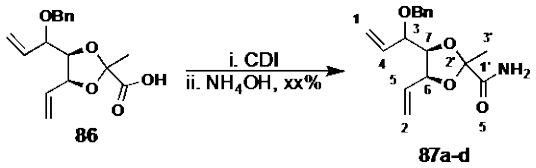

Scheme 46: Preparation of Diastereomer 86

8.1.19 Preparation of amide 87a-d

To a 25 mL, single-necked round bottom flask equipped with a Teflon-coated stir bar was sequentially added carboxylic acid **86** (740 mg, 2.43 mmol) and CH_2Cl_2 (12 mL, 0.2 M). The resulting solution was cooled to 0 °C with a ice/water bath for 10 min upon which was added CDI (591 mg, 3.65 mmol) in one portion. The reaction was stirred at this temperature for 20 min until TLC analysis revealed complete consumption of starting material. Next, ammonium hydroxide (14.8 M; 1.38 mL, 20.4 mmol) was added via syringe drop-wise over 5 min at 0 °C. TLC analysis immediately following addition revealed total conversion of the CDI-activated carboxylic acid intermediate, and the reaction was then poured over H_2O (20 mL). The organic layer was separated and the remaining aqueous phase was extracted with CH_2Cl_2 (3 x 10 mL). Combined organic layers were dried over Na_2SO_4 and solvents removed *in vacuo* yielding a crude oil. The crude was subjected to purification by flash chromatography (100% hexanes to 100 % EtOAc in hexanes) using silica gel (66 mL) to yield four separable isomers (517 mg, 46%, dr ~1:1:1:1).

8.1.20 Compound 47a

R_f = 0.42 (70% EtOAc in hexanes); IR (thin film): 3475, 3030, 1700 (C=O), 1200, 1068 cm^{-1}; ^1H NMR (400 MHz, 293K, $CDCl_3$): δ 7.39-7.28 (m, 5H, x-Ar), 5.99-5.83 (m, 2H, 4-H, 5-H), 5.45-5.26 (m, 4H, 1-H, 2-H), 4.80 (t, *J* = 5.2 Hz, 1H, 6-H), 4.53 (d, *J* = 11.2 Hz, 1H, Bn-CH_2), 4.22 (d, *J* = 11.2 Hz, 1H, x-H), 4.23 (app t, *J* ~ 6 Hz, 1H, 7-H), 3.86 (t, *J* = 8.0 Hz, 1H, 3-H), 1.54 (s, 3H, 3'-Me); 13C NMR (400 MHz, 293K, $CDCl_3$): δ 173.4, 137.7, 135.3, 132.4, 128.5, 128.1, 127.9, 120.5, 118.6, 106.0, 80.3, 80.1, 79.0, 70.2, 22.6; HRSM (ESI+) calcd for $C_{17}H_{21}NO_4Na$ $[M+Na]^+$ 326.1368, found 326.1347

8.1.21 Compound 47b

R_f = 0.30 (70% EtOAc in hexanes); IR (thin film): 3473, 3030, 1692 (C=O), 1211, 1068 cm^{-1}; ^1H NMR (400 MHz, 293K, $CDCl_3$): δ 7.40-7.25 (m, 5H, H-Ar), 5.94-5.81 (m, 2H, 4-H, 5-H), 5.45-5.24 (m, 4H, 1-H, 2-H), 4.69 (t, *J* = 6.0 Hz, 1H, 6-H), 4.53 (d, *J* = 11.2 Hz, 1H, Bn-CH_2), 4.24 (d, 11.2 Hz, 1H, Bn-CH_2), 4.12 (t , *J* = 6.8 Hz, 1H, 7-H), 3.81 (t, *J* = 7.6 Hz, 1H, 3-H), 1.63 (s, 3H, 3'-Me); 13C NMR (400 MHz, 293K, $CDCl_3$): δ 174.2, 137.8, 135.0, 132.5, 128.5, 128.1, 127.9, 120.2, 118.2, 105.8, 80.3, 79.6, 78.8, 70.2, 23.3; HRSM (ESI+) calcd for $C_{17}H_{22}NO_4$ $[M+H]^+$ 304.1560, found 304.1549

8.1.22 Compound 87c

R_f = 0.23 (70% EtOAc in hexanes); IR (thin film): 3324, 3029, 1687 (C=O), 1211, 1061 cm^{-1}; ^1H NMR (400 MHz, 293K, $CDCl_3$): δ 7.41-7.22 (m, 5H, H-Ar), 5.96-5.789 (app dddd, *J* = 36.8, 18.0, 10.4, 7.6, 2H, 4-H, 5-H), 5.40-5.25 (m, 4H, 1-H, 2-H), 4.63 (d, *J* = 12.0 Hz, 1H, Bn-CH_2), 4.54 (app t, *J* = 6.8 Hz, 1H, 6-H), 4.40 (d, 12.0 Hz, 1H, Bn-CH_2), 4.16 (t, *J* = 5.6 Hz, 1H, 7-H), 3.85 (dd, *J* = 7.6, 5.6 Hz, 1H, 3-H), 1.67 (s, 3H, 3'-Me); 13C NMR (400 MHz, 293K, $CDCl_3$): δ

174.5, 138.2, 134.2, 132.9, 128.4, 127.7, 127.6, 120.3, 120.1, 106.2, 81.7, 80.0, 78.8, 70.2, 23.2; HRSM (ESI+) calcd for $C_{17}H_{22}NO_4$ $[M+H]^+$ 304.1549, found 304.1568

8.1.23 Compound 87d

Rf = 0.07 (70% EtOAc in hexanes): Currently purifying by HPLC.

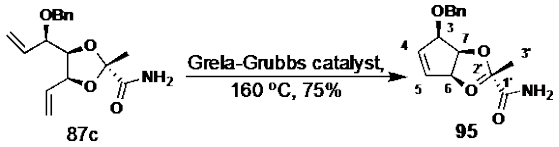

Scheme 47: Preparation of Amide 95

8.1.24 Preparation of bi-cyclic amide 95

To a 10-mL sealed tube equipped with a Teflon-coated stir bar was sequentially added a single diastereomer of amide **87c** (R_f = 0.23 from previous reaction, 66 mg, 217 μmol) and toluene (11.0 mL, 0.02 M). Afterwards, Grela-Grubbs catalyst (73 mg, 109 μmol) was added in one portion and the resulting mixture was heated to 160 °C for 1 h. Upon complete consumption of the starting material by TLC analysis, the reaction solution was cooled to 25 °C and filtered through a plug of silica (~20 mL) using hexanes (20 mL) to remove xylenes. The product was then removed from the column using EtOAc as eluting solvent. After removal of solvents by rotary evaporation, the resulting dark brown material was purified by silica gel (10 mL) flash chromatography (100% hexanes to 100% EtOAc). Rotary evaporation of solvents yielded an impure material that was further purified using preparatory-TLC (70% EtOAc in hexanes). The silica gel containing the UV-active spot was separated and placed in a fine frit. The product was removed from the silica with EtOAc (100 mL) washing . To remove colored Ru by-products 3.0 g activated carbon was added to this EtOAc solution and the mixture was stirred for 12 h at 25

°C. Filtering activated carbon using a fine frit, followed by removal of solvents *in vacuo* yielded a bright white amorphous solid (25 mg, 42%)

8.1.25 Compound 95

R_f = 0.29 (80% EtOAc in hexanes); mp 109.5-110.2°; $[\alpha]_D$ = +62.8° (c 0.010, 22 °C, CH_2Cl_2); IR (thin film): 3406, 1665(C=O), 1399, 1027 cm^{-1}; ^1H NMR (600 MHz, 293K, $CDCl_3$): δ 7.37-7.28 (m, 5H, H-Ar), 6.04 (app d, *J* = 5.4, 1H, 5-H), 5.97 (app dd, *J* = 6.0, 5.4 Hz, 1H, 4-H), 5.30 (d, *J* = 6.0 Hz, 1H, 6-H), 4.69 (d, *J* = 11.4 Hz, 1H, Bn-CH_2), 4.61 (app t, *J* = 6.0 Hz, 2H, 7-H, 3-H), 4.58 (d, *J* = 11.4 Hz, 1H, Bn-CH_2), 1.56 (s, 3H, 3'-Me); 13C NMR (600 MHz, 293K, $CDCl_3$): δ 173.8, 137.8, 134.6, 134.2, 128.7, 128.1, 108.5, 87.6, 85.3, 84.1, 72.1, 29.9, 23.4; HRSM (ESI+) calcd for $C_{15}H_{17}NO_4Na$ $[M+Na]^+$ 298.1055, found 298.1048

9.0 NMR SPECTRUMS

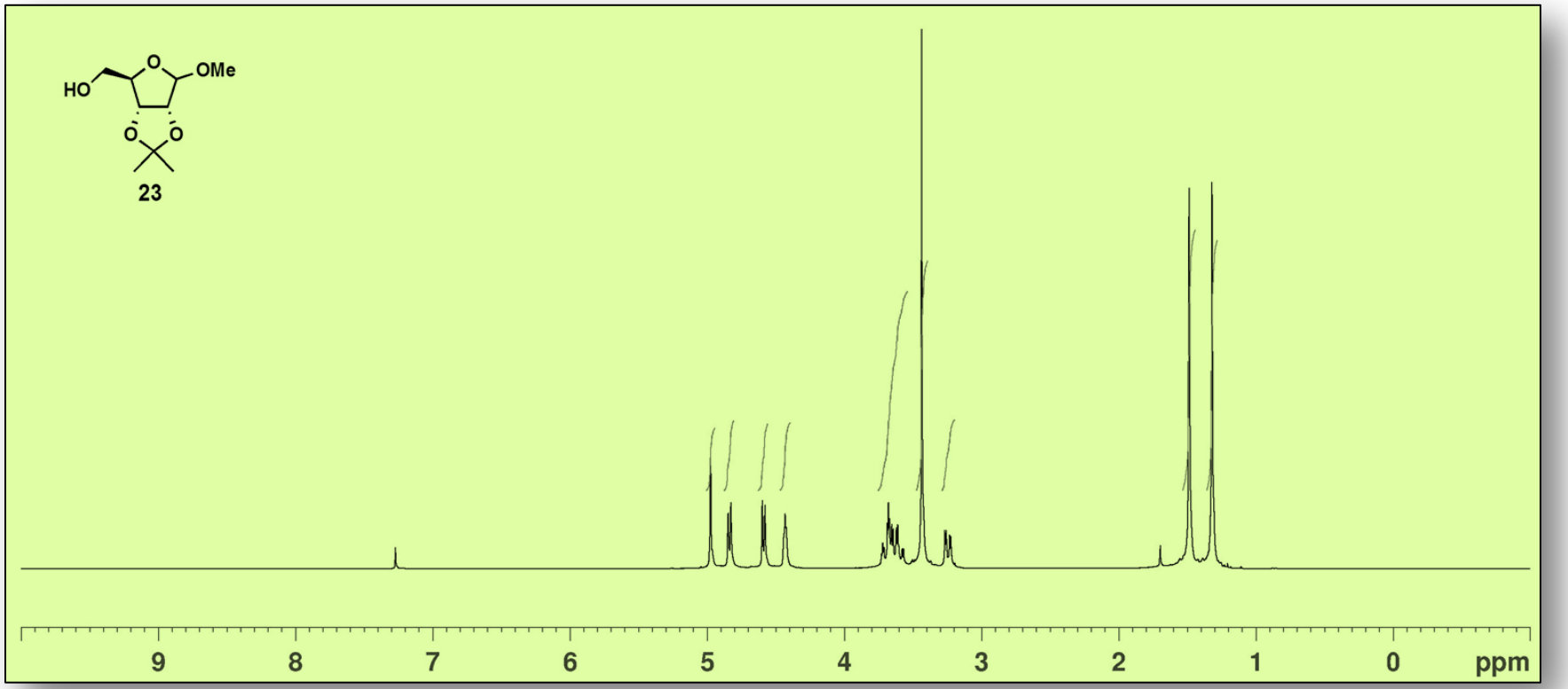

Figure 22: ^{1}H NMR spectrum of compound **23** (300 MHz, $CDCl_3$, 293K)

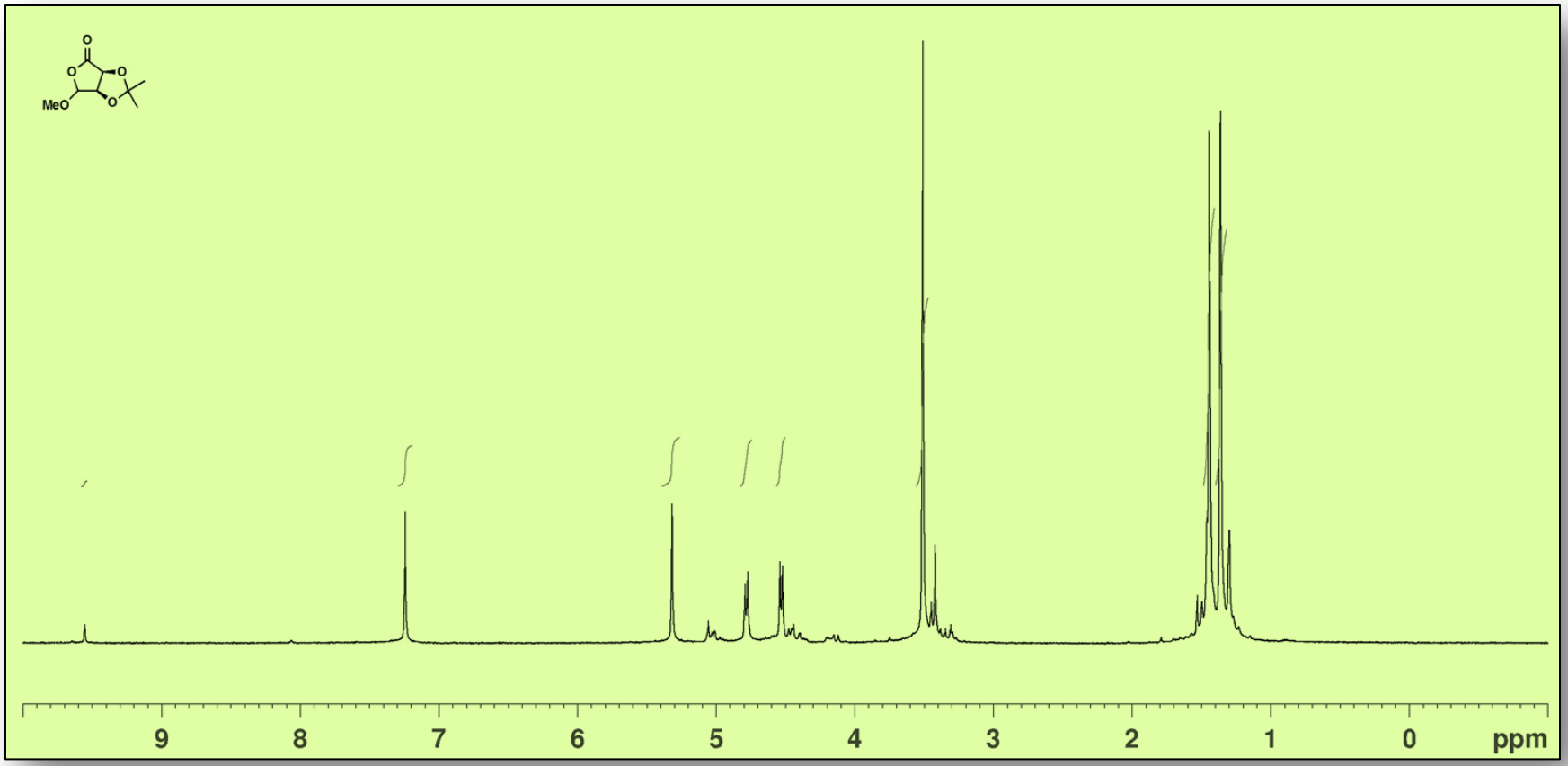

Figure 23: ^{1}H NMR spectrum of compound 22 (300 MHz, $CDCl_3$, 293K)

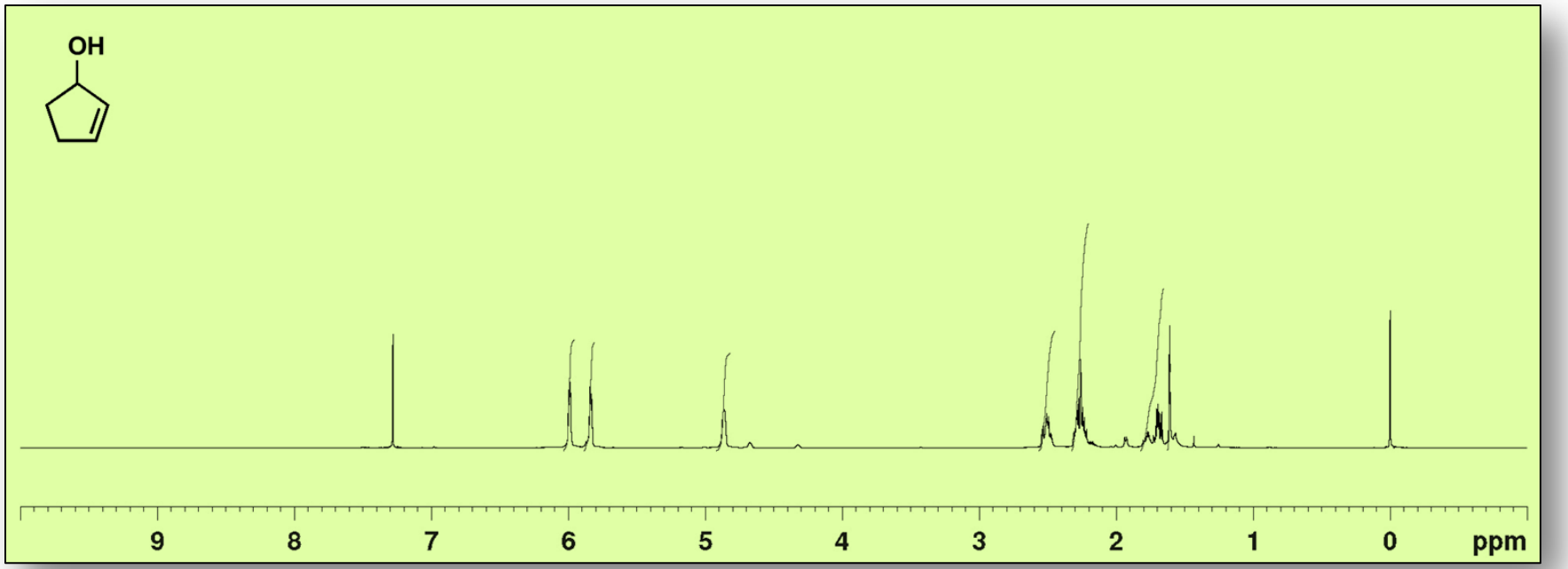

Figure 24: ^{1}H NMR spectrum of compound 35 (300 MHz, $CDCl_3$, 293K)

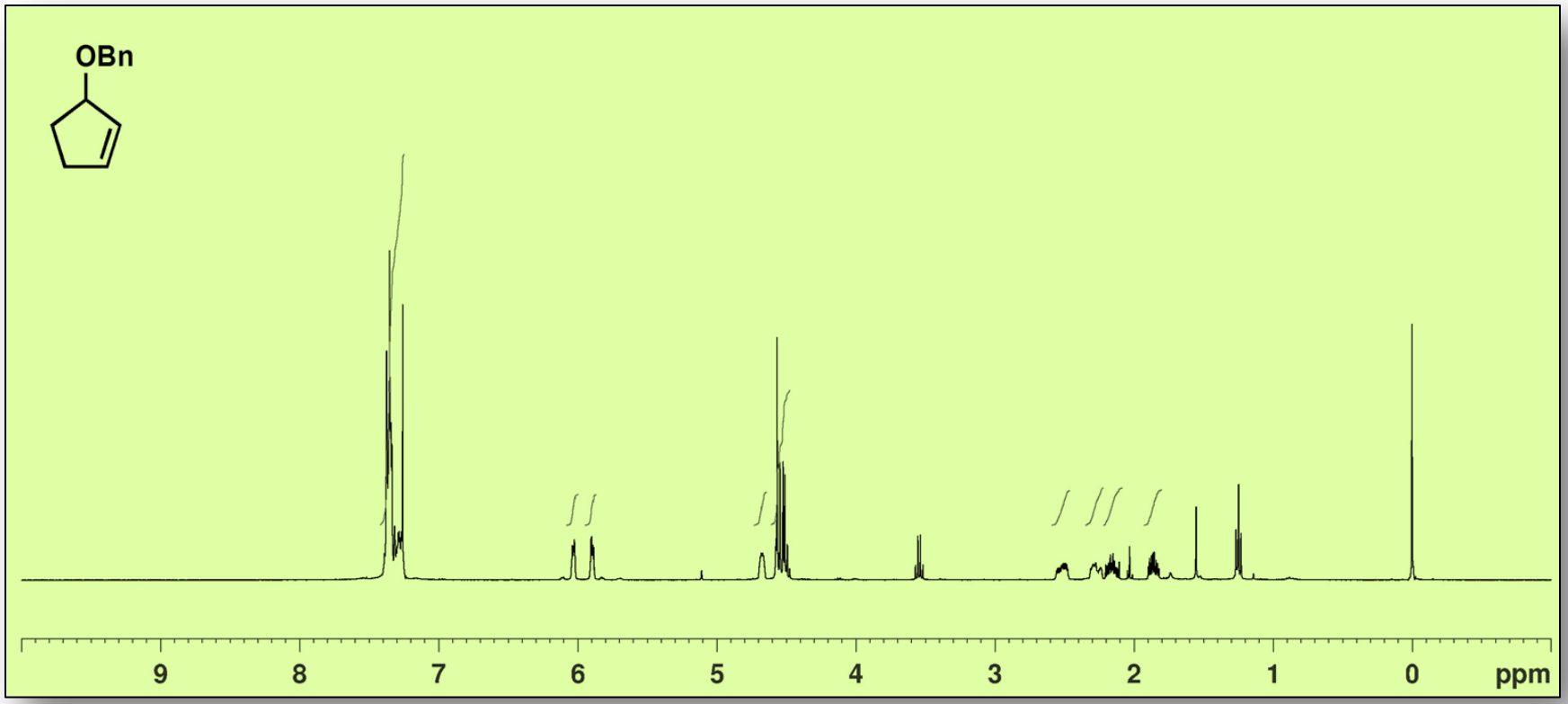

Figure 25: ^{1}H NMR spectrum of compound 37 (300 MHz, $CDCl_3$, 293K)

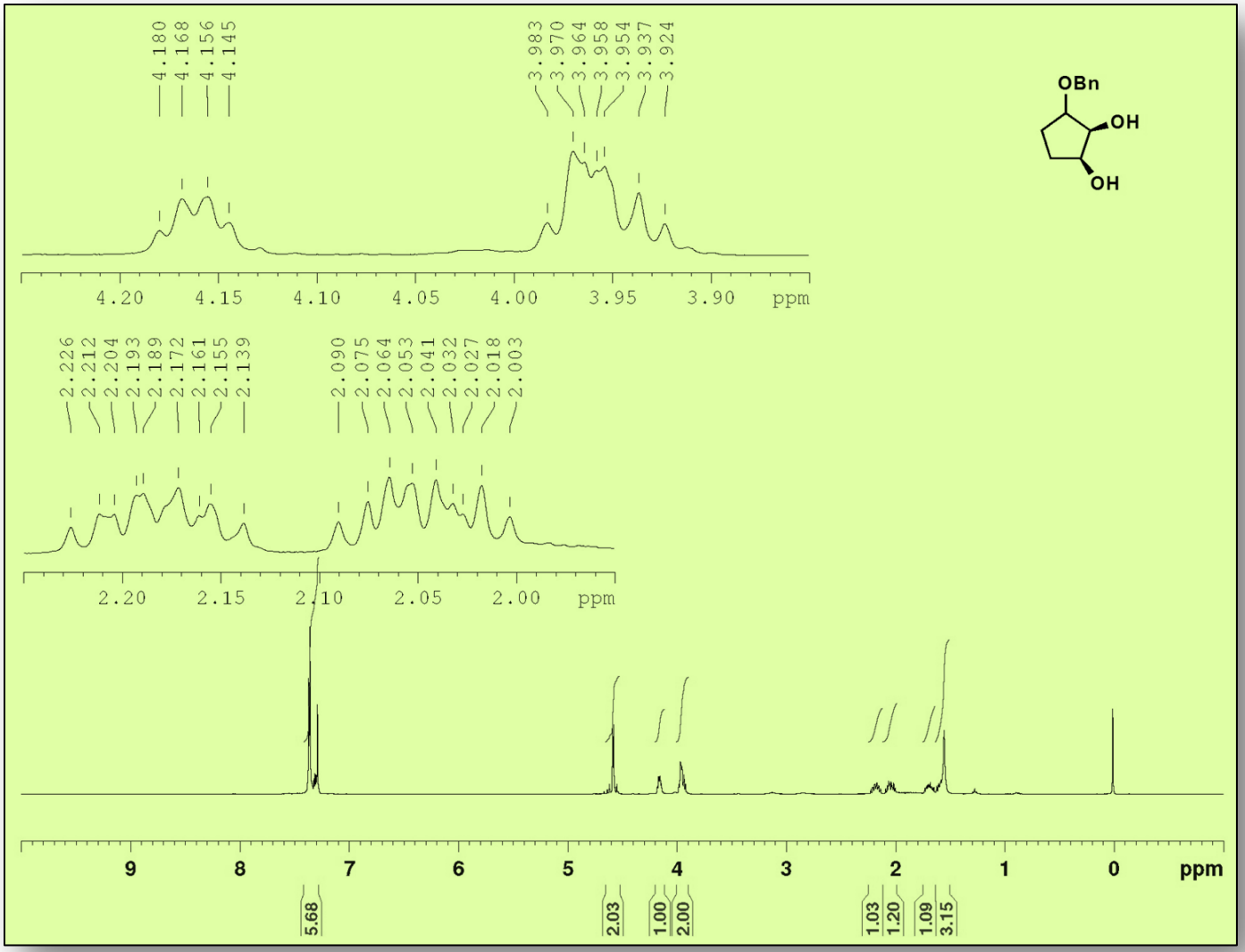

Figure 26: ^{1}H NMR spectrum of compound 34 (300 MHz, $CDCl_3$, 293K)

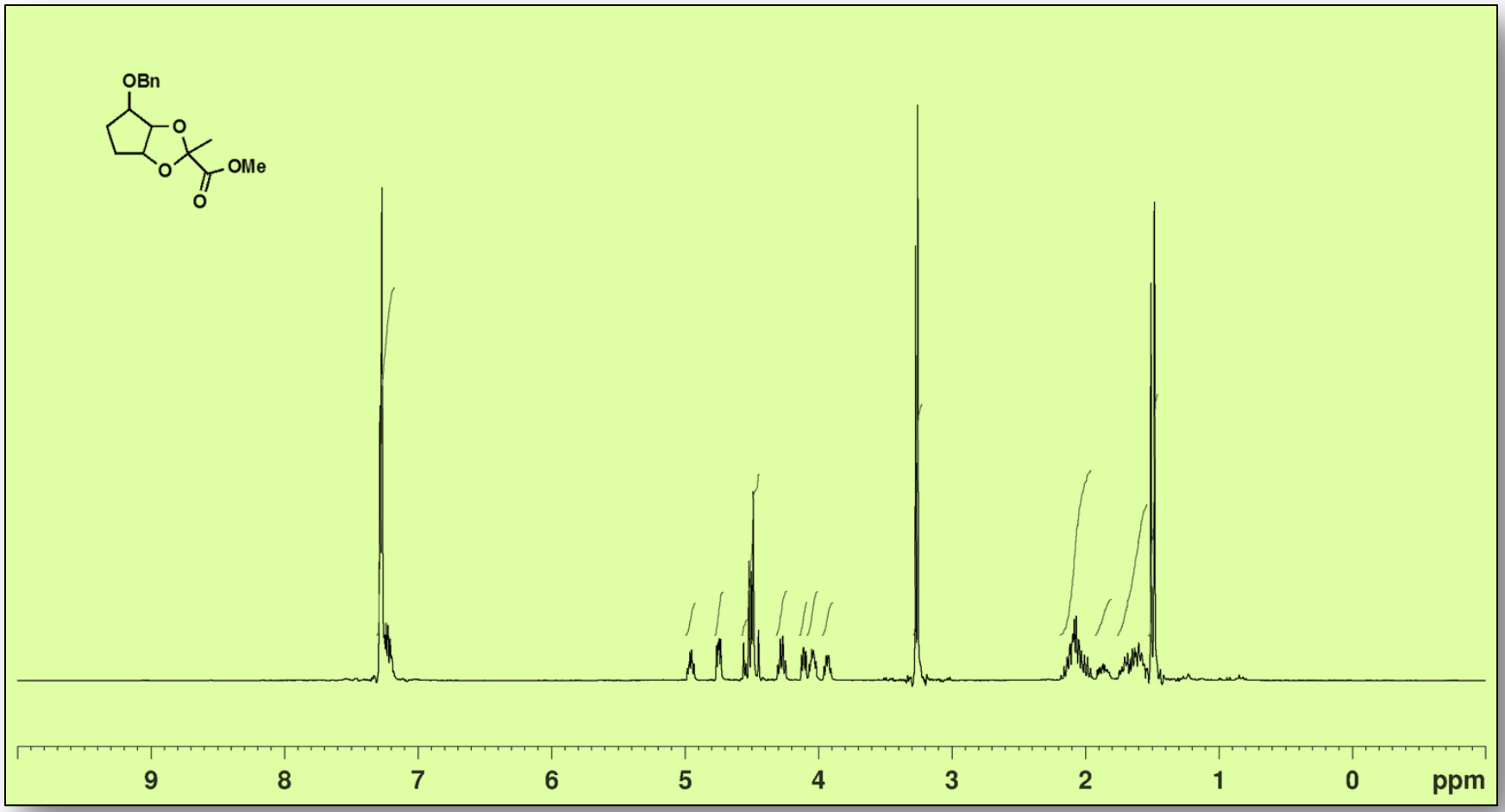

Figure 27: ^{1}H NMR spectrum of compound 40 R_f=0 .60 (300 MHz, $CDCl_3$, 293K)

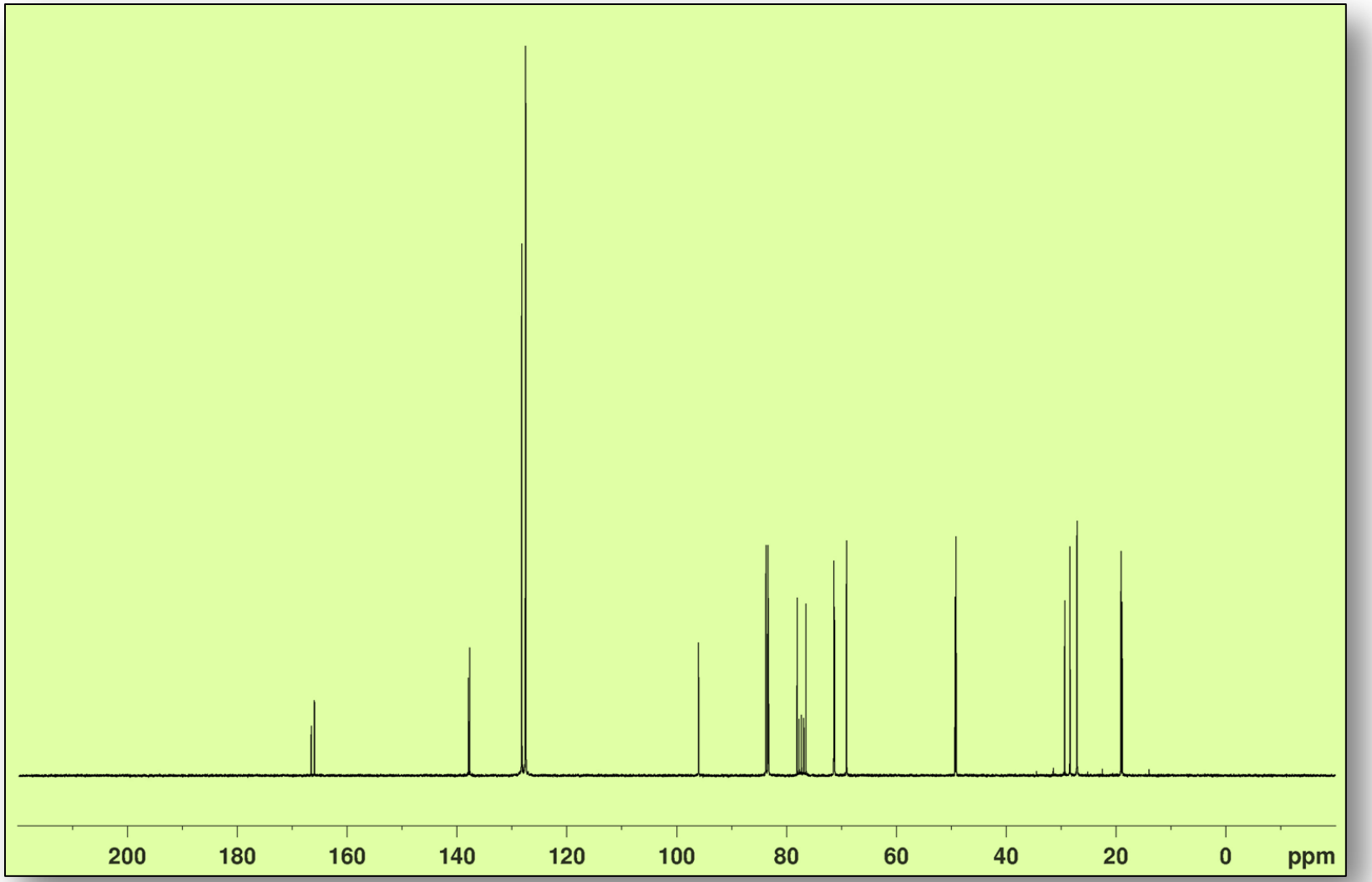

Figure 28: ^{13}C NMR spectrum of compound 40 R_f=0 .60 (300 MHz, $CDCl_3$, 293K)

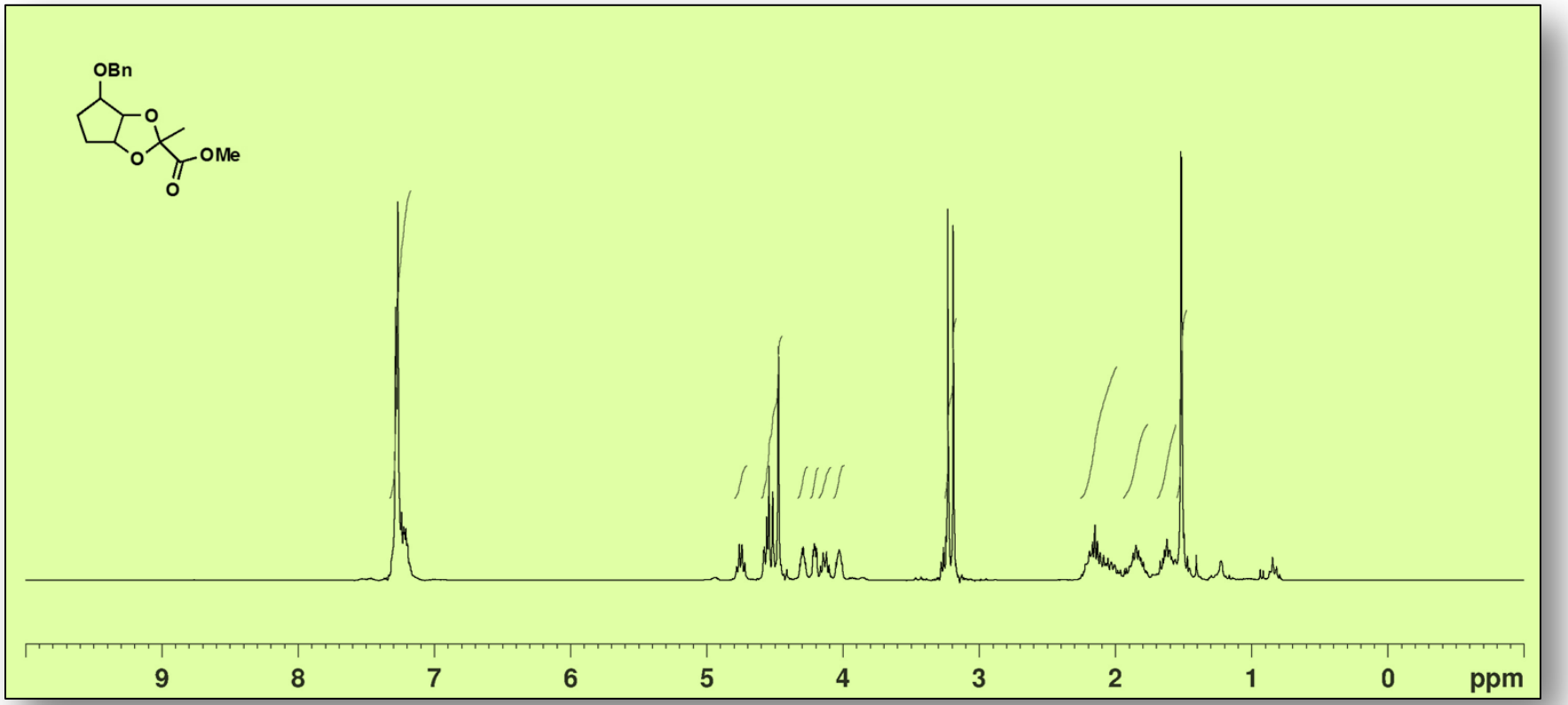

Figure 29: ^{1}H NMR spectrum of compound 40 R_f=0 .47 (300 MHz, $CDCl_3$, 293K)

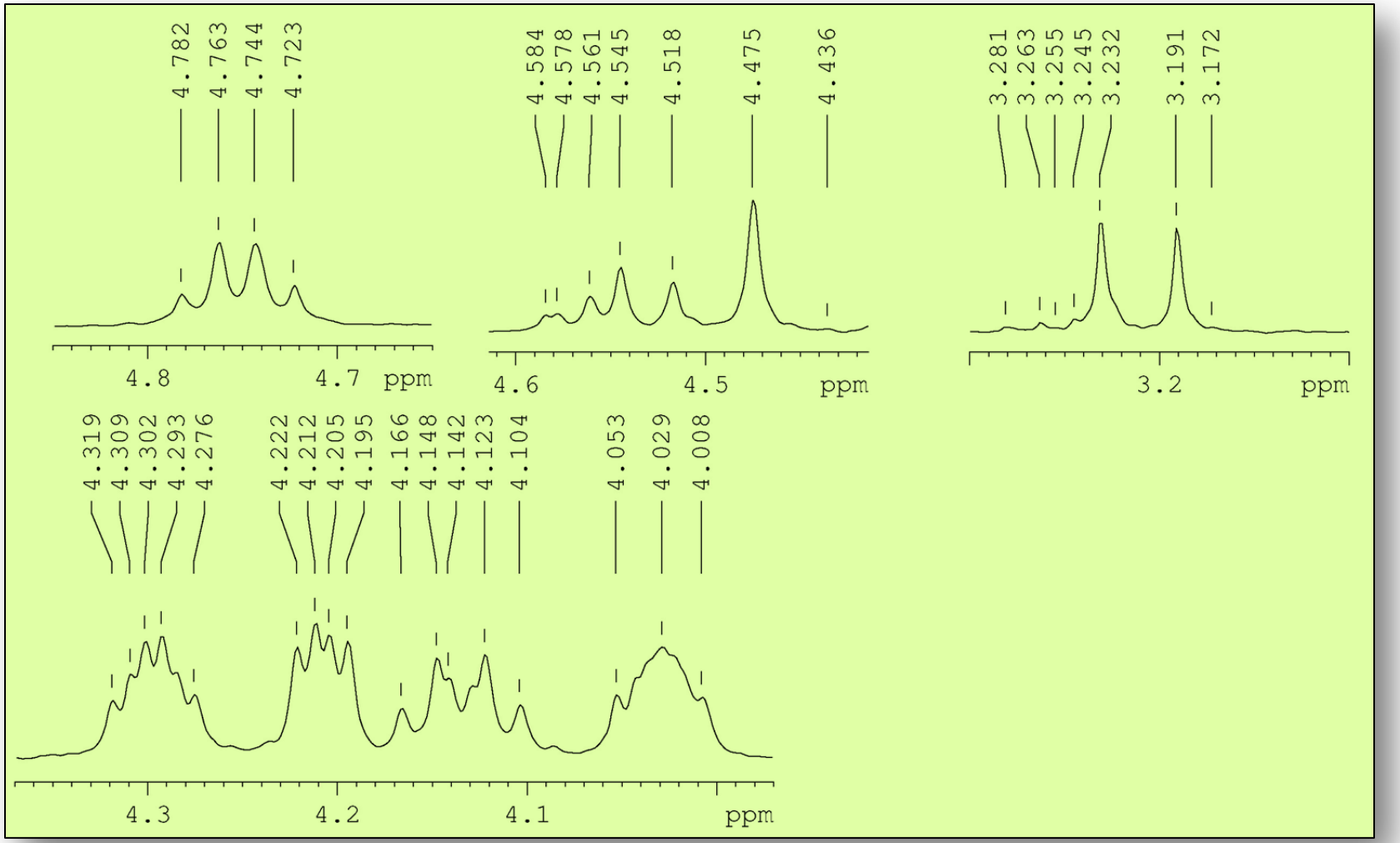

Figure 30: ^{1}H NMR spectrum of compound 40 R_f=0 .47 (continued)

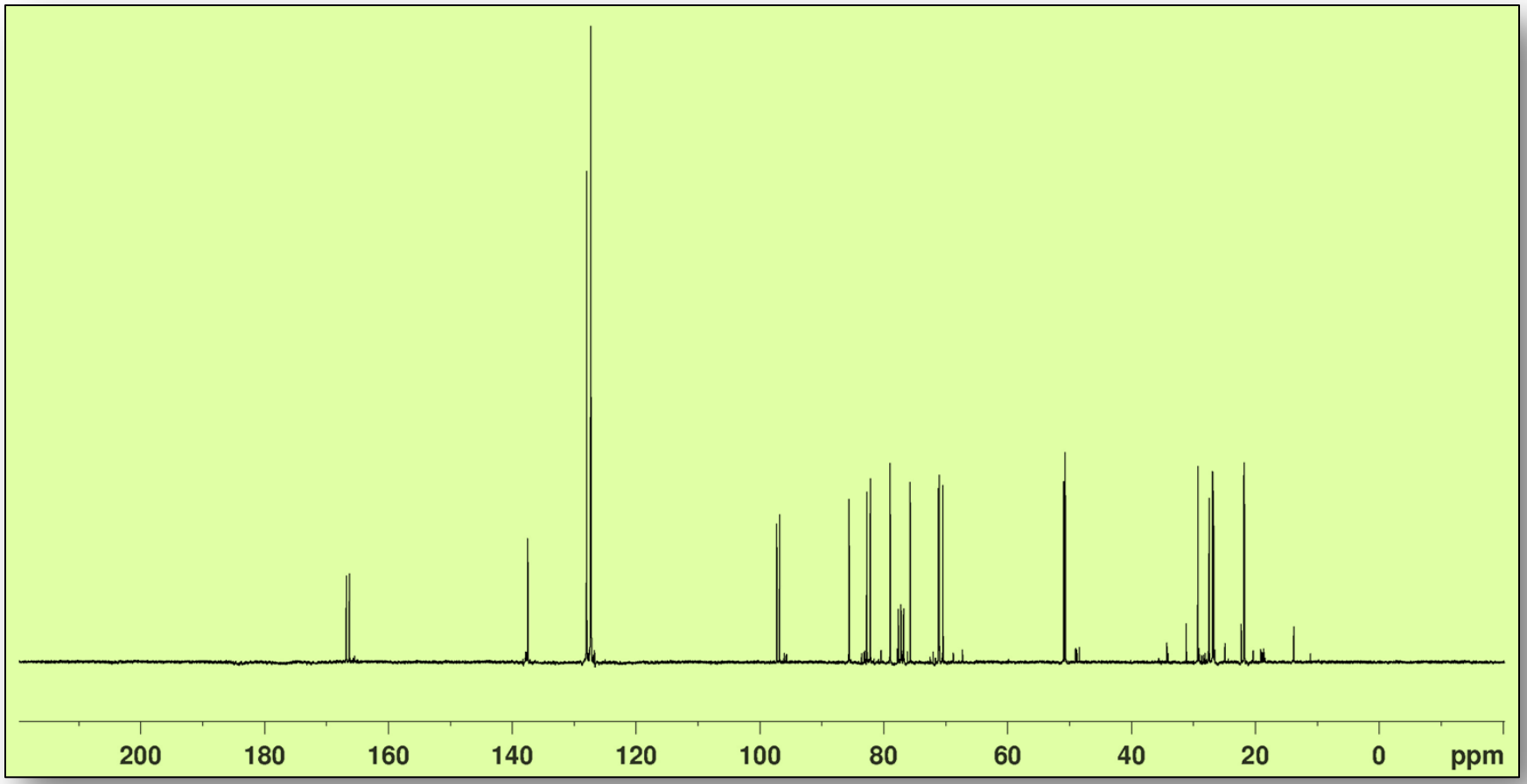

Figure 31: ^{13}H NMR spectrum of compound 40 R_f=0 .47 (300 MHz, $CDCl_3$, 293K)

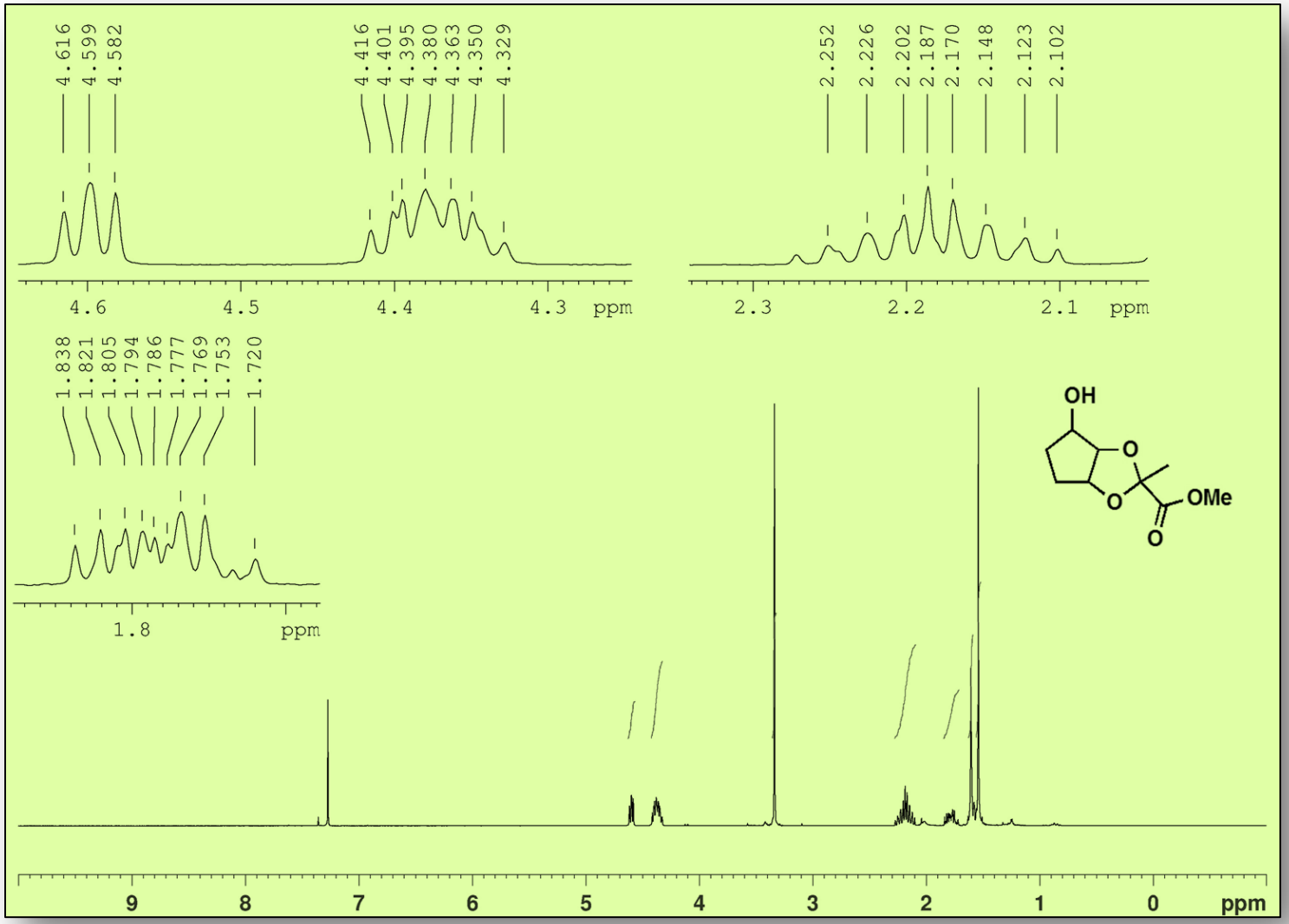

Figure 32: ^{1}H NMR spectrum of compound 45 R_f=0 .38 (300 MHz, $CDCl_3$, 293K)

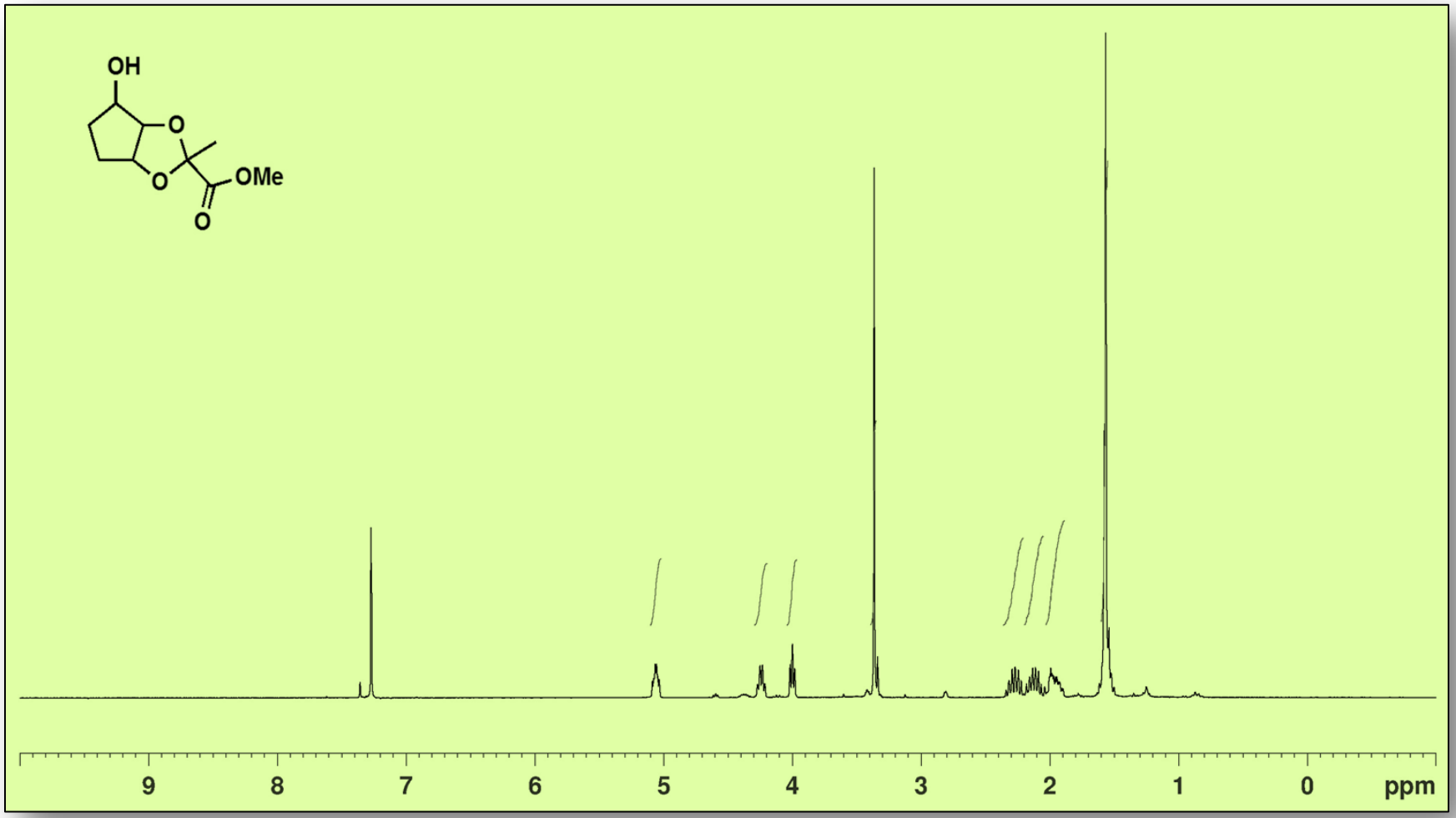

Figure 33: ^{1}H NMR spectrum of compound 45 R_f=0 .28 (300 MHz, $CDCl_3$, 293K)

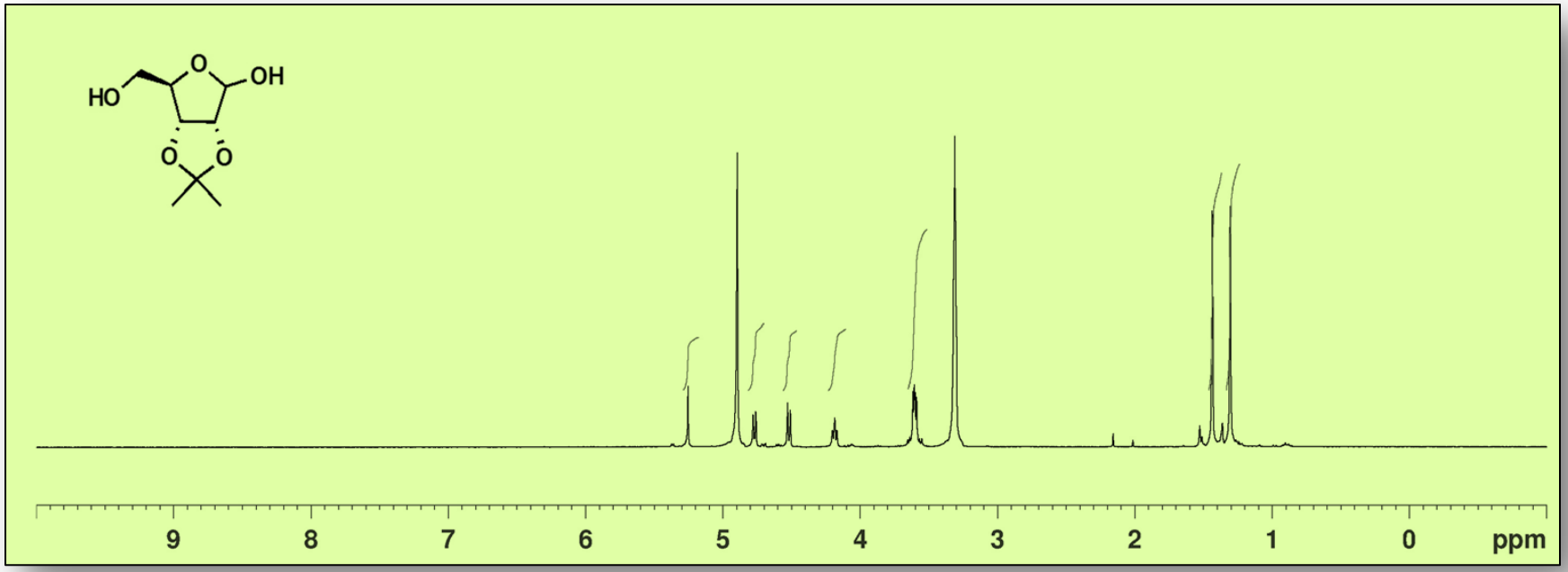

Figure 34: ^{1}H NMR spectrum of compound 52 (300 MHz, $CDCl_3$, 293K)

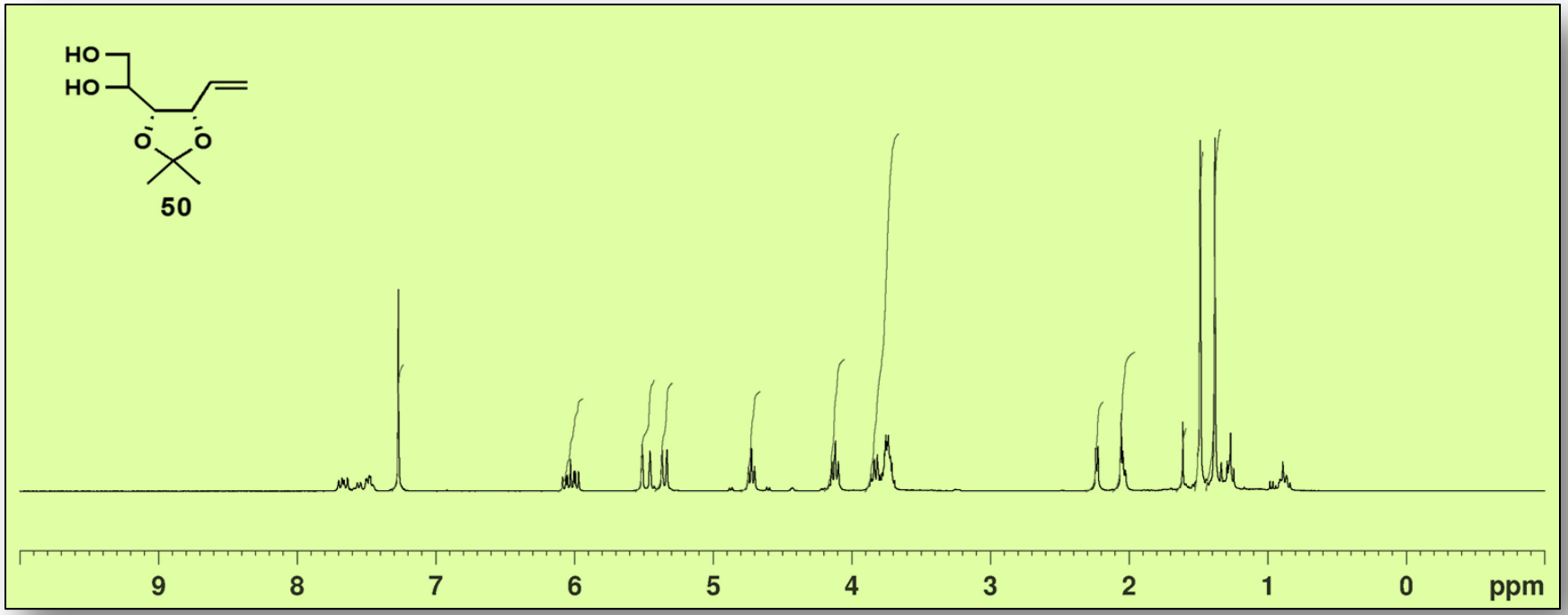

Figure 35: ^{1}H NMR spectrum of compound **50** (300 MHz, $CDCl_3$, 293K)

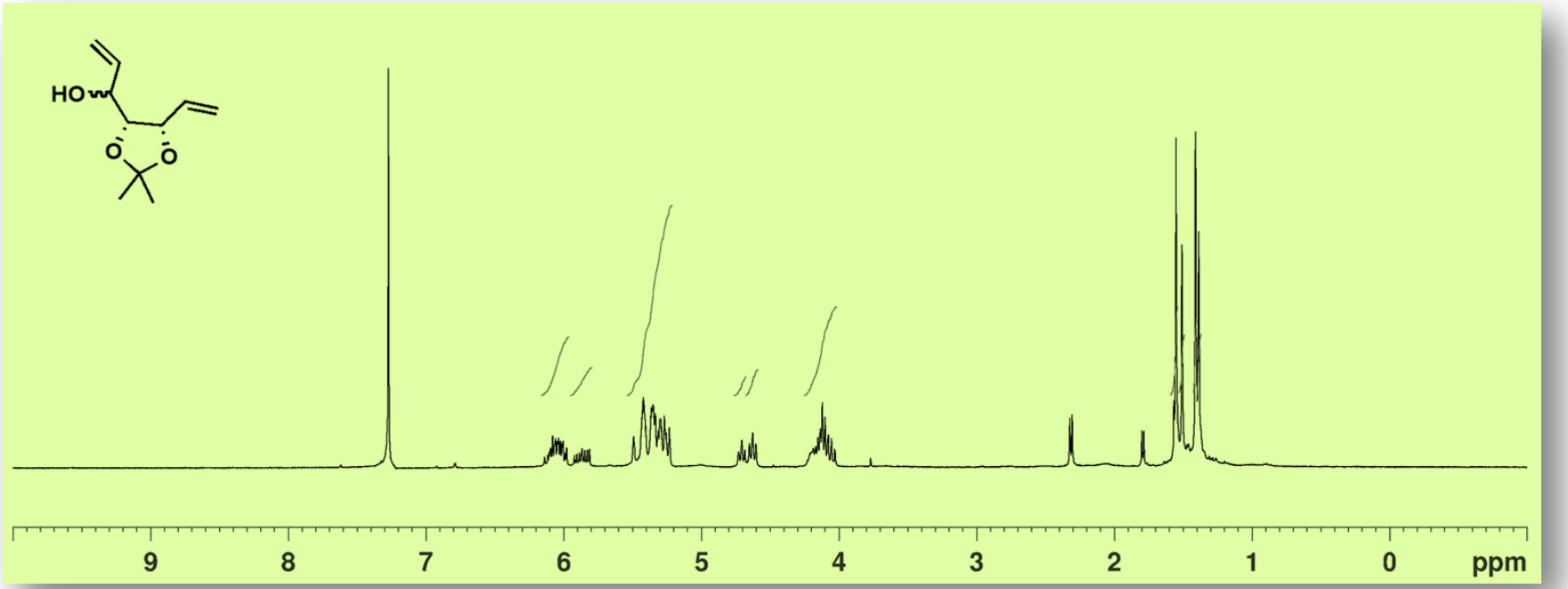

Figure 36: ^{1}H NMR spectrum of compound 48 (300 MHz, $CDCl_3$, 293K)

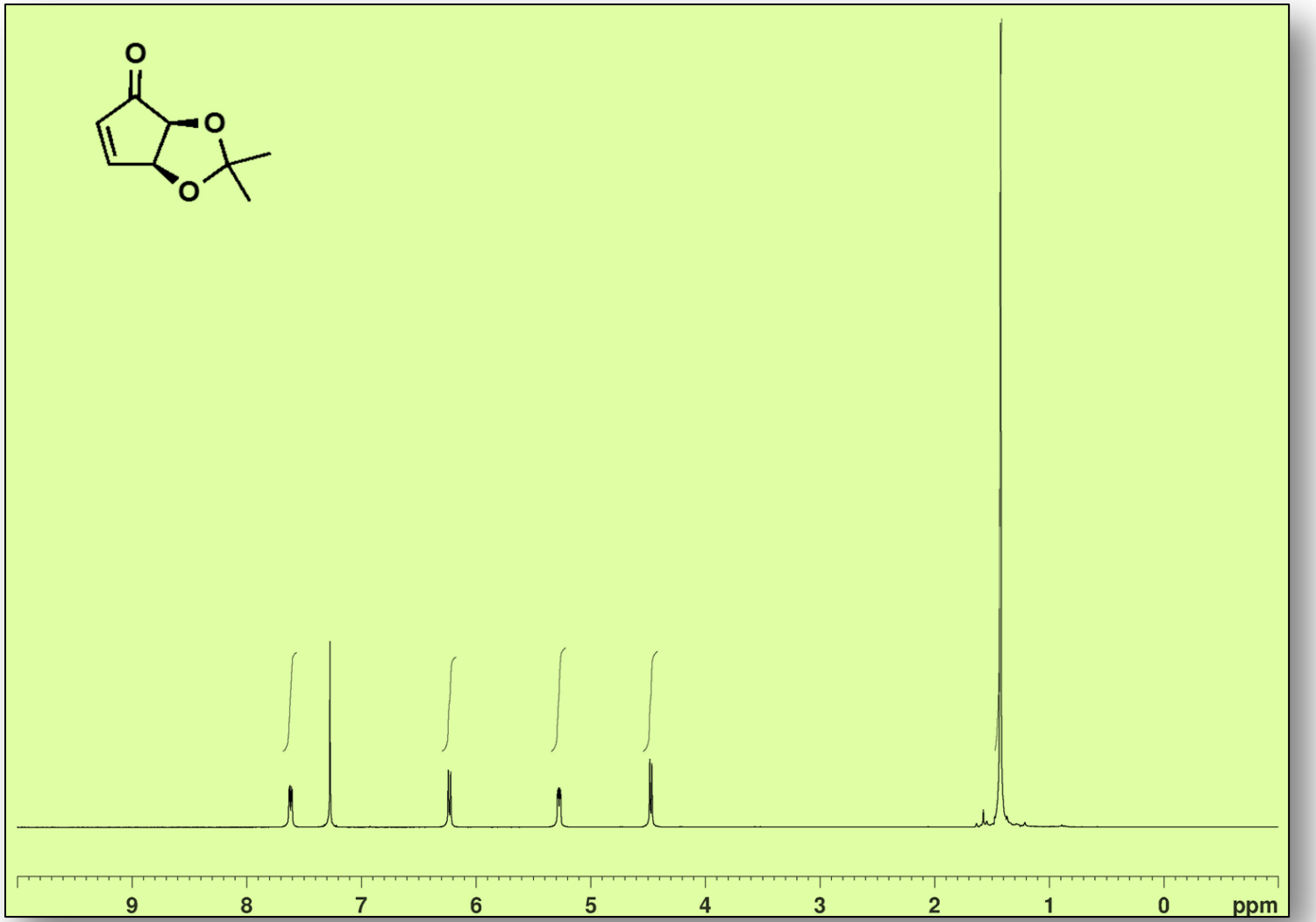

Figure 37: ^{1}H NMR spectrum of compound 2 (300 MHz, $CDCl_3$, 293K)

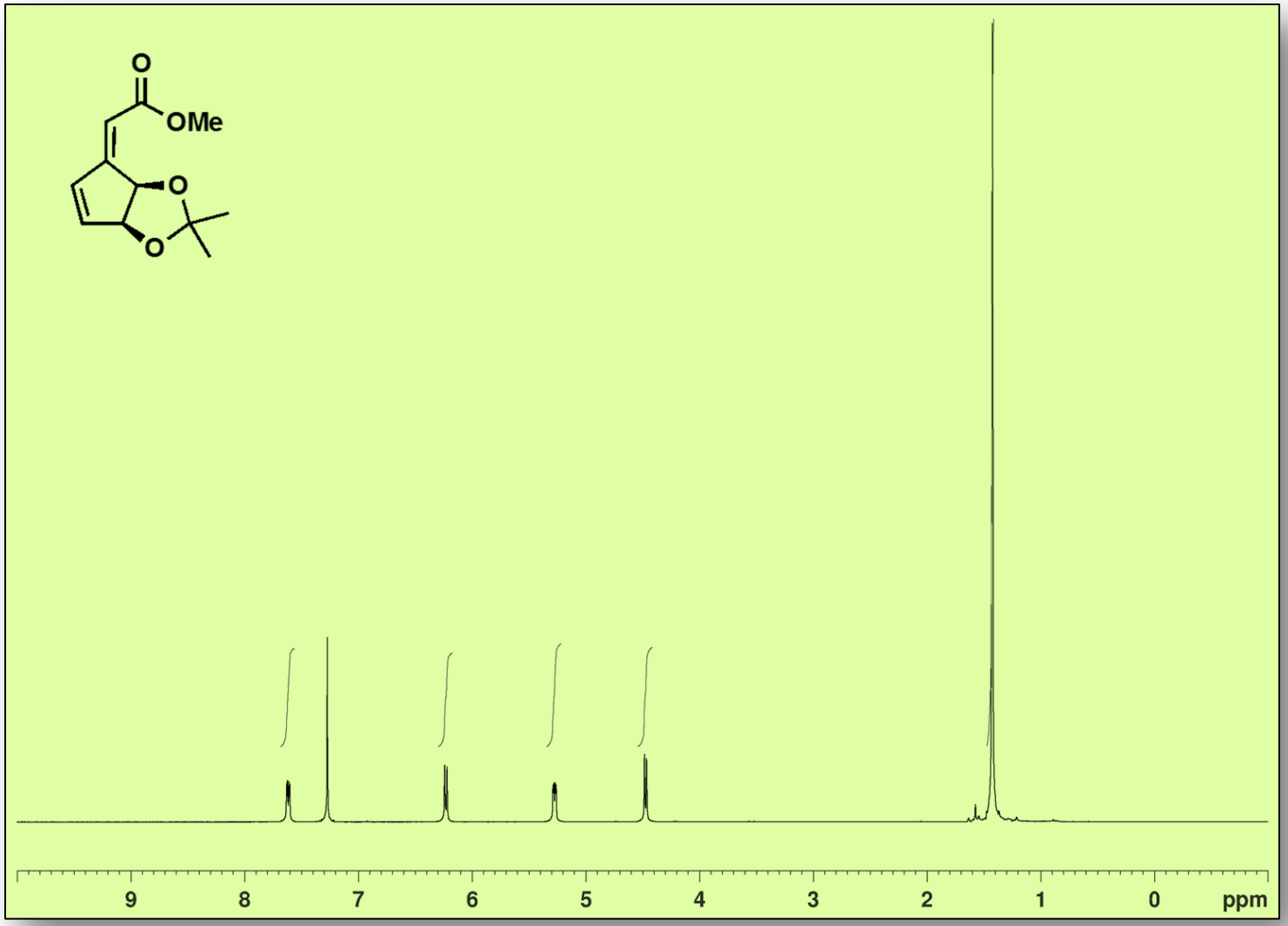

Figure 38: ^{1}H NMR spectrum of compound 51-Z (300 MHz, $CDCl_3$, 293K)

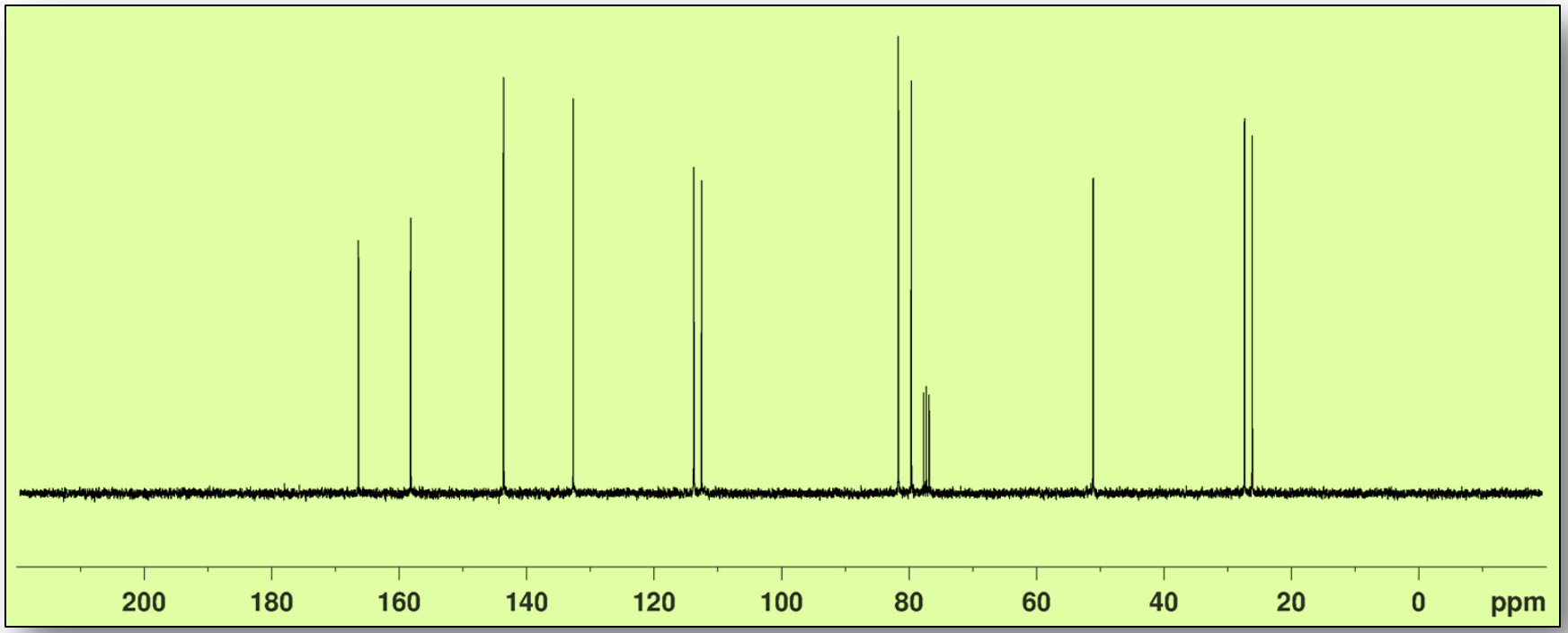

Figure 39: ^{13}C NMR spectrum of compound 51-Z (300 MHz, $CDCl_3$, 293K)

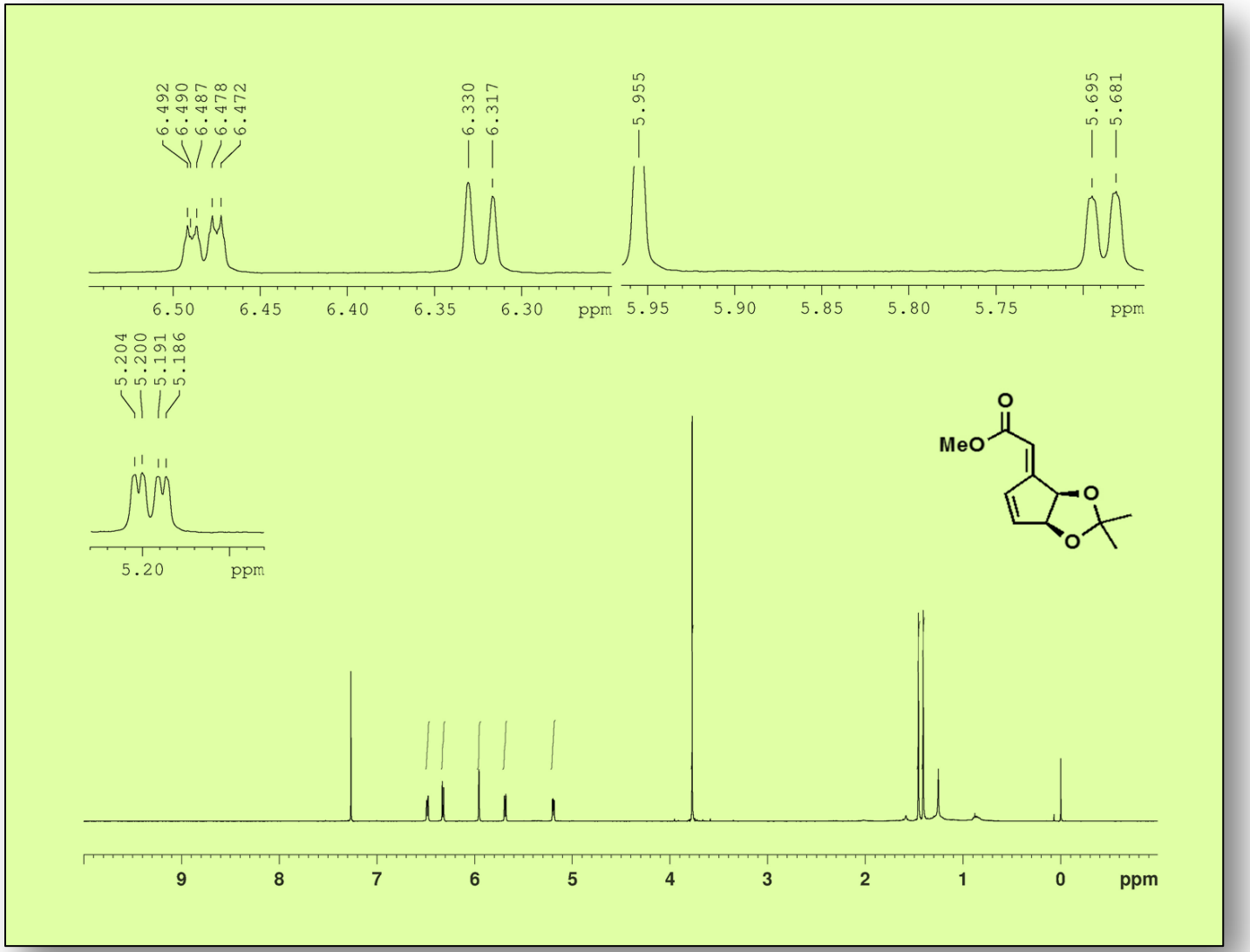

Figure 40: ^{1}H NMR spectrum of compound 51-E (300 MHz, $CDCl_3$, 293K)

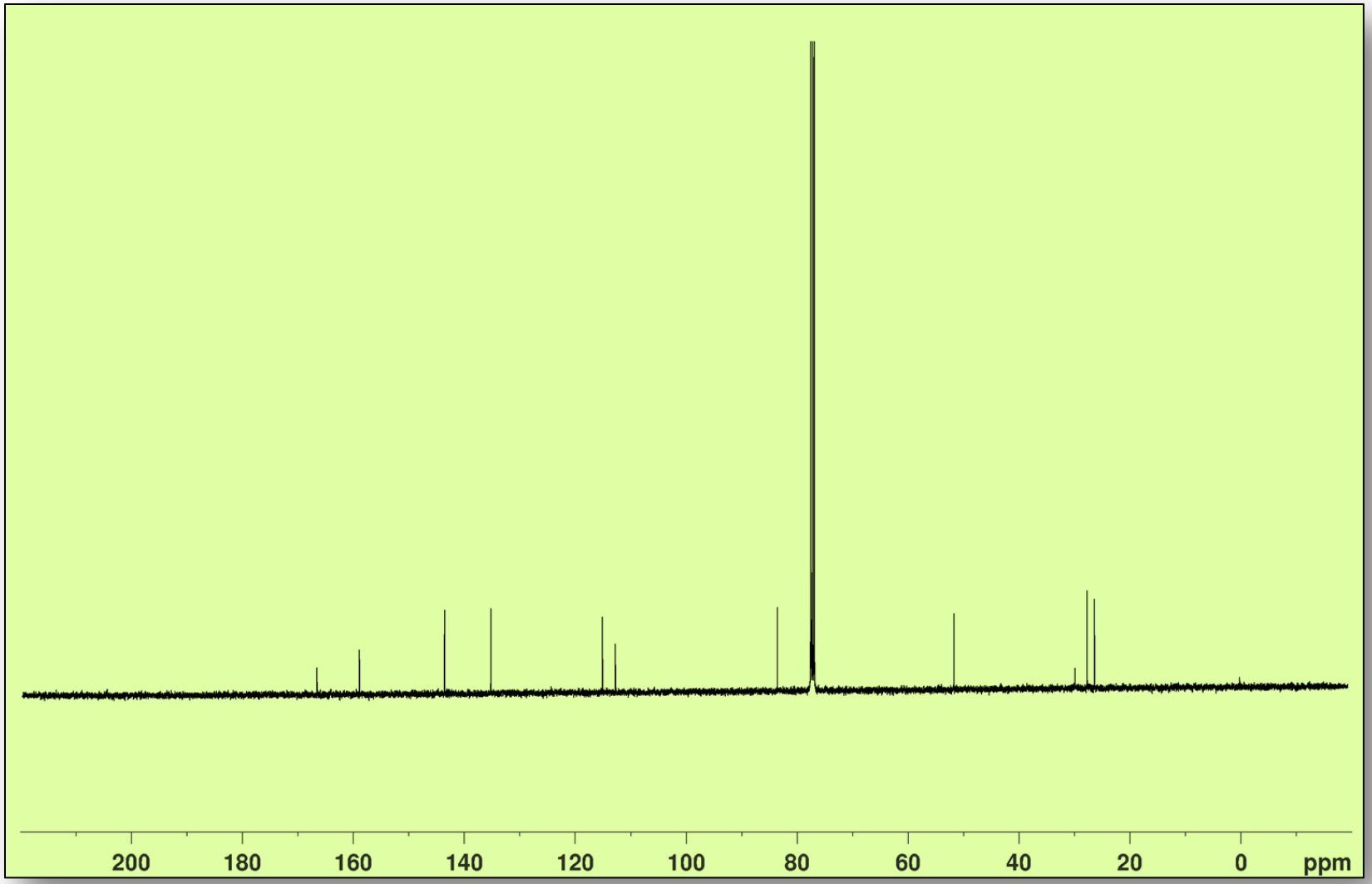

Figure 41: ^{13}C NMR spectrum of compound 51-E (300 MHz, $CDCl_3$, 293K)

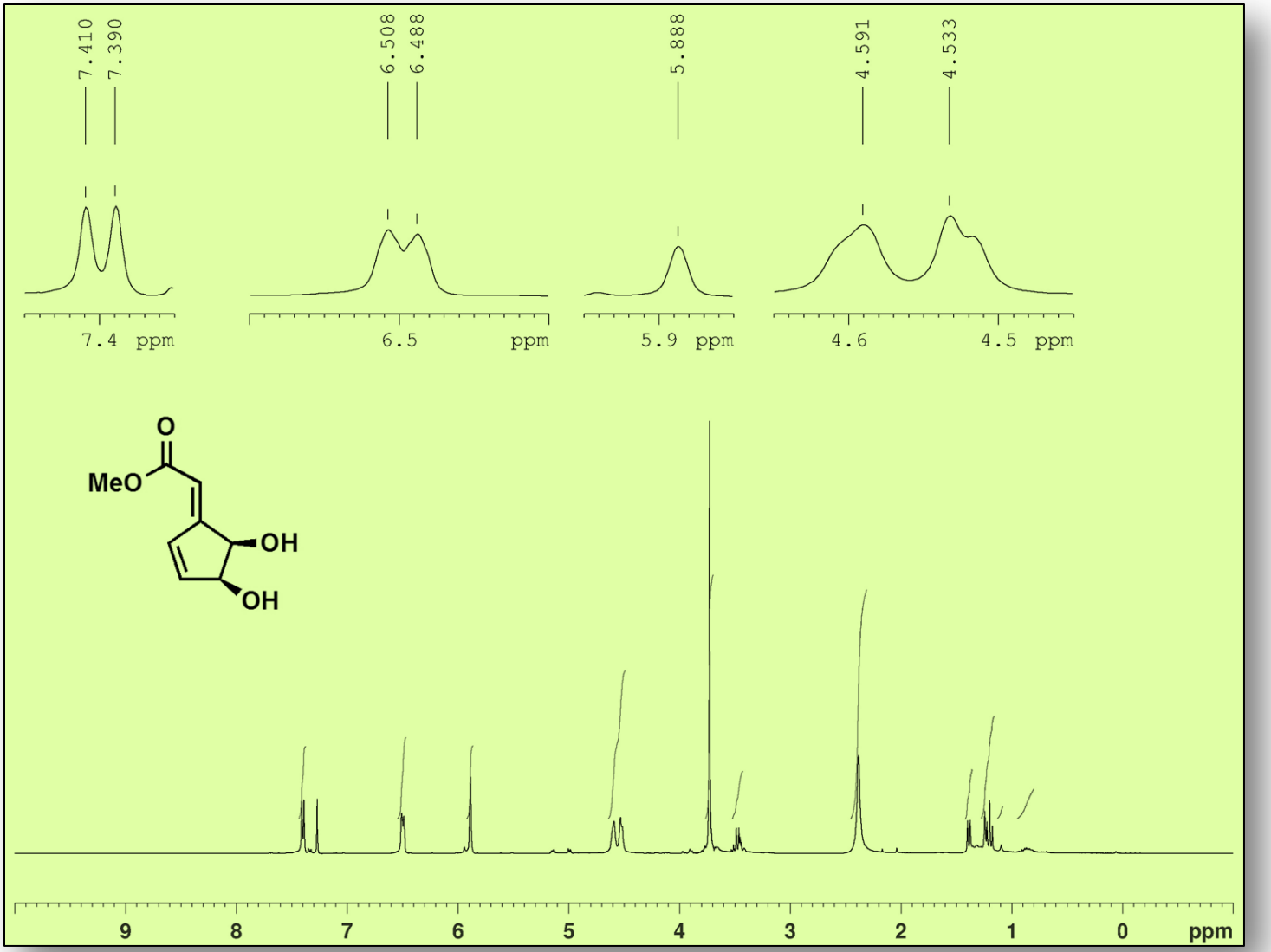

Figure 42: ^{1}H NMR spectrum of compound 73 (300 MHz, $CDCl_3$, 293K)

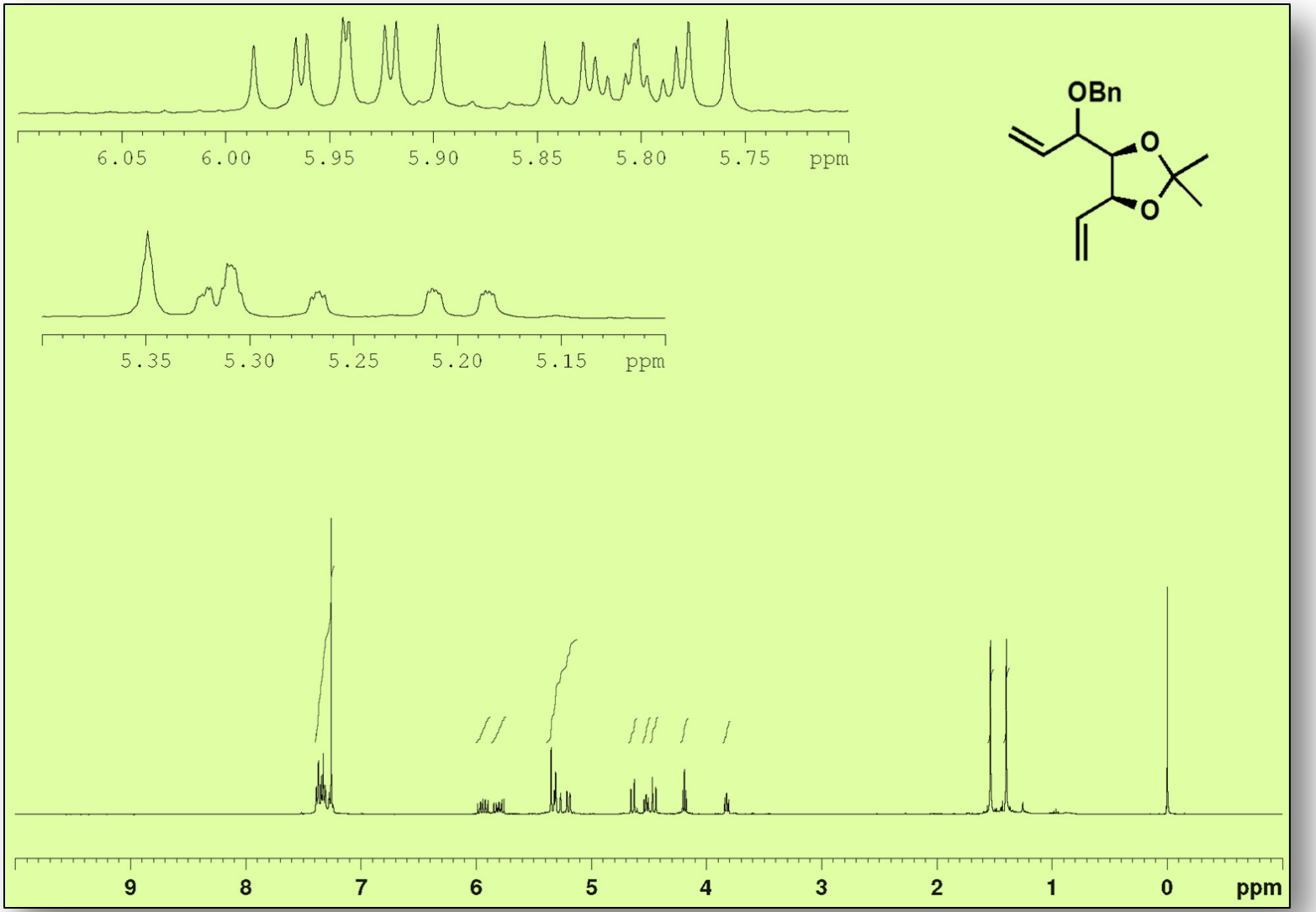

Figure 43: ^{1}H NMR spectrum of compound 83 (400 MHz, $CDCl_3$, 293K)

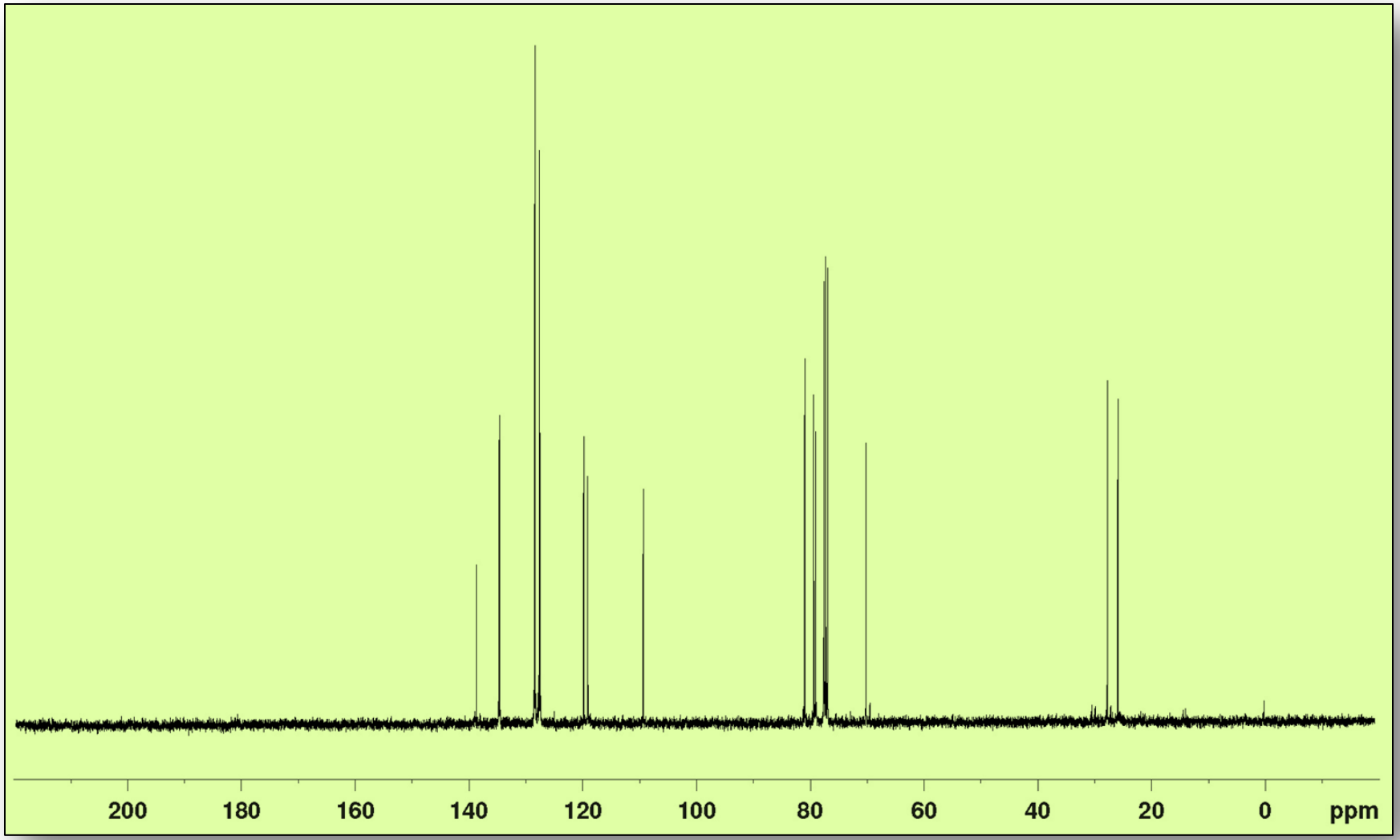

Figure 44: ^{13}C NMR spectrum of compound 83 (400 MHz, $CDCl_3$, 293K)

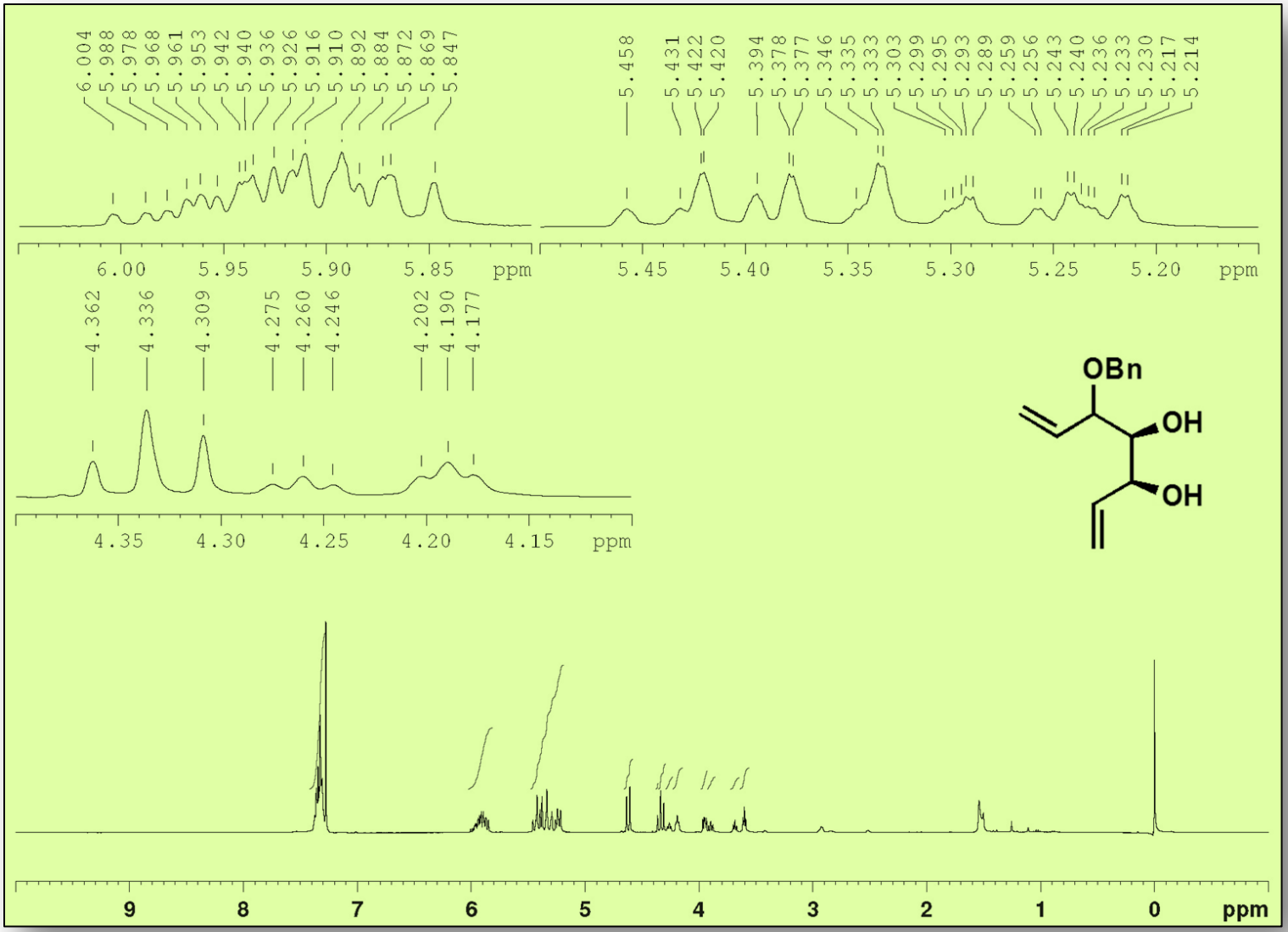

Figure 45: ^{1}H NMR spectrum of compound 80 mixture diastereomers (400 MHz, $CDCl_3$, 293K)

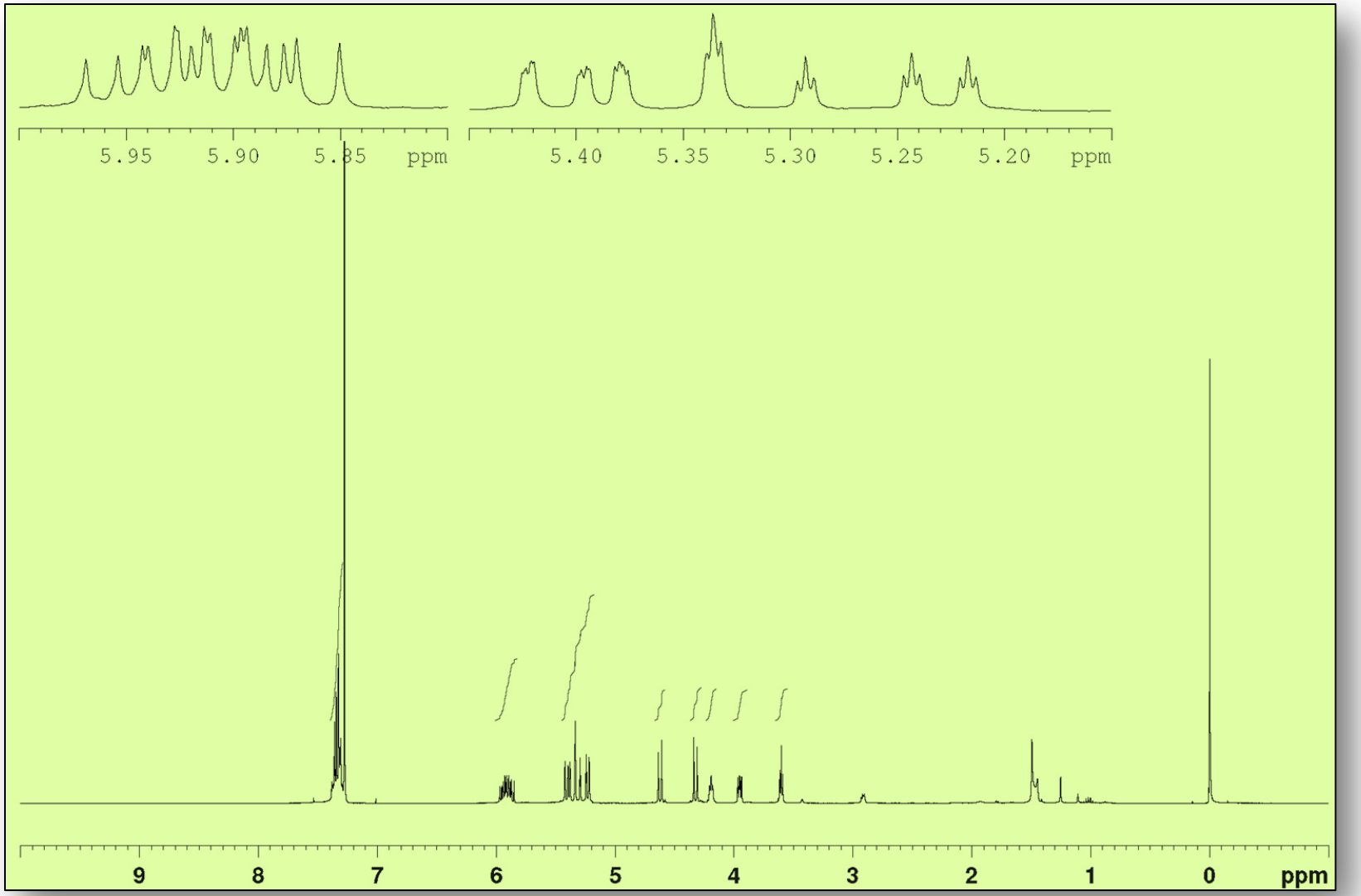

Figure 46: ^{1}H NMR spectrum of compound 80 mixture diastereomers (400 MHz, $CDCl_3$, 293K)

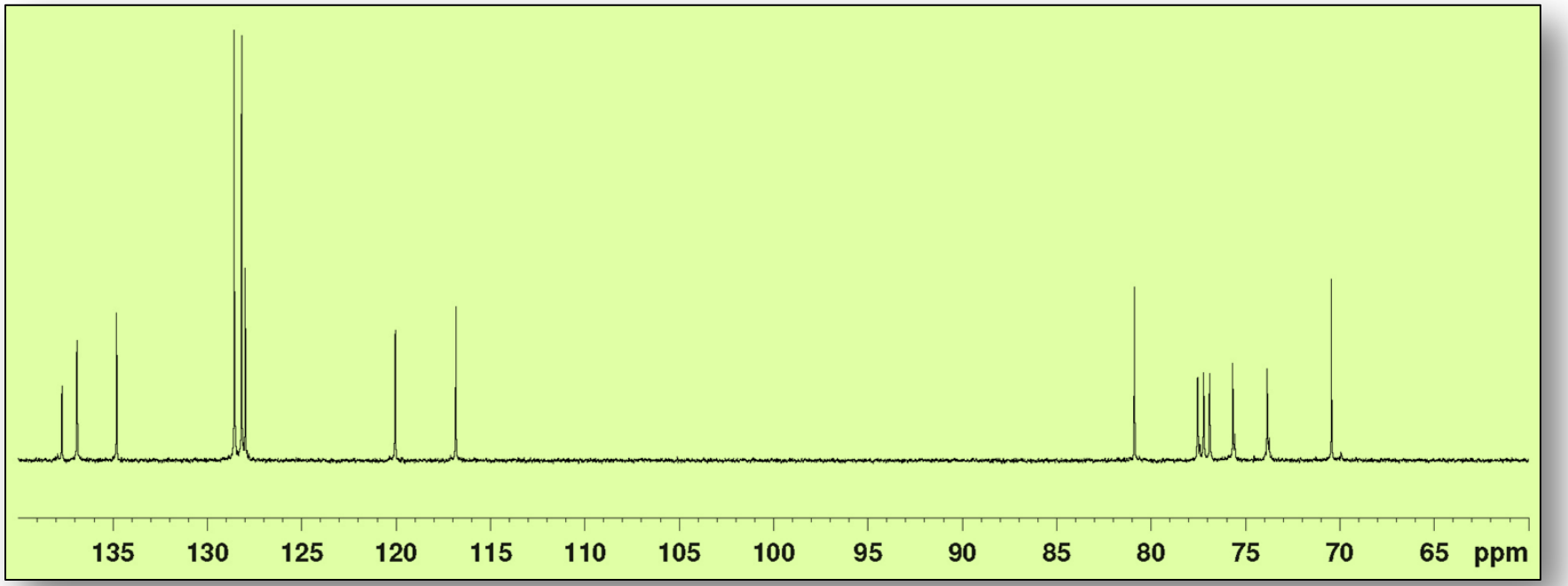

Figure 47: ^{13}C NMR spectrum of compound **80** single diastereomer (400 MHz, $CDCl_3$, 293K)

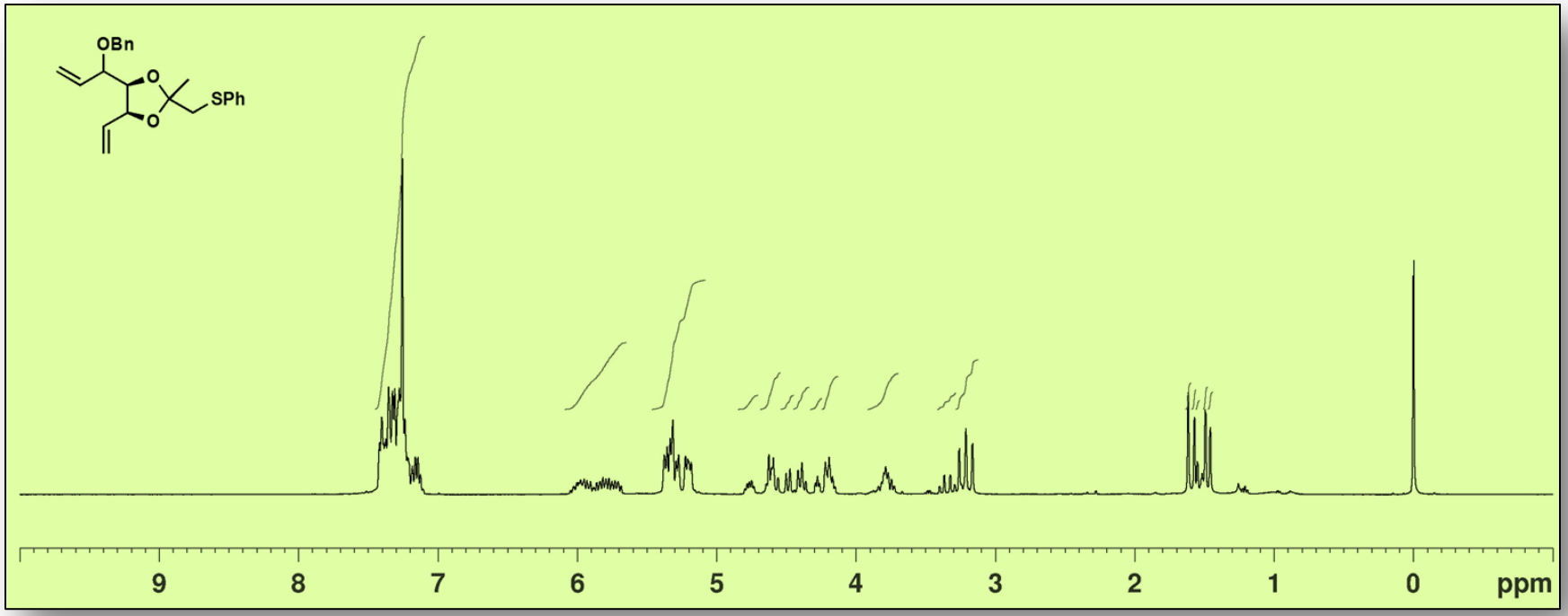

Figure 48: ^{1}H NMR spectrum of compound 79 (400 MHz, $CDCl_3$, 293K)

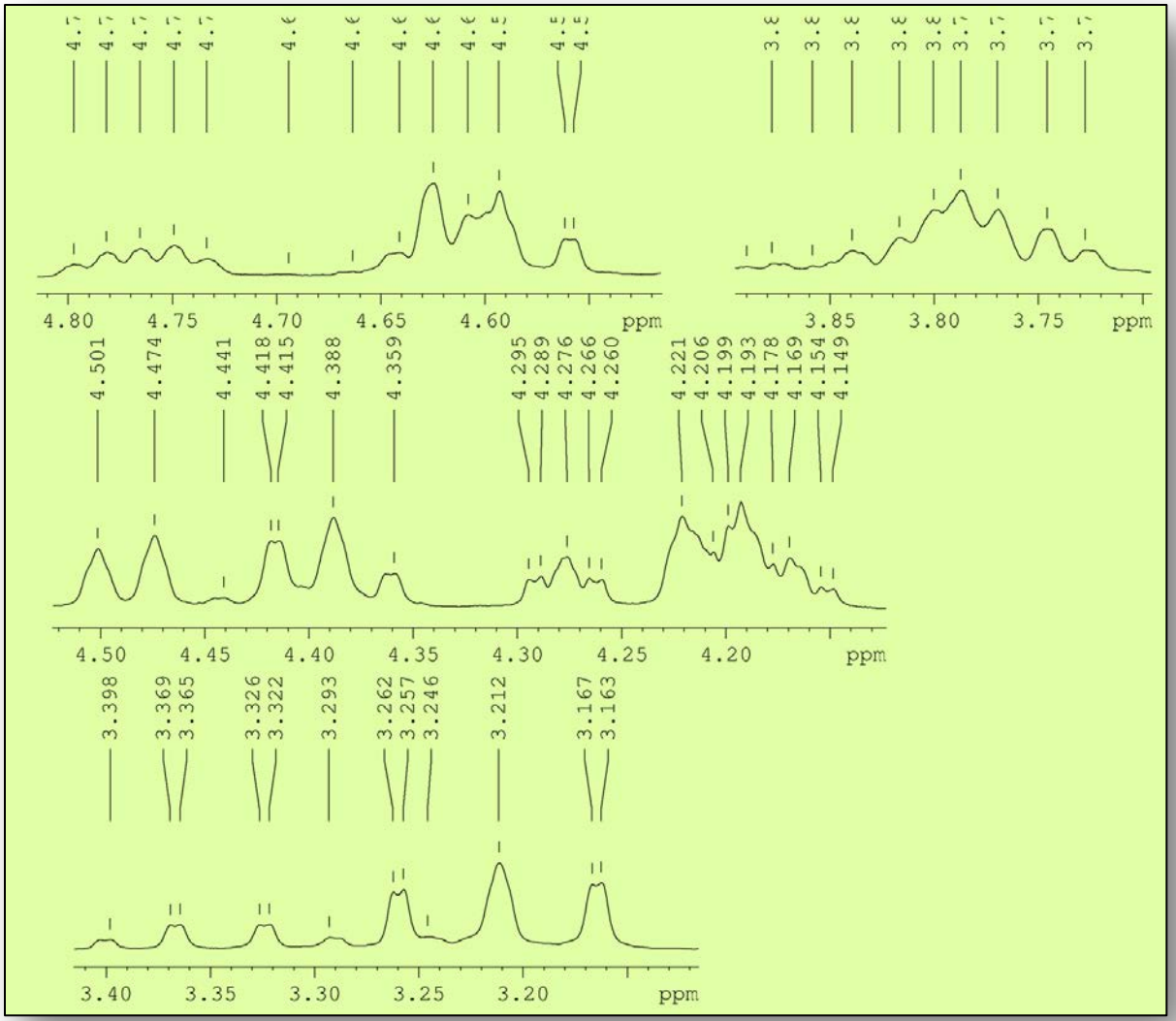

Figure 49: ^{1}H NMR spectrum of compound 79 (continued)

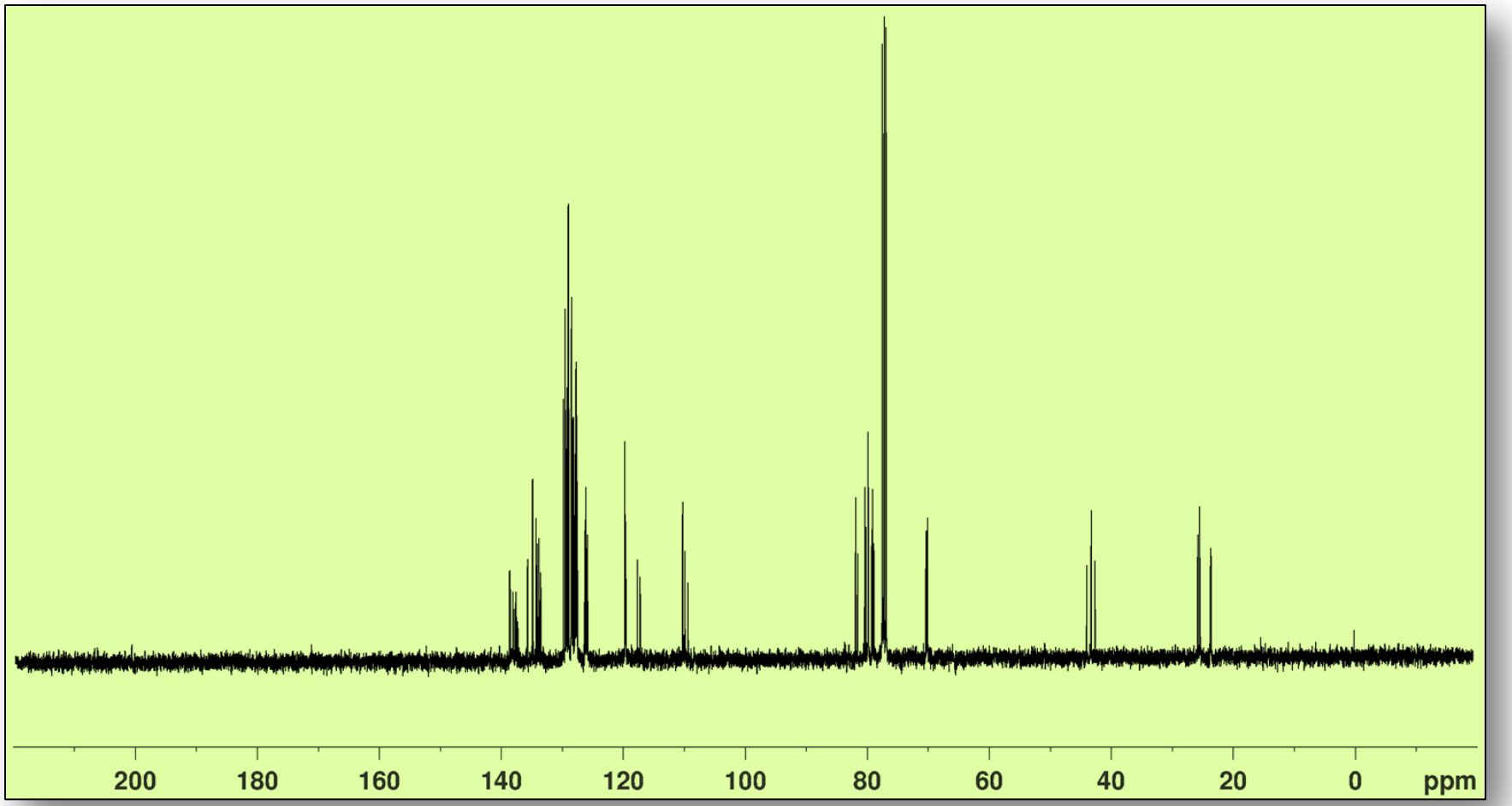

Figure 50: ^{13}C NMR spectrum of compound 79 (400 MHz, $CDCl_3$, 293K)

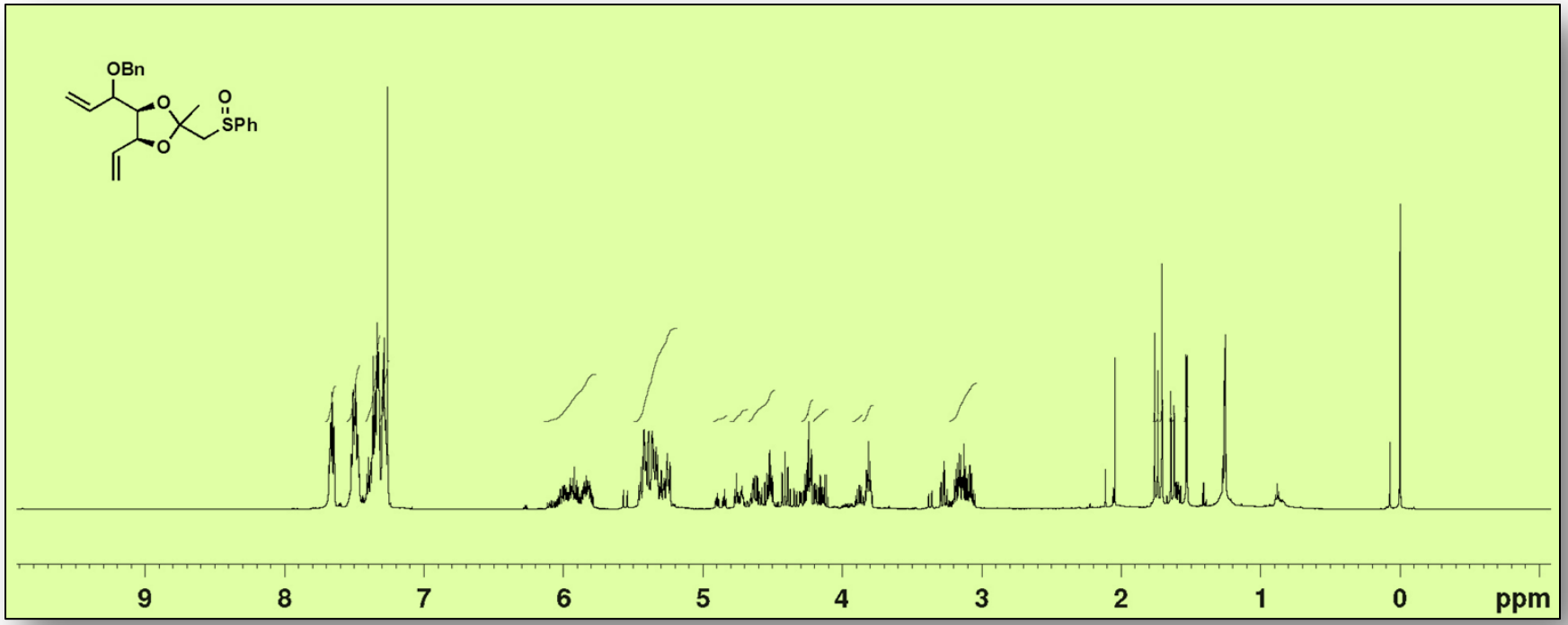

Figure 51: ^{1}H NMR spectrum of compound **84** (400 MHz, $CDCl_3$, 293K)

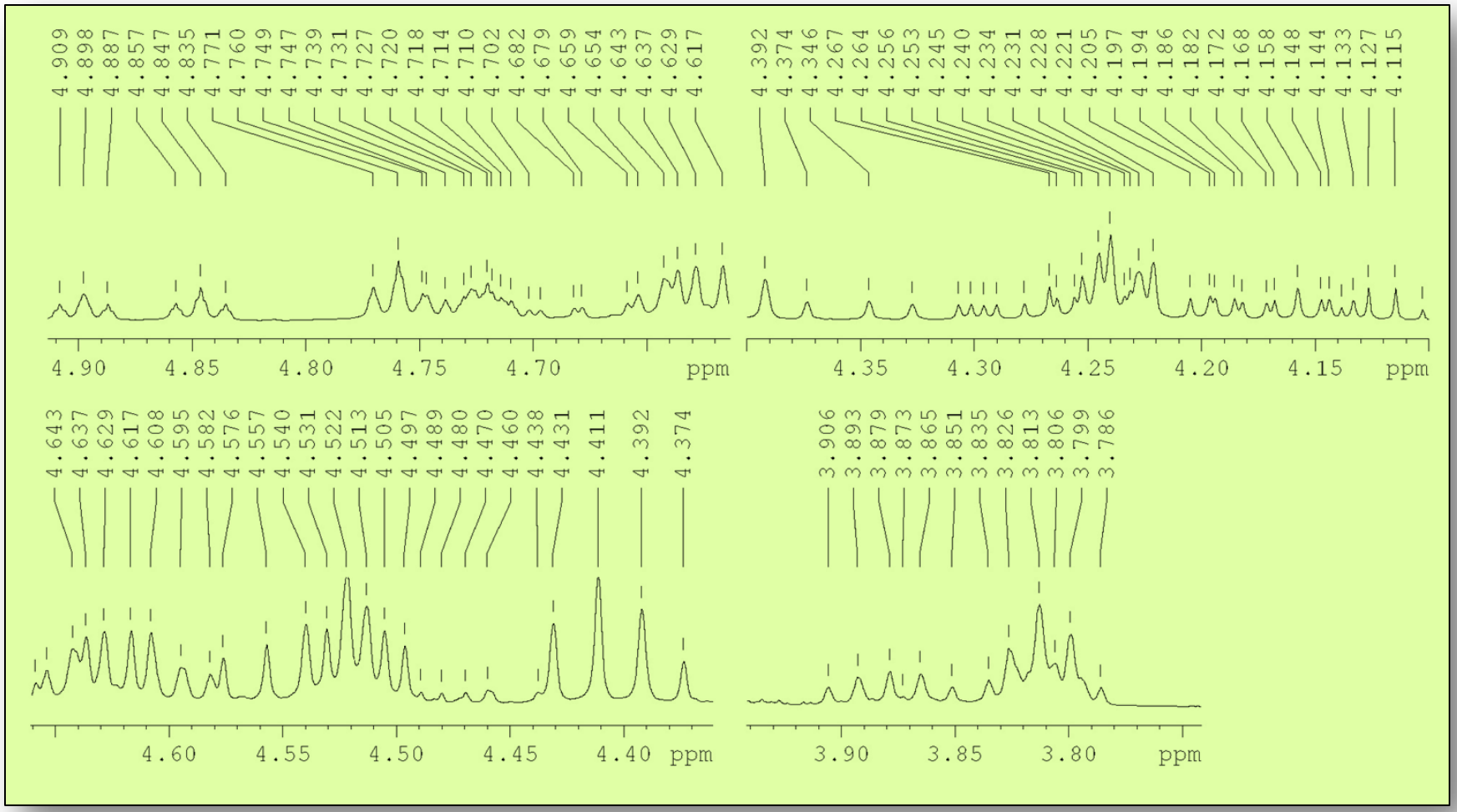

Figure 52: ^{1}H NMR spectrum of compound **84** (continued)

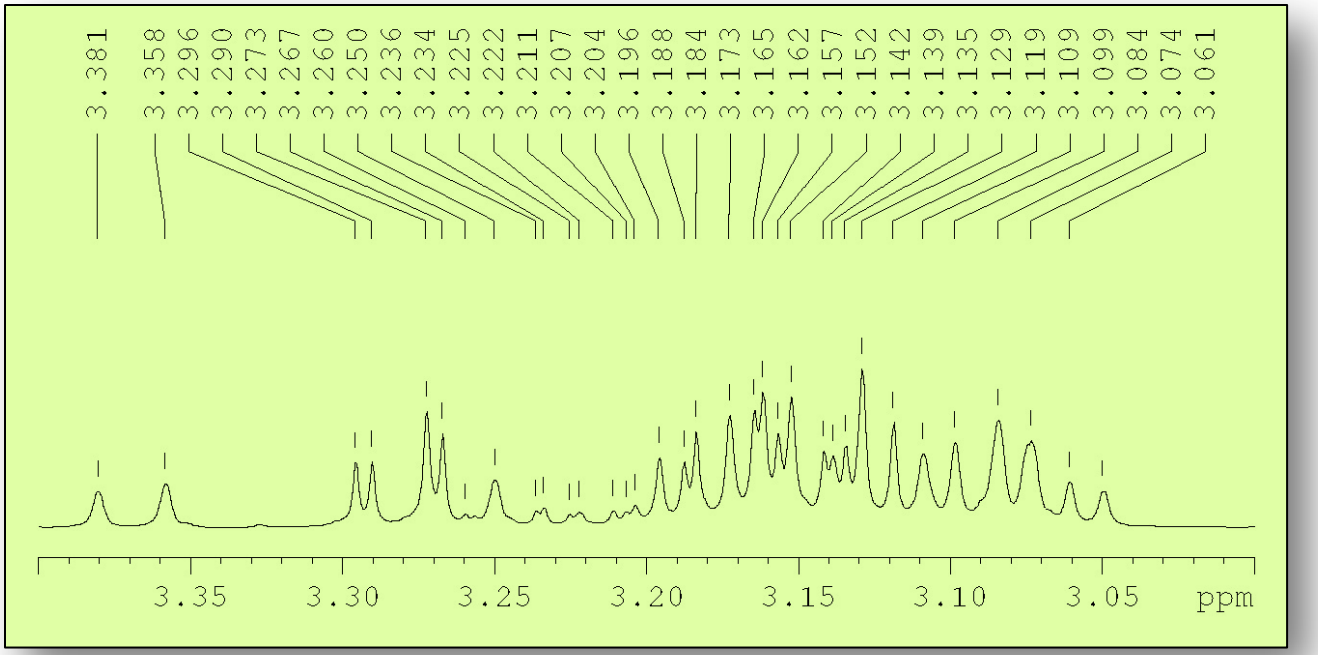

Figure 53: ^{1}H NMR spectrum of compound **84** (continued)

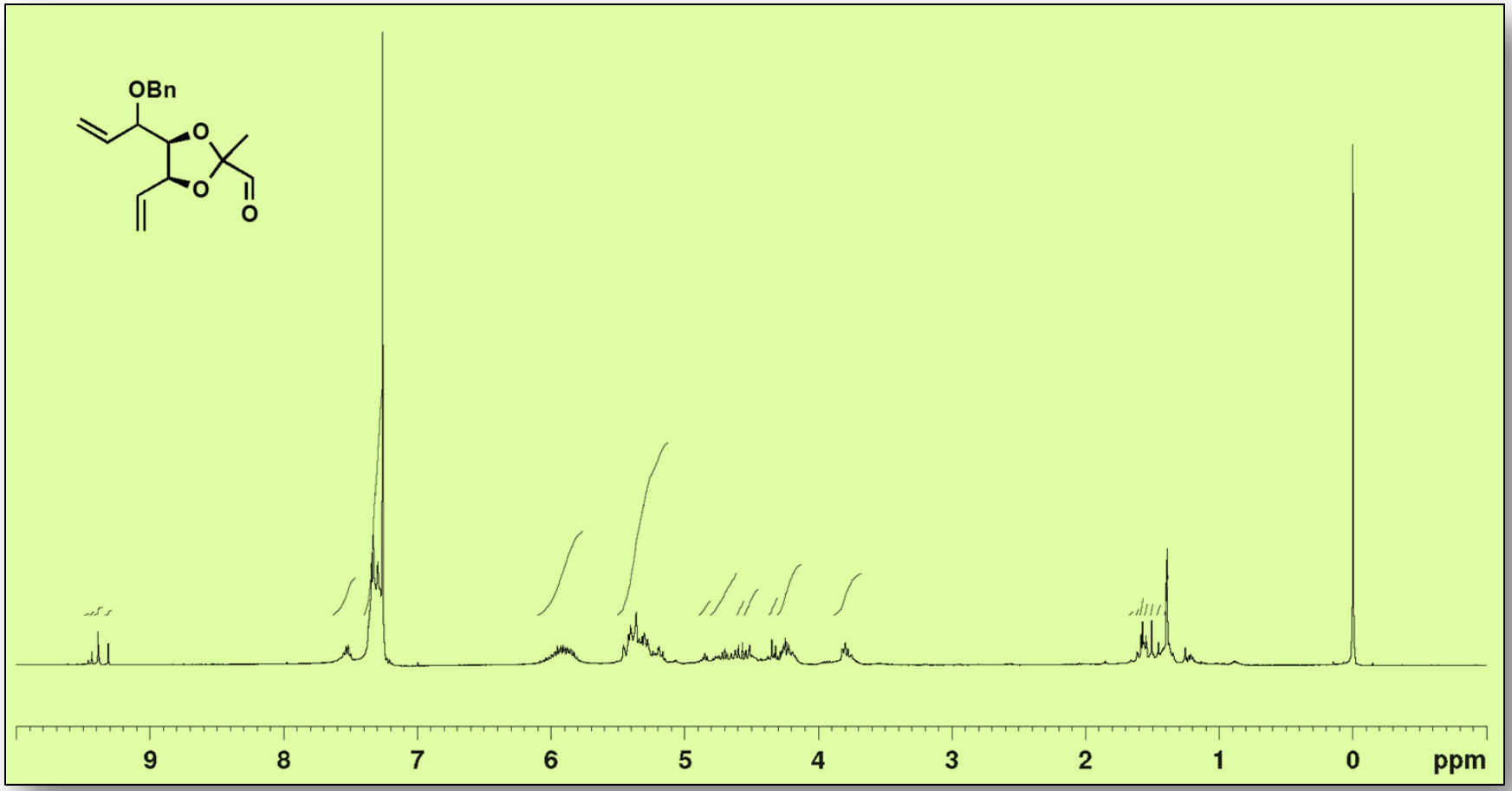

Figure 54: ^{1}H NMR spectrum of compound **85** (400 MHz, $CDCl_3$, 293K)

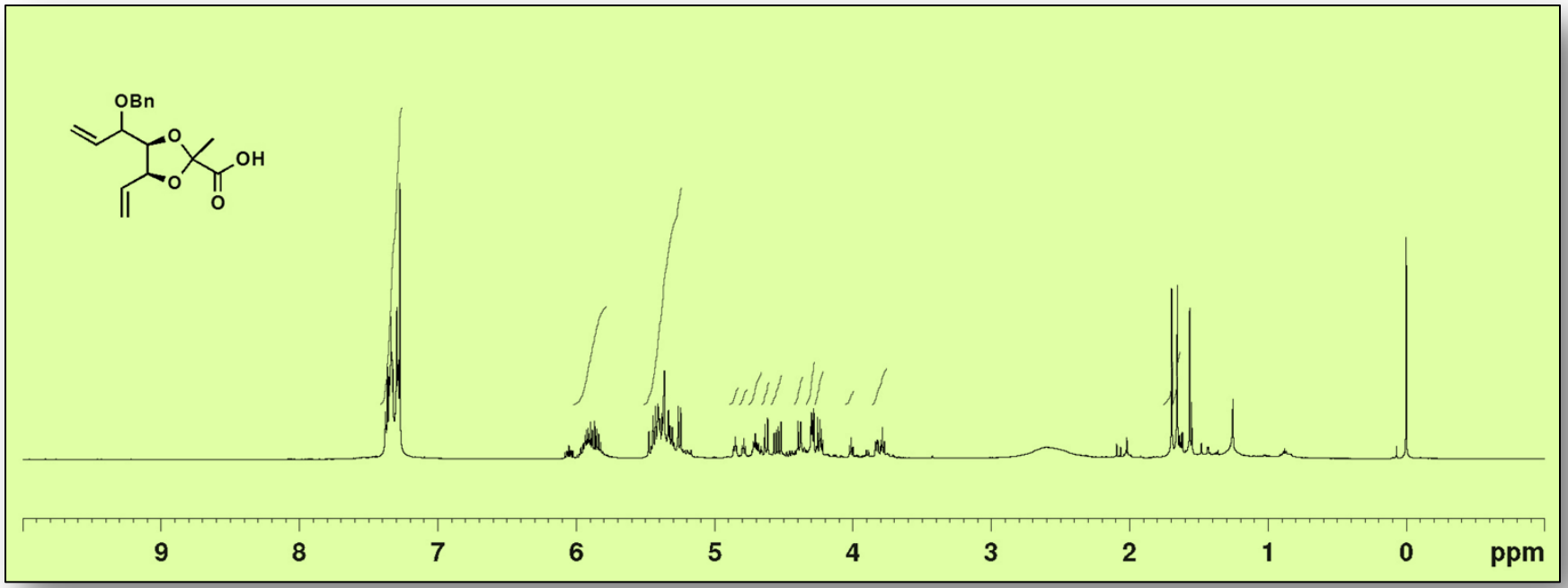

Figure 55: ^{1}H NMR spectrum of compound **85** (400 MHz, $CDCl_3$, 293K)

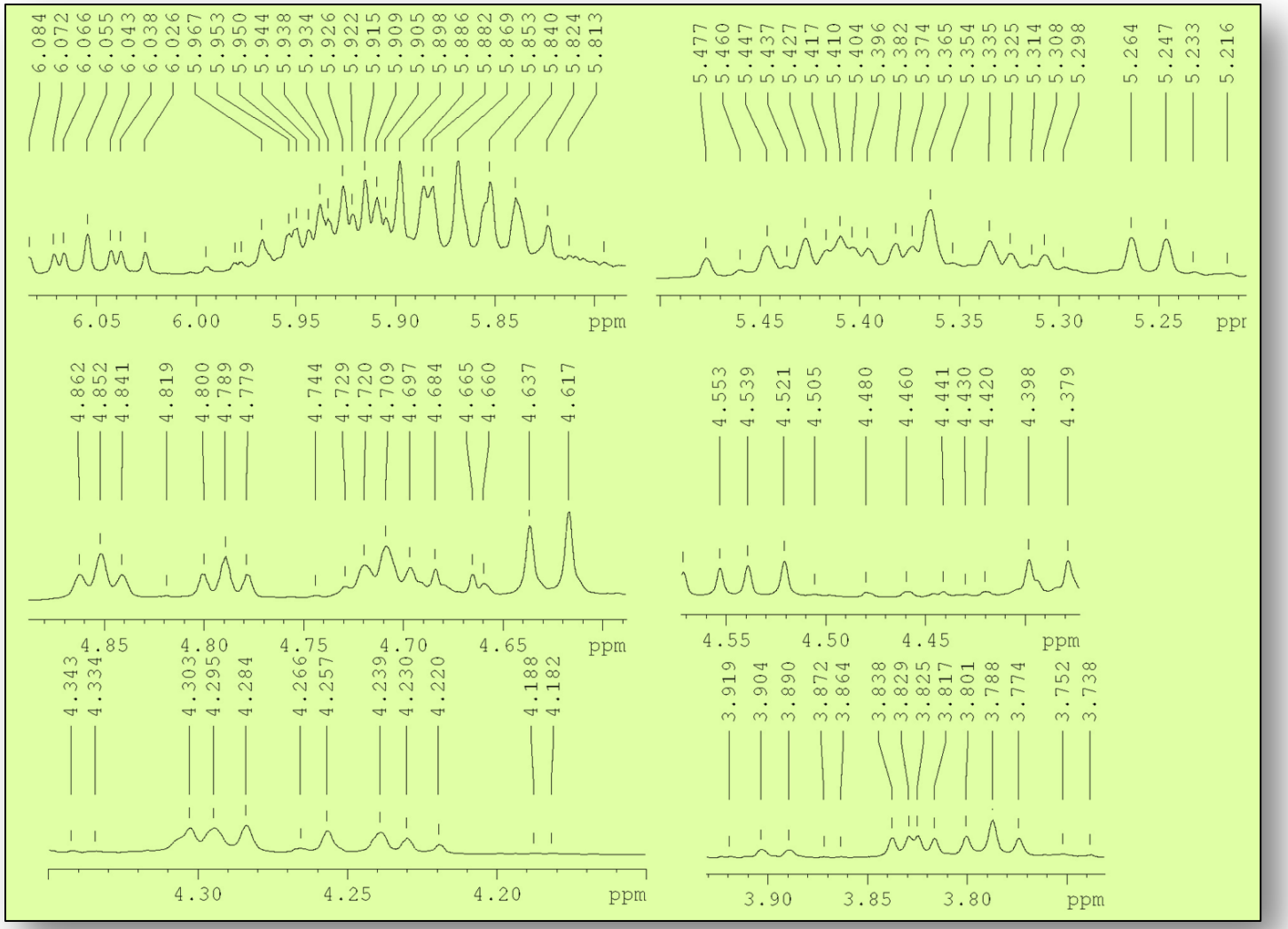

Figure 56: ^{1}H NMR spectrum of compound 85 (continued)

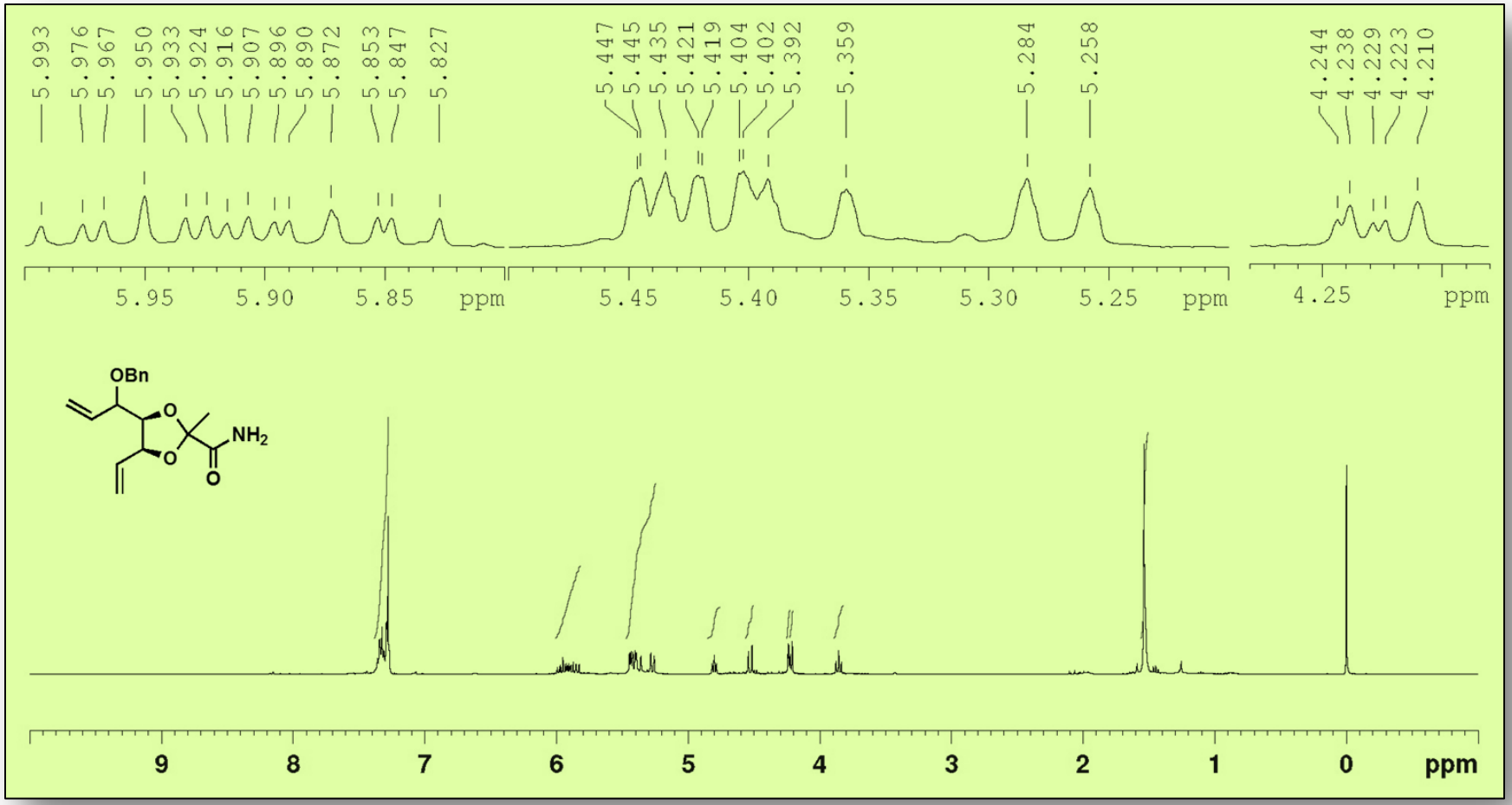

Figure 57: ^{1}H NMR spectrum of compound 87a (400 MHz, $CDCl_3$, 293K)

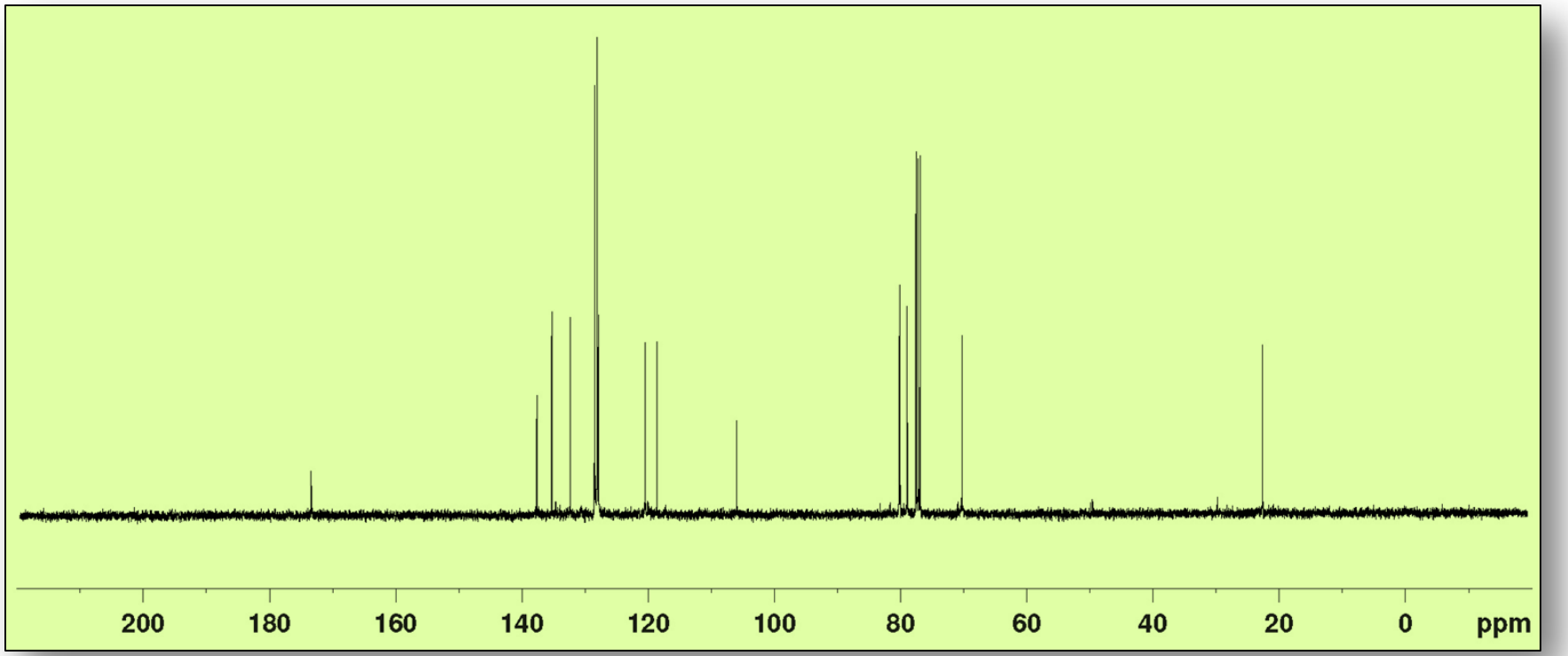

Figure 58: ^{13}C NMR spectrum of compound 87a (400 MHz, $CDCl_3$, 293K)

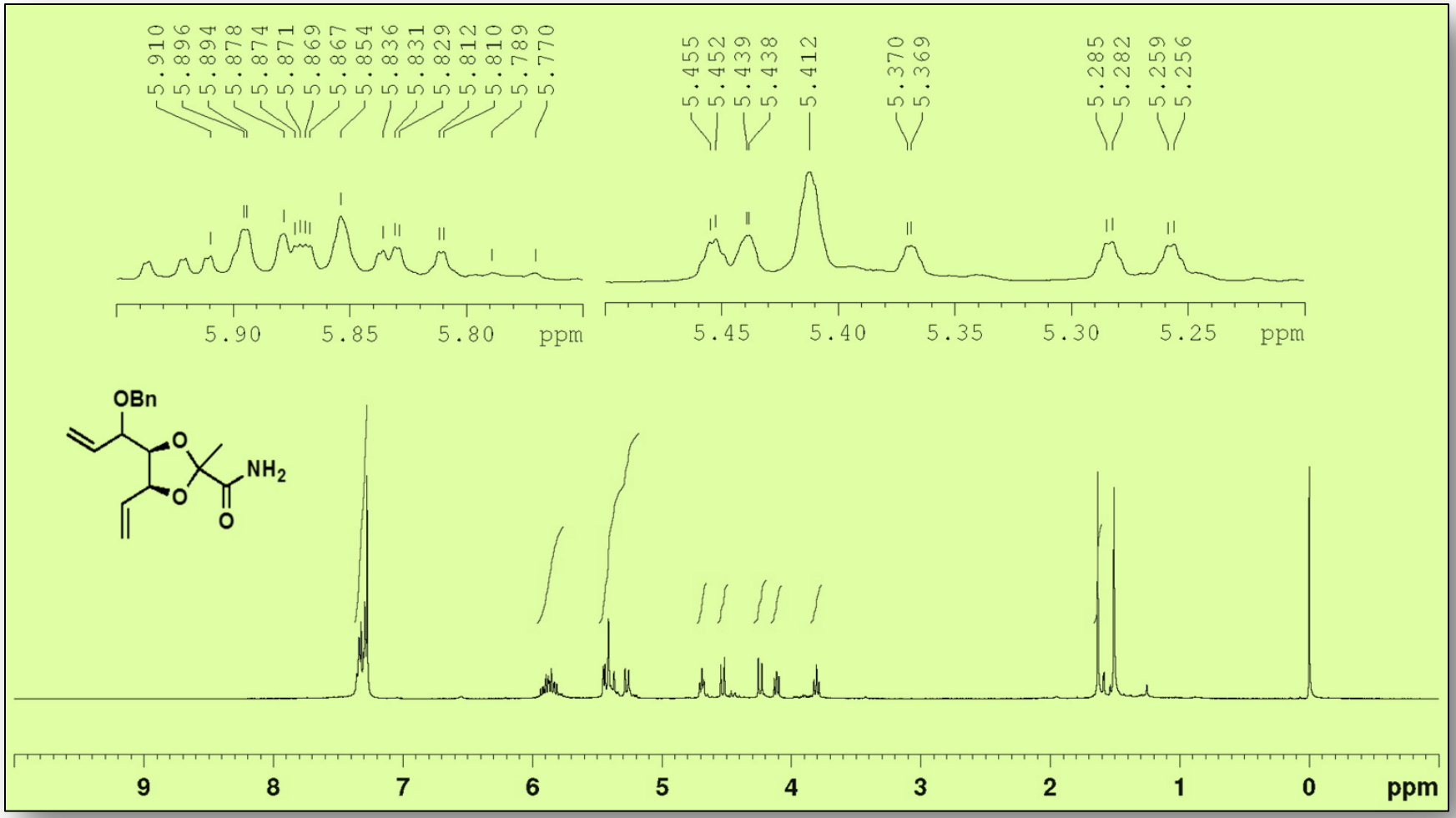

Figure 59: ^{1}H NMR spectrum of compound 87b (400 MHz, $CDCl_3$, 293K)

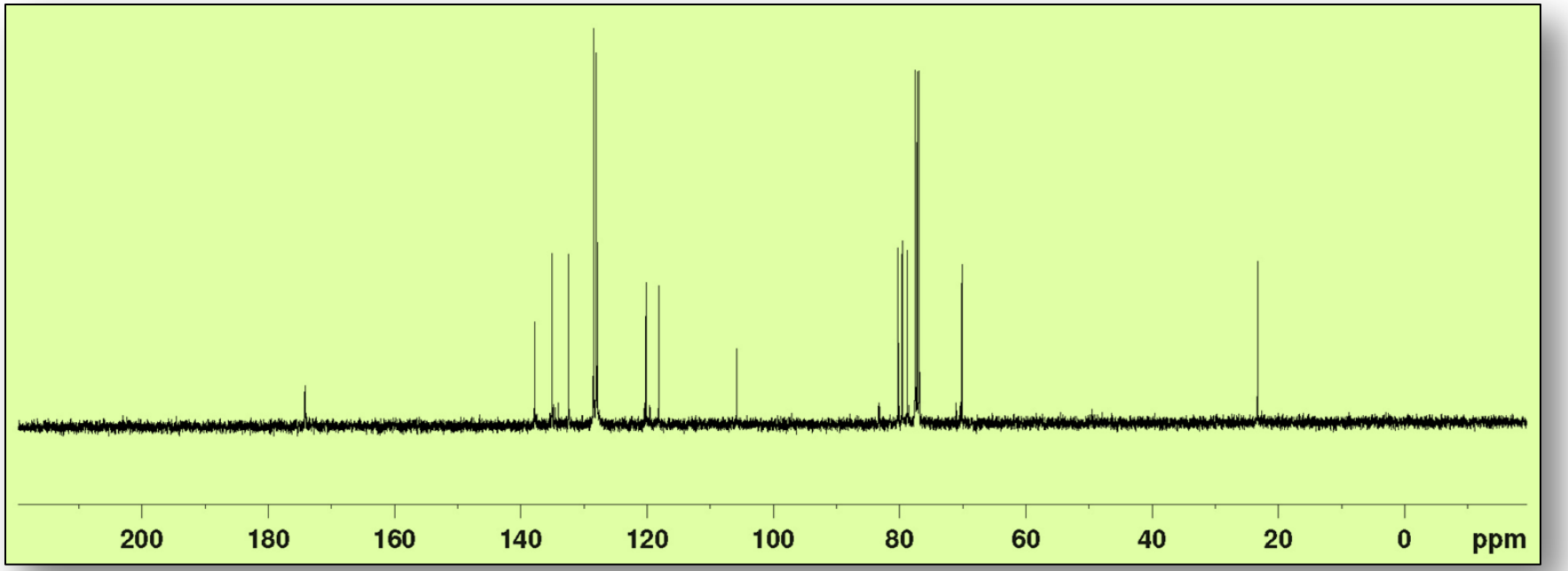

Figure 60: ^{13}C NMR spectrum of compound 87b (400 MHz, $CDCl_3$, 293K)

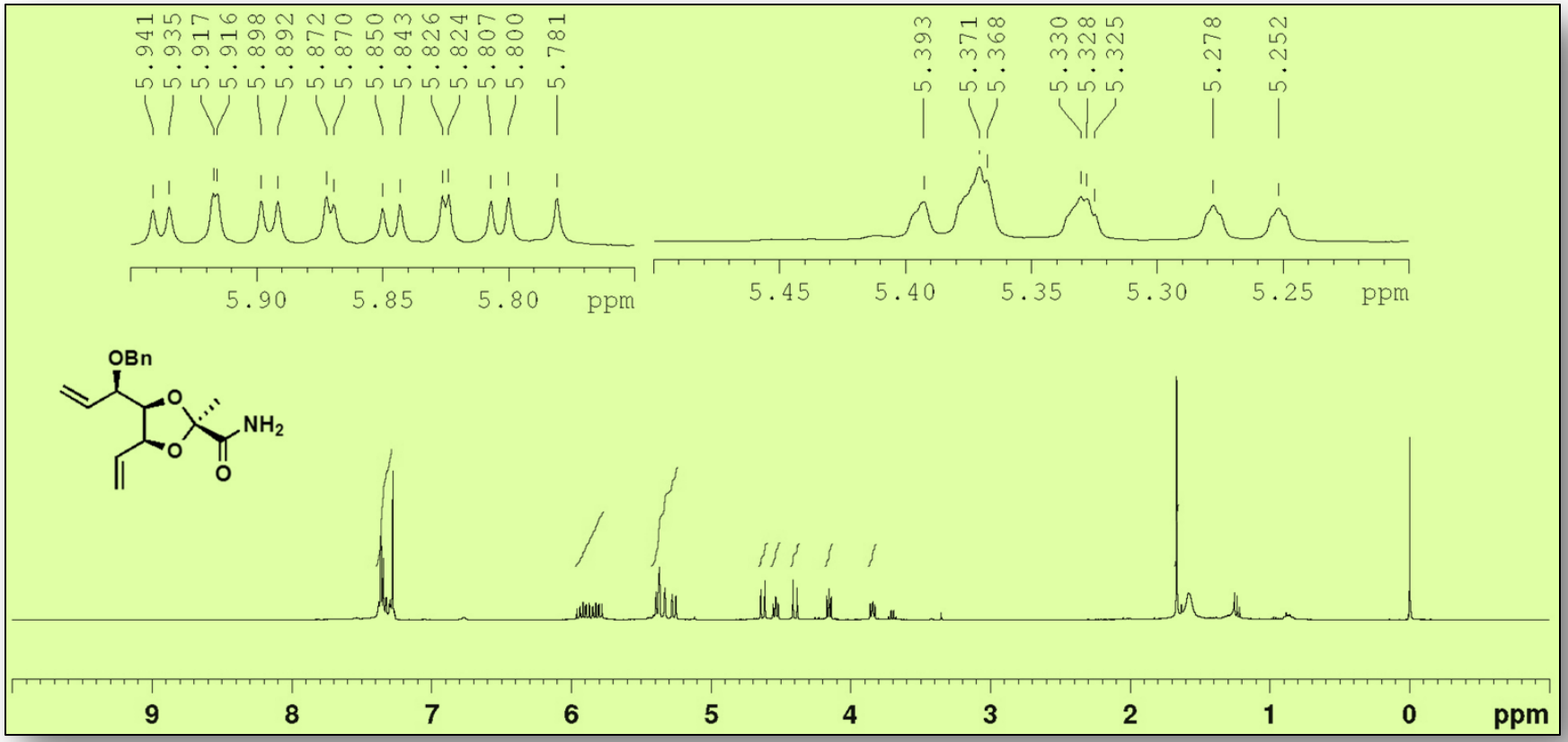

Figure 61: ^{1}H NMR spectrum of compound 87c (400 MHz, $CDCl_3$, 293K)

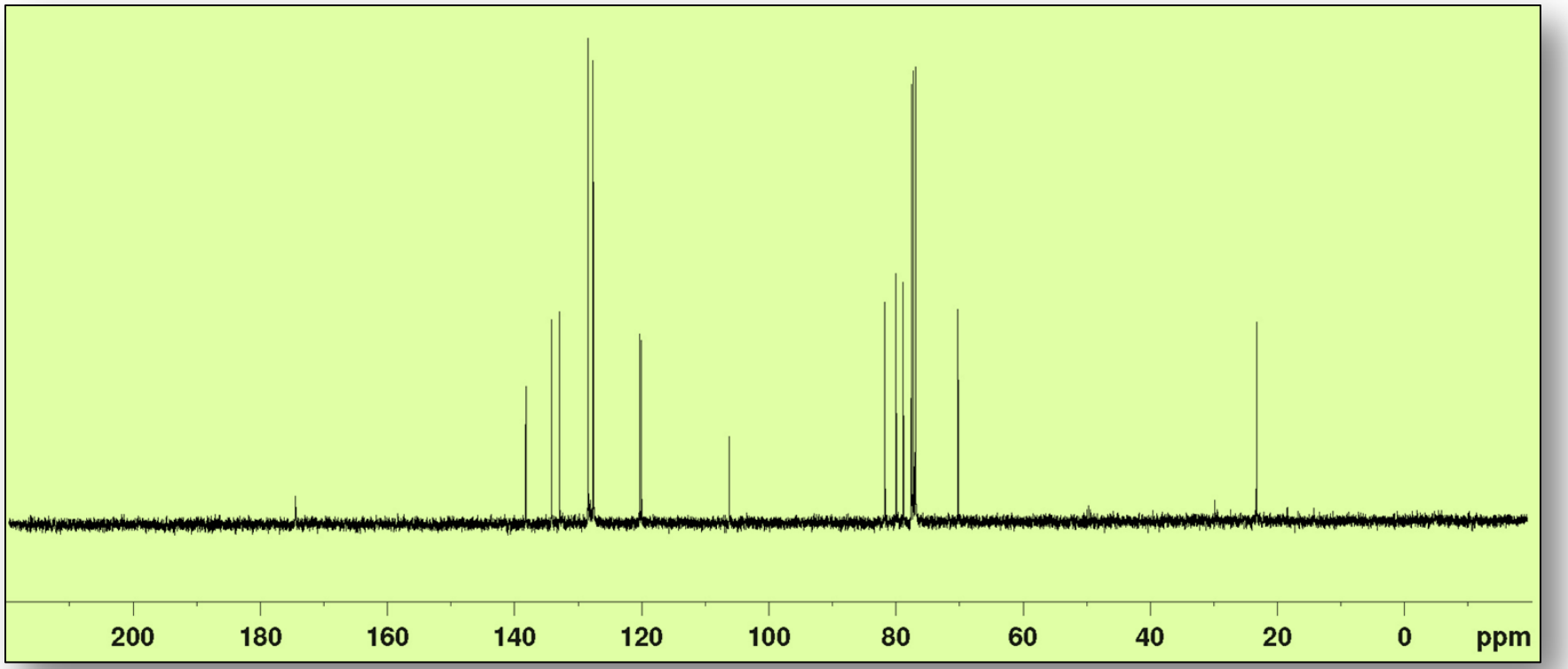

Figure 62: ^{13}C NMR spectrum of compound 87c (400 MHz, $CDCl_3$, 293K)

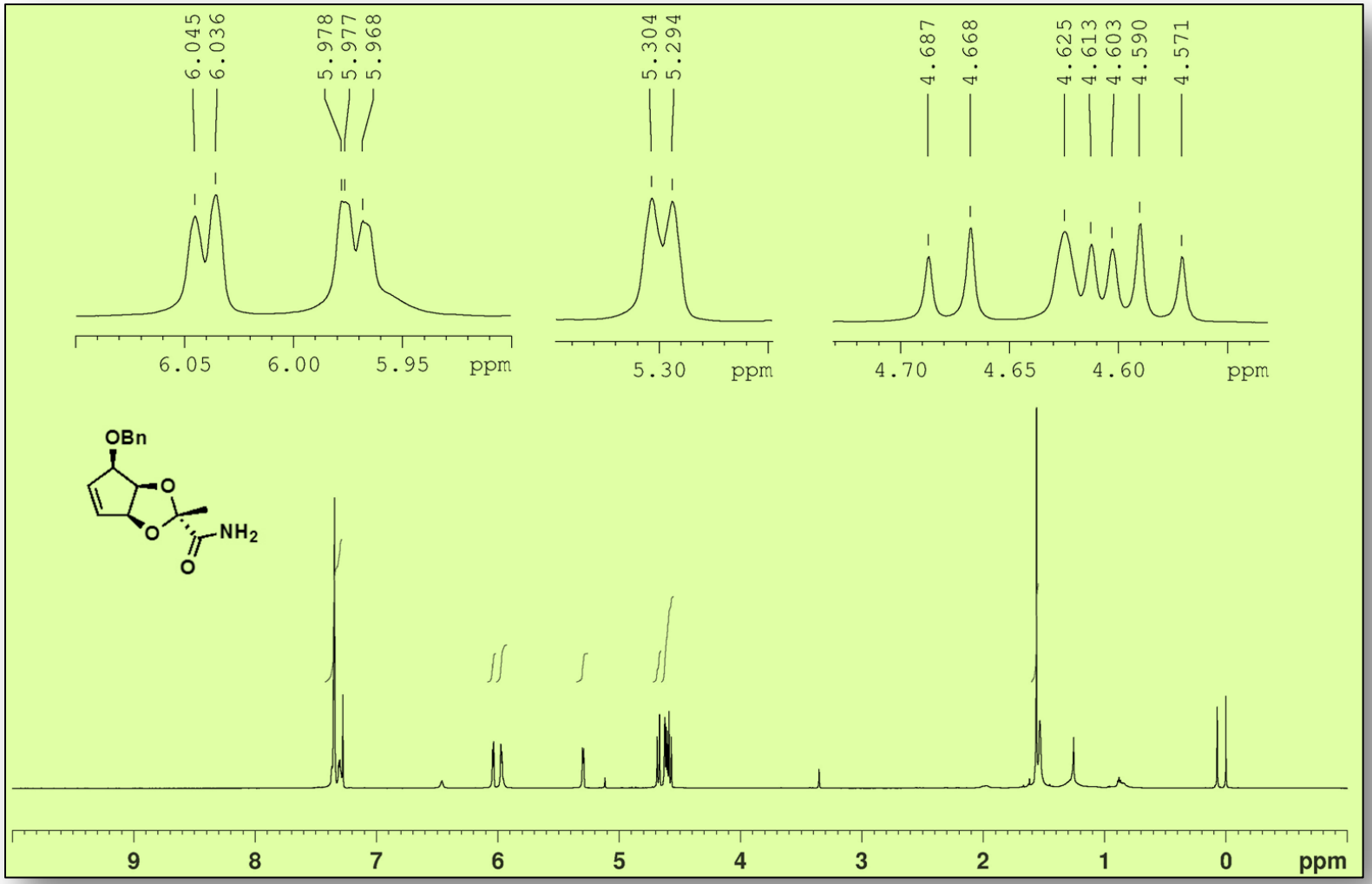

Figure 63: ^{1}H NMR spectrum of compound (600 MHz, $CDCl_3$, 293K)

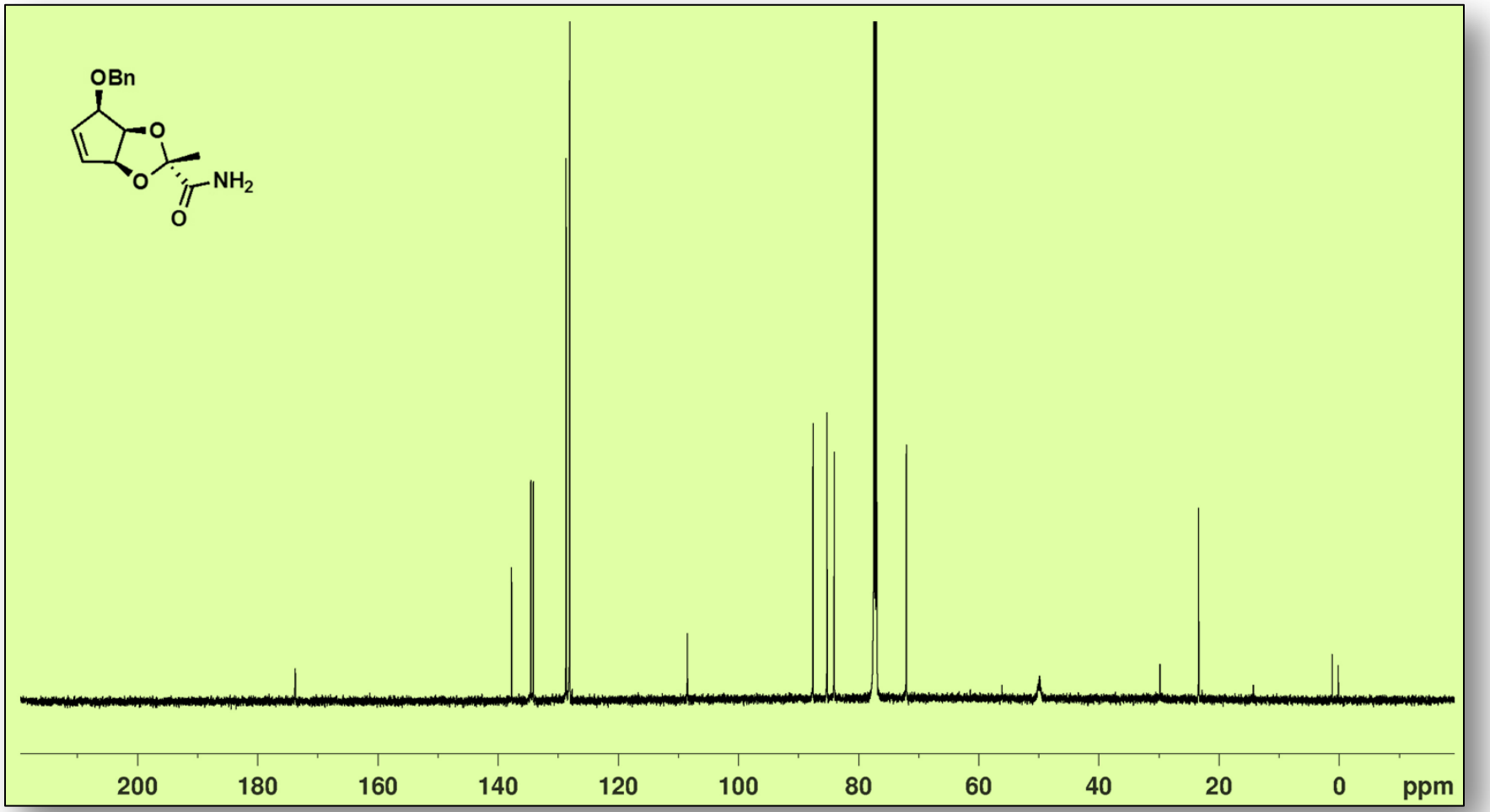

Figure 64: ^{13}C NMR spectrum of compound 95 (600 MHz, $CDCl_3$, 293K)

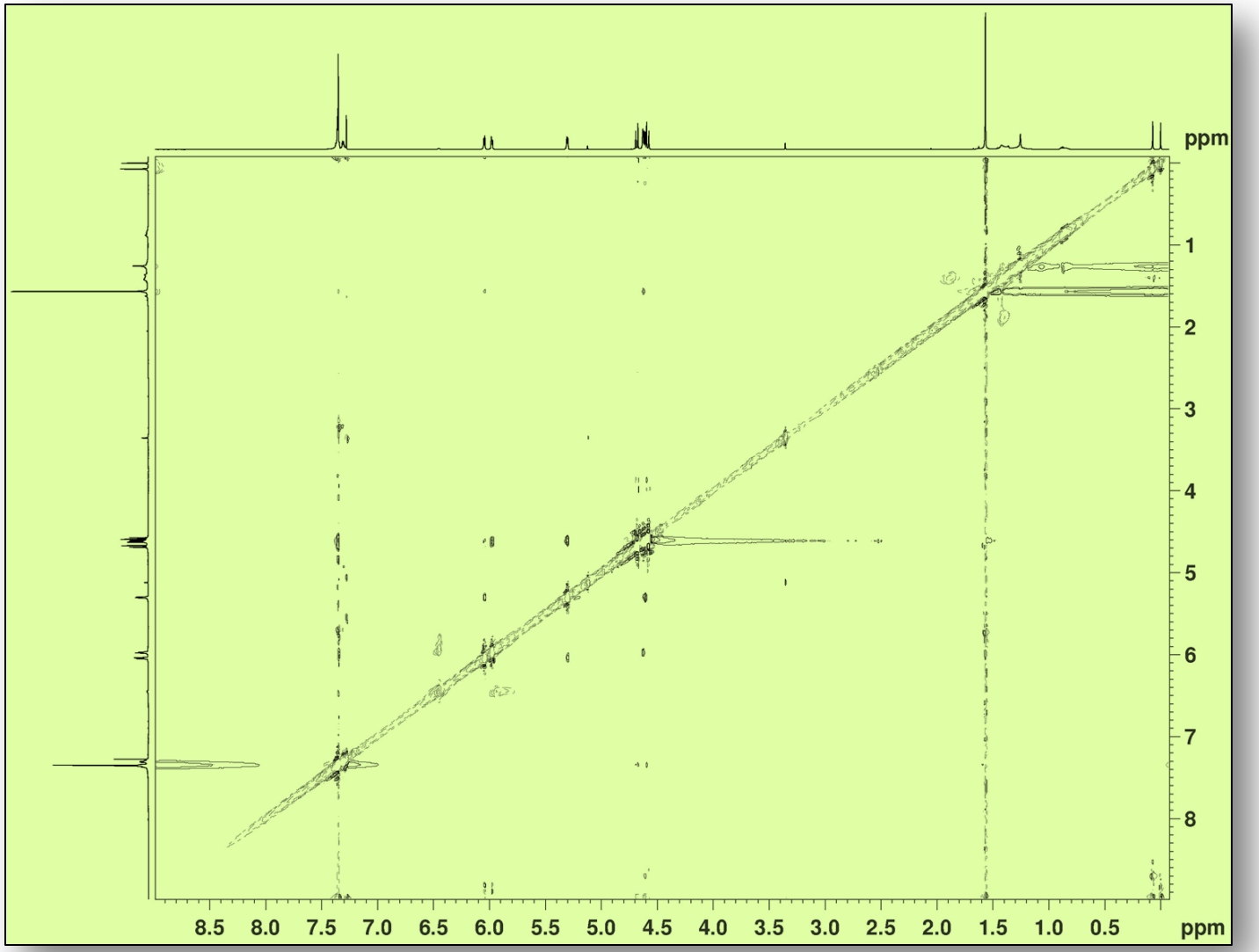

Figure 65: NOESY correlation spectrum of compound **87a** (600 MHz, $CDCl_3$, 293K)

10.0 BIBLIOGRAPHY

1. Isaacs, J. S.; Xu, W. P.; Neckers, L. Heat shock protein 90 as a molecular target for cancer therapeutics. *Cancer Cell.* **2003,** 3, 213-217.
2. Ritossa, F. New Puffing Pattern Induced by Temperature Shock and Dnp in Drosophila. *Experientia.* **1962,** 18, 571-&.
3. Georgopoulos, C.; Welch, W. J. Role of the Major Heat-Shock Proteins as Molecular Chaperones. *Ann. Rev. Cell. Bio.* **1993,** 9, 601-634.
4. Sreedhar, A. S.; Kalmar, E.; Csermely, P.; Shen, Y. F. Hsp90 isoforms: functions, expression and clinical importance. *FEBS Lett.* **2004,** 562, 11-15.
5. Prodromou, C.; Roe, S. M.; Piper, P. W.; Pearl, L. H. A molecular clamp in the crystal structure of the N-terminal domain of the yeast Hsp90 chaperone. *Nat. Struct. Biol.* **1997,** 4, 477-482.
6. Scheibel, T.; Buchner, J. The Hsp90 complex - A super-chaperone machine as a novel drug target. *Biochem. Pharmacol.* **1998,** 56, 675-682.
7. Scheibel, T.; Siegmund, H. I.; Jaenicke, R.; Ganz, P.; Lilie, H.; Buchner, J. The charged region of Hsp90 modulates the function of the N-terminal domain. *P. Natl. Acad. Sci. U.S.A.* **1999,** 96, 1297-1302.
8. Scheibel, T.; Weikl, T.; Buchner, J. Two chaperone sites in Hsp90 differing in substrate specificity and ATP dependence. *P. Natl. Acad. Sci. U.S.A.* **1998,** 95, 1495-1499.
9. Scheibel, T.; Weikl, T.; Rimerman, R.; Smith, D.; Lindquist, S.; Buchner, J. Contribution of N- and C-terminal domains to the function of Hsp90 in Saccharomyces cerevisiae. *Mol. Microbiol.* **1999,** 34, 701-713.
10. Young, J. C.; Schneider, C.; Hartl, F. U. In vitro evidence that hsp90 contains two independent chaperone sites. *FEBS Lett.* **1997,** 418, 139-143.
11. Spiess, C.; Meyer, A. S.; Reissmann, S.; Frydman, J. Mechanism of the eukaryotic chaperonin: protein folding in the chamber of secrets. *Trends. Cell. Biol.* **2004,** 14, 598-604.
12. Young, J. C.; Agashe, V. R.; Siegers, K.; Hartl, F. U. Pathways of chaperone-mediated protein folding in the cytosol. *Nat. Rev. Mol. Cell. Bio.* **2004,** 5, 781-791.
13. Young, J. C.; Moarefi, I.; Hartl, F. U. Hsp90: a specialized but essential protein-folding tool. *J. Cell Biol.* **2001,** 154, 267-273.
14. Picard, D.; Khursheed, B.; Garabedian, M. J.; Fortin, M. G.; Lindquist, S.; Yamamoto, K. R. Reduced Levels of Hsp90 Compromise Steroid-Receptor Action Invivo. *Nature.* **1990,** 348, 166-168.
15. Xu, Y.; Lindquist, S. Heat-Shock Protein Hsp90 Governs the Activity of Pp60(V-Src) Kinase. *P. Natl. Acad. Sci. U.S.A.* **1993,** 90, 7074-7078.
16. Karapanagiotou, E. M.; Syrigos, K.; Saif, M. W. Heat shock protein inhibitors and vaccines as new agents in cancer treatment. *Expert. Opin. Inv. Drug.* **2009,** 18, 161-174.

17. Fisher, D. L.; Mandart, E.; Doree, M. Hsp90 is required for c-Mos activation and biphasic MAP kinase activation in Xenopus oocytes. *EMBO J,* **2000,** 19, 1516-1524.
18. Helmbrecht, K.; Zeise, E.; Rensing, L. Chaperones in cell cycle regulation and mitogenic signal transduction: a review. *Cell Proliferat.* **2000,** 33, 341-365.
19. Lange, B. M. H.; Bachi, A.; Wilm, M.; Gonzalez, C. Hsp90 is a core centrosomal component and is required at different stages of the centrosome cycle in Drosophila and vertebrates. *EMBO J.* **2000,** 19, 1252-1262.
20. Zou, J. Y.; Guo, Y. L.; Guettouche, T.; Smith, D. F.; Voellmy, R. Repression of heat shock transcription factor HSF1 activation by HSP90 (HSP90 complex) that forms a stress-sensitive complex with HSF1. *Cell.* **1998,** 94, 471-480.
21. Dai, C.; Whitesell, L.; Rogers, A. B.; Lindquist, S. Heat shock factor 1 is a powerful multifaceted modifier of carcinogenesis. *Cell.* **2007,** 130, 1005-1018.
22. Deboer, C.; Meulman, P. A.; Wnuk, R. J.; Peterson, D. H. Geldanamycin, a New Antibiotic. *J. Antibiot* . **1970,** 23, 442-&.
23. Whitesell, L.; Shifrin, S. D.; Schwab, G.; Neckers, L. M. Benzoquinonoid Ansamycins Possess Selective Tumoricidal Activity Unrelated to Src Kinase Inhibition. *Cancer Res.* **1992,** 52, 1721-1728.
24. Grenert, J. P.; Sullivan, W. P.; Fadden, P.; Haystead, T. A. J.; Clark, J.; Mimnaugh, E.; Krutzsch, H.; Ochel, H. J.; Schulte, T. W.; Sausville, E.; Neckers, L. M.; Toft, D. O. The amino-terminal domain of heat shock protein 90 (hsp90) that binds geldanamycin is an ATP/ADP switch domain that regulates hsp90 conformation. *J. Biol. Chem.* **1997,** 272, 23843-23850.
25. Hostein, I.; Robertson, D.; DiStefano, F.; Workman, P.; Clarke, P. A. Inhibition of signal transduction by the Hsp90 inhibitor 17-allylamino-17-demethoxygeldanamycin results in cytostasis and apoptosis. *Cancer Res.* **2001,** 61, 4003-4009.
26. Supko, J. G.; Hickman, R. L.; Grever, M. R.; Malspeis, L. Preclinical Pharmacological Evaluation of Geldanamycin as an Antitumor Agent. *Cancer. Chemoth. Pharmacol.* **1995,** 36, 305-315.
27. Whitesell, L.; Sutphin, P.; An, W. G.; Schulte, T.; Blagosklonny, M. V.; Neckers, L. Geldanamycin-stimulated destabilization of mutated p53 is mediated by the proteasome in vivo. *Oncogene.* **1997,** 14, 2809-2816.
28. Schulte, T. W.; An, W. G.; Neckers, L. M. Geldanamycin-induced destabilization of Raf-1 involves the proteasome. *Biochem. Bioph. Res. Co.* **1997,** 239, 655-659.
29. Tian, Z. Q.; Liu, Y. Q.; Zhang, D.; Wang, Z.; Dong, S. D.; Carreras, C. W.; Zhou, Y. Q.; Rastelli, G.; Santi, D. V.; Myles, D. C. Synthesis and biological activities of novel 17-aminogeldanamycin derivatives. *Bioorgan. Med. Chem.* **2004,** 12, 5317-5329.
30. Delmotte, P.; Delmotteplaquee, J. A New Antifungal Substance of Fungal Origin. *Nature.* **1953,** 171, 344-344.
31. Mccapra, F.; Scott, A. I.; Delmotte, P.; Delmotteplaquee, J. The Constitution of Monorden, an Antibiotic with Tranquilising Action. *Tetrahedron Lett.* **1964**, 869-875.
32. Roe, S. M.; Prodromou, C.; O'Brien, R.; Ladbury, J. E.; Piper, P. W.; Pearl, L. H. Structural basis for inhibition of the Hsp90 molecular chaperone by the antitumor antibiotics radicicol and geldanamycin. *J. Med. Chem.* **1999,** 42, 260-266.
33. Kelland, L. R.; Sharp, S. Y.; Rogers, P. M.; Myers, T. G.; Workman, P. DT-diaphorase expression and tumor cell sensitivity to 17-allylamino,17-demethoxygeldanamycin, an inhibitor of heat shock protein 90. *J. Natl. Cancer. I.* **1999,** 91, 1940-1949.

34. Ali, J. A.; Jackson, A. P.; Howells, A. J.; Maxwell, A. The 43-Kilodalton N-Terminal Fragment of the DNA Gyrase-B Protein Hydrolyzes Atp and Binds Coumarin Drugs. *Biochemistry.* **1993,** 32, 2717-2724.
35. Marcu, M. G.; Schulte, T. W.; Neckers, L. Novobiocin and related coumarins and depletion of heat shock protein 90-dependent signaling proteins. *J. Natl. Cancer. I.* **2000,** 92, 242-248.
36. Marcu, M. G.; Chadli, A.; Bouhouche, I.; Catelli, M.; Neckers, L. M. The heat shock protein 90 antagonist novobiocin interacts with a previously unrecognized ATP-binding domain in the carboxyl terminus of the chaperone. *J. Biol. Chem.* **2000,** 275, 37181-37186.
37. Chiosis, G.; Timaul, M. N.; Lucas, B.; Munster, P. N.; Zheng, F. F.; Sepp-Lorenzino, L.; Rosen, N. A small molecule designed to bind to the adenine nucleotide pocket of Hsp90 causes Her2 degradation and the growth arrest and differentiation of breast cancer cells. *Chem. Biol.* **2001,** 8, 289-299.
38. Chiosis, G.; Lucas, B.; Shtil, A.; Huezo, H.; Rosen, N. Development of a purine-scaffold novel class of Hsp90 binders that inhibit the proliferation of cancer cells and induce the degradation of Her2 tyrosine kinase. *Bioorgan. Med. Chem.* **2002,** 10, 3555-3564.
39. Biamonte, M. A.; Shi, J. D.; Hong, K.; Hurst, D. C.; Zhang, L.; Fan, J. H.; Busch, D. J.; Karjian, P. L.; Maldonado, A. A.; Sensintaffar, J. L.; Yang, Y. C.; Kamal, A.; Lough, R. E.; Lundgren, K.; Burrows, F. J.; Timony, G. A.; Boehm, M. F.; Kasibhatla, S. R. Orally active purine-based inhibitors of the heat shock protein 90. *J. Med. Chem.* **2006,** 49, 817-828.
40. Akagawa, H.; Takano, Y.; Ishii, A.; Mizuno, S.; Izui, R.; Sameshima, T.; Kawamura, N.; Dobashi, K.; Yoshioka, T. Stresgenin B, an inhibitor of heat-induced heat shock protein gene expression, produced by Streptomyces sp AS-9. *J. Antibiot.* **1999,** 52, 960-970.
41. Roberts, S. M.; Santoro, M. G.; Sickle, E. S. The emergence of the cyclopentenone prostaglandins as important, biologically active compounds. *J .Chem. Soc. Perk. T. 1.* **2002**, 1735-1742.
42. Johnson, C. R., Penning, T. D. Triply Convergent Synthesis of (-)-Prostaglandin E2. *J. Am. Chem. Soc.* **1986,** 108, 5655-5656.
43. Armstrong, A.; Hayter, B. R. Concise synthesis of (4S,5S)-4,5-(isopropylidenedioxy)-2-cyclopentenone and a novel C-2-symmetric ketone. *Tetrahedron-Asymmetry.* **1997,** 8, 1677-1684.
44. Stone, K. J.; Little, R. D. An Exceptionally Simple and Efficient Method for the Preparation of a Wide Variety of Fulvenes. *J. Org. Chem.* **1984,** 49, 1849-1853.
45. Ali, S. M.; Ramesh, K.; Borchardt, R. T. Efficient Enantioselective Syntheses of Carbocyclic Nucleoside and Prostaglandin Synthons. *Tetrahedron Lett.* **1990,** 31, 1509-1512.
46. Gemal, A. L.; Luche, J. L. Lanthanoids in Organic-Synthesis .6. The Reduction of Alpha-Enones by Sodium-Borohydride in the Presence of Lanthanoid Chlorides - Synthetic and Mechanistic Aspects. *J. Am. Chem. Soc.* **1981,** 103, 5454-5459.
47. Vanrheenen, V.; Kelly, R. C.; Cha, D. Y. Improved Catalytic Oso4 Oxidation of Olefins to Cis-1,2-Glycols Using Tertiary Amine Oxides as Oxidant. *Tetrahedron Lett.* **1976**, 1973-1976.
48. Nicolaou, K. C.; Baran, P. S.; Zhong, Y. L. Selective oxidation at carbon adjacent to aromatic systems with IBX. *J. Am. Chem. Soc.* **2001,** 123, 3183-3185.
49. Nicolaou, K. C.; Montagnon, T.; Baran, P. S.; Zhong, Y. L. Iodine(V) reagents in organic synthesis. Part 4. o-iodoxybenzoic acid as a chemospecific tool for single electron transfer-based oxidation processes. *J. Am. Chem. Soc.* **2002,** 124, 2245-2258.

50. Parikh, J. R.; Doering, W. V. E. Sulfur Trioxide in Oxidation of Alcohols by Dimethyl Sulfoxide. *J. Am. Chem. Soc.* **1967,** 89, 5505-&.
51. Jin, Y. H.; Liu, P.; Wang, J. N.; Baker, R.; Huggins, J.; Chu, C. K. Practical synthesis of D- and L-2-cyclopentenone and their utility for the synthesis of carbocyclic antiviral nucleosides against orthopox viruses (smallpox, monkeypox, and cowpox virus). *J. Org. Chem.* **2003,** 68, 9012-9018.
52. Moon, H. R.; Choi, W. J.; Kim, H. O.; Jeong, L. S. Improved and alternative synthesis of D- and L-cyclopentenone derivatives, the versatile intermediates for the synthesis of carbocyclic nucleosides. *Tetrahedron-Asymmetry.* **2002,** 13, 1189-1193.
53. Christoffers, J. a. J. A. B. *Quaternary Stereocenters*. Wiley-VHC: 2005; Vol. 5.
54. Wuts, T. W. G. a. P. G. M. *Protective Groups in Organic Synthesis*. 3 ed.; John Wiley & Sons: New York, 1999.
55. Singh, G.; Vankayalapati, H. Efficient stereocontrolled synthesis of C-glycosides using glycosyl donors substituted by propane 1,3-diyl phosphate as the leaving group. *Tetrahedron-Asymmetry.* **2001,** 12, 1727-1735.
56. Robiette, R.; Richardson, J.; Aggarwal, V. K.; Harvey, J. N. On the origin of high E selectivity in the Wittig reaction of stabilized ylides: Importance of dipole-dipole interactions. *J. Am. Chem. So.c* **2005,** 127, 13468-13469.
57. Vedejs, E.; Fleck, T.; Hara, S. Evidence against Reversible Wittig Reaction of a Stabilized Ylide - High (E)-Olefin Selectivity under Kinetic Control. *J. Org. Chem.* **1987,** 52, 4637-4639.
58. Vedejs, E.; Fleck, T. J. Kinetic (Not Equilibrium) Factors Are Dominant in Wittig Reactions of Conjugated Ylides. *J. Am. Chem. Soc.* **1989,** 111, 5861-5871.
59. Vedejs, E.; Marth, C. F. Mechanism of the Wittig Reaction - the Role of Substituents at Phosphorus. *J. Am. Chem. Soc.* **1988,** 110, 3948-3958.
60. Vedejs, E.; Marth, C. F.; Ruggeri, R. Substituent Effects and the Wittig Mechanism - the Case for Stereospecific Oxaphosphetane Decomposition. *J. Am. Chem. Soc.* **1988,** 110, 3940-3948.
61. Blanchette, M. A.; Choy, W.; Davis, J. T.; Essenfeld, A. P.; Masamune, S.; Roush, W. R.; Sakai, T. Horner-Wadsworth-Emmons Reaction - Use of Lithium-Chloride and an Amine for Base Sensitive Compounds. *Tetrahedron Lett.* **1984,** 25, 2183-2186.
62. Toutchkine, A.; Aebisher, D.; Clennan, E. L. Substituent-dictated partitioning of intermediates on the sulfide singlet oxygen reaction surface. A new mechanism for oxidative C-S bond cleavage in alpha-hydroperoxy sulfides. *J. Am. Chem. Soc.* **2001,** 123, 4966-4973.
63. Sugihara, H.; Tanikaga, R.; Kaji, A. Useful Method for Conversion of Sulfoxides to Aldehydes. *Synthesis.* **1978**, 881-881.
64. Jung, M. E.; Lyster, M. A. Quantitative Dealkylation of Alkyl Ethers Via Treatment with Trimethylsilyl Iodide - New Method for Ether Hydrolysis. *J. Org. Chem.* **1977,** 42, 3761-3764.
65. Jung, M. E.; Lyster, M. A. Quantitative Dealkylation of Alkyl Esters Via Treatment with Trimethylsilyl Iodide - New Method for Ester Hydrolysis. *Abstr. Pap. Am. Chem. Soc.* **1977,** 173, 89-89.
66. Jung, M. E.; Lyster, M. A. Quantitative Dealkylation of Alkyl Esters Via Treatment with Trimethylsilyl Iodide - New Method for Ester Hydrolysis. *J. Am. Chem. Soc.* **1977,** 99, 968-969.

67. Alzeer, J.; Vasella, A. Oligosaccharide Analogs of Polysaccharides .2. Regioselective Deprotection of Monosaccharide-Derived Monomers and Dimers. *Helv. Chim. Acta.* **1995,** 78, 177-193.
68. Angibeaud, P.; Utille, J. P. Cyclodextrin Chemistry .1. Application of a Regioselective Acetolysis Method for Benzyl Ethers. *Synthesis.* **1991**, 737-738.
69. Ikemoto, N.; Schreiber, S. L. Total Synthesis of (-)-Hikizimycin Employing the Strategy of 2-Directional Chain Synthesis. *J. Am. Chem. So.c* **1992,** 114, 2524-2536.
70. Floreancig, P. E.; Liu, L. 2,3-Dichloro-5,6-dicyano-1,4-benzoquinone-Catalyzed Reactions Employing MnO(2) as a Stoichiometric Oxidant. *Org. Lett.* **2010,** 12, 4686-4689.